DEVELOPMENT AND CHARACTERIZATION OF MAGNESIUM ALGINATE HYDROGELS FOR 3D CELL CULTURE FORMATION

A Thesis Submitted to
the Graduate School of Engineering and Science of
Izmir Institute of Technology
in Partial Fulfillment of the Requirements for the Degree of

MASTER OF SCIENCE

in Bioengineering

by
Başak ÇOBAN

July 2021
İZMİR

ACKNOWLEDGEMENTS

Firstly, I would like to mention my deep and sincere gratitude to my supervisor Assoc. Prof. Dr. Ahu ARSLAN YILDIZ for all of her patience, counseling, encouragement, and support throughout my graduate studies. I acknowledge TUBITAK 2210/C National MSc Scholarship Program in the Priority Fields in Science and Technology for financal support. I would like to thank Prof. Hasan Şahin and CENT group member Mehmet Başkurt for his contributions in the computational part of the thesis.

I am very thankful to my co-worker Rabia Önbaş for her guide, suggestions, encourage and support throughout my Master of Science thesis study. I am grateful to Biomimetics Research Group members; Alper Baran Sözmen, Ece Özmen, Duygu Arslantaş, Meltem Güzelgülgen, Özüm Yıldırım, and Rümeysa Bilginer for their friendship, support, help, and patience. I also want to express special thanks to Gamze Yazgeldi and Azime Akçaöz for their encouragement, patience and support during my whole graduate life.

Finally, I would like to show my deepest appreciation to my family for their everlasting excellent encouragement.

.

ABSTRACT

DEVELOPMENT AND CHARACTERIZATION OF MAGNESIUM ALGINATE HYDROGEL FOR 3D CELL CULTURE FORMATION

Three-dimensional (3D) cell culture allows cells to growth in their 3D physical shape and interact with their surroundings which represent the natural microenvironment. Hydrogels are crosslinked networks, have become increasingly used biomaterial for 3D cell culture. In this thesis, a new methodology based on bio-patterning was developed to fabricate (3D) cellular structures by using Mg-alginate hydrogel and fabricated 3D cellular structures was utilized for drug screening studies. Mg-alginate hydrogel has a specific gelation/de-gelation characteristics compared to other types of hydrogels due to its weak polymer-ion interaction. In this study, slow gelation and de-gelation property of Mg-alginate hydrogel was used for biopatterning of 3D cellular structures. Plackett-Burman and Box-Behnken design models were used to optimize parameters of Mg alginate-based biopatterning method while using HeLa cells as a model cell line. The applicability of biopatterning was successfully demonstrated by using SaOS-2 and SH-SY5Y cells. Cell proliferation and viability of long-term cultured tumor models were analyzed and immunostaining was done to investigate cellular and extracellular components of 3D cellular structures. The dose-response of fabricated 3D structures was evaluated and compared with standard 2D cell culture by applying doxorubicin (DOX). The IC_{50} values were calculated for 3D cellular structure of HeLa, SaOS-2 and SH-SY5Y cells as 8.2, 7.8, and 2.1 μM respectively while IC_{50} values of 2D controls obtained as 3.2, 4.4, and 0.2 μM respectively. These results were also statistically analyzed and dose responses were found significantly different according to t-test, which means 3D cellular structures were more resistant to drug exposure compared to 2D cell culture.

ÖZET

3B HÜCRE KÜLTÜRÜ OLUŞUMU İÇİN MAGNEZYUM ALJİNAT HİDROJELLERİN GELİŞTİRİLMESİ VE KARAKTERİZASYONU

Üç boyutlu (3B) hücre kültürü, hücrelerin 3B fiziksel şekillerinde büyümesine ve doğal mikro ortamı temsil eden çevreleriyle etkileşime girmesine olanak tanır. Hidrojeller çapraz bağlı ağlardır ve çoğu yumuşak dokunun doğasını taklit etme yetenekleriyle 3B hücre kültürü için kullanılmaktadır. Bu tezde, Mg-aljinat hidrojel kullanılarak 3 boyutlu (3B) tümör modelleri üretmek için biyo-kalıplandırmaya dayalı yeni bir metodoloji geliştirilmiş ve ilaç tarama çalışmaları için üretilen 3B tümör modelleri kullanılmıştır. Mg-aljinat hidrojel, zayıf polimer-iyon etkileşimi nedeniyle diğer hidrojel türlerine kıyasla spesifik bir jelleşme/ayrılma özelliklerine sahiptir. Bu çalışmada, Mg-aljinat hidrojelin yavaş jelleşme ve kendi kendine ayrılma özelliği kullanılmıştır. Plackett-Burman ve Box-Behnken tasarım modelleri, model hücre hattı olarak HeLa hücreleri kullanılırken Mg-aljinat bazlı biyo-modelleme yönteminin parametrelerini optimize etmek için kullanıldı. Yeni geliştirilen metodolojinin uygulanabilirliği, 3B tümör modelleri üretmek için SaOS-2 ve SH-SY5Y hücreleri kullanılarak başarıyla gösterildi. Ardından, uzun süreli kültürlenmiş tümör modellerinin hücre proliferasyonu ve canlılığı analiz edildi ve 3B tümör modellerinin hücresel ve hücre dışı bileşenlerini araştırmak için immün boyama yapıldı. Son olarak, üretilen 3B tümör modellerinin doz yanıtı değerlendirildi ve doksorubisin (DOX) uygulanarak standart 2B hücre kültürü ile karşılaştırıldı. HeLa, SaOS-2 ve SH-SY5Y hücrelerinin 3B tümör modeli için IC_{50} değerleri sırasıyla 8.2, 7.8 ve 2.1 μM olarak hesaplanırken, 2B kontrollerin IC_{50} değerleri sırasıyla 3.2, 4.4 ve 0.2 μM olarak elde edildi. Bu sonuçlar da istatistiksel olarak analiz edildi ve doz tepkileri t-testine göre önemli ölçüde farklı bulundu, bu da 3B tümör modellerinin 2B hücre kültürüne kıyasla ilaca maruz kalmaya karşı daha dirençli olduğu anlamına gelmektedir.

TABLE OF CONTENTS

LIST OF FIGURES

Figures **Page**

LIST OF TABLES

Tables **Page**

CHAPTER 1

INTRODUCTION

1.1. Scope of thesis

This study aims to develop a new method based on bio-patterning approach to fabricate patterned 3-dimensional (3D) cellular structures by using Mg-alginate-based bio-ink. In the biopatterning method, the bio-ink comprised of Mg-alginate, magnetic nanoparticles, and cells in the optimized formulation. Prepared bio-ink was patterned onto the well surface as a shape of a disc magnet while applying an external magnetic force. Mg-alginate was the main component of bio-ink and it was used as a carrier of cells and magnetic nanoparticles due to its specific gelation/de-gelation property. Alginate hydrogels are commonly prepared in the presence of multivalent ions like Ba, Sr, Ca and Co ions through ionotropic gelation. Different from other commonly used multivalent ions, magnesium ion has weak polymer-ion interaction and it was recently shown that gelation occurs via highly concentrated magnesium ions and alginate (Topuz et al. 2012). Moreover, Mg-alginate hydrogel has another significant property which is easy self-dissociation of hydrogel in water. That provides an important advantage while obtaining patterned 3D cellular structures without applying any extra dissociation step in the newly developed bio-patterning method. Optimization of the bio-patterning was method performed with HeLa cells by using Plackett-Burman and Box Behnken experimental design models to fabricate 3D cellular structure. Also, 3D cellular structure by using SaOS-2 and SH-SY5Y cells were fabricated to investigate applicability of bio-patterning method. Finally, drug responses of patterned 3D cellular structures were investigated by applying doxorubicin (Dox). According to IC_{50} values, dose response of 3D cellular structures were showed significant differences compared to conventional 2-dimensional (2D) cell culture.

1.2. Cell culture models in tissue engineering

Tissue engineering is an interdisciplinary field that uses engineering and life sciences in combination to develop biological tissues (Langer and Vacanti 1993). Cells, scaffolds and growth factor are main tools that used by tissue engineering (Ikada 2006). Cell source has a crucial influence on the success of tissue engineering and also scaffold should be convenient to both cell type and tissues so that they could regenerate. Cell culture has become an essential tool to help understand biophysical and biomolecular mechanisms of tissues and organs (Kirkpatrick et al. 2007). Cell cultures make it easier to recognize tissue morphology, cell biology, mechanisms of disease and drug effect. Also, they are widely used in biomedical research (Blomme 2016), preclinical research of many drugs and tissue engineering studies (Duval et al. 2017; Kapałczyńska et al. 2018). The choice of the appropriate cell culture method depends on the type of research performed and allows for a better understanding of cell biology and therefore conduct a more effective study (Lovitt, Shelper, and Avery 2014). For over a century, 2D cell cultures have been used as in vitro models. Although the 2D cell culture approach is very informative about cell behavior, its effectiveness was questioned after it was understood that the environment was far different from *in vivo* state (Kapałczyńska et al. 2018). For example, some characteristic features of cancer cells cannot be modeled in 2D cultures (Choi et al. 2010). To overcome these limitations and better mimic in vivo situations, three-dimensional (3D) cell culture platforms were being developed by researchers (Jong 2005; Lovitt, Shelper, and Avery 2014; Alhaque, Themis, and Rashidi 2018) 3D studies have shown that increased dimensionality of extracellular matrix around cells has a significant impact on cell viability, proliferation, differentiation, and cellular responses (Anton et al. 2015). Moreover, traditional 2D cell culture systems needed a flat surface where the cells adhere and spread. The surface which is commonly made of polystyrene is important to provide mechanical support for cells (Duval et al. 2017; Edmondson et al. 2014). 2D monolayer settings allow cells to receive an even amount of nutrients and growth factors from the medium and this lead to homogenous growth and proliferation (Edmondson et al. 2014). 2D cell culture methods have been used in varied areas; cancer research (Katt et al. 2016), stem cell research (Saji Joseph, Tebogo Malindisa, and Ntwasa 2019), and drug discovery (Stock et

al. 2016). However, 2D cultured cells are usually flattered and more stretched and do not mimic the normal cell morphology and natural structures of tissues (Duval et al. 2017). Also, lack of cell-cell and cell-extracellular environment interactions affect many cellular functions such as cell differentiation, proliferation, gene and protein expression, drug metabolism (Kapałczyńska et al. 2018; Edmondson et al. 2014). Since the 2D cell culture system has many limitations, 2D-cultured cells do not sufficiently mimic the *in vivo* microenvironment (Saji Joseph, Tebogo Malindisa, and Ntwasa 2019). As a result, 2D cell culture systems can cause misleading and unexpected information for *in vivo* responses due to their inability to form natural tissue-like structures (Kapałczyńska et al. 2018). Furthermore, 3D environment is important in tissue engineering for development of physiological *in vitro* models (Heberer et al. 2021). Cells grow naturally in a 3D environment and interact with each other, the ECM and their microenvironment which are essential for cell proliferation, differentiation, morphology and cellular responses (Saji Joseph, Tebogo Malindisa, and Ntwasa 2019). 3D cell culture systems have been developed to mimic the actual microenvironment where the cells reside in tissues. The 3D culture models are closer to the *in vivo* conditions and increase the physiological relevancy of experiments performed *in vitro* (Ravi et al. 2015). Also, the additional dimensionality allows greater cell-to-cell contact which increases intercellular signaling, catalyzes developmental processes, and enhances cell differentiation into more complex structures (Knight and Przyborski 2015; Edmondson et al. 2014). 3D culture systems are being utilized in varied research areas such as drug discovery and development (Verjans et al. 2018), cancer cell biology (Brancato et al. 2020) stem cell biology (Willerth et al. 2006), tissue engineering (Matai et al. 2019) and other cell-based analysis and providing excellent *in vitro* models as opposed to 2D monolayer cell culture.

1.3. Conventional drug discovery and development process

Drug discovery and development process is a long and costly business. Development and availability of a new drug takes about 15 years and it require an expense of between $ 800 million and $ 2 billion (Saji Joseph, Tebogo Malindisa, and Ntwasa

2019). Discovery and development process of a new candidate drug molecule consists of four phases: drug discovery, preclinical development, clinical development, and regulatory approval as seen in Figure 1 (Breslin and O'Driscoll 2013). Nevertheless, phase II and phase III clinical stages are critical, because most drugs fail at these steps due to inadequate efficacy and safety issues including an insufficient therapeutic index (Saji Joseph, Tebogo Malindisa, and Ntwasa 2019; Langhans 2018). The main reasons for long drug development and high failure rate are strongly related to inappropriate preclinical testing methods (Stock et al. 2016) because *in vitro* cell culture and *in vivo* animal models lack a true recapitulation *in vivo* biology and micro-environmental factors (Saji Joseph, Tebogo Malindisa, and Ntwasa 2019; Langhans 2018). Preclinical testing is required to determine which of the candidate molecules are target-specific and have high efficiency (Imamura et al. 2015). Preclinical testing includes *in vitro* analyses of appropriate cell lines and *in vivo* experiments in related animal models, but due to lack of clinical efficacy or unexpected toxicity, data generated from their use generally can not reflect to what occurs *in vivo* (Breslin and O'Driscoll 2013). Cell-based assays are an essential element of drug discovery process; therefore, the cell line used must successfully mimic the phenotype of cells within the target tissue (Saji Joseph, Tebogo Malindisa, and Ntwasa 2019; Breslin and O'Driscoll 2013). Cell culture systems are simple, fast, and cost-effective when compared to cost-intensive animal models. Up to now, 2D cell cultures constitute the majority of cell cultures used in drug discovery (Langhans 2018). It provided information on essential biological processes; however, the limitations of 2D culture showed that it does not mimic the complex microenvironment of tissue. The most important limitations are the lack of cell-cell and cell-extracellular matrix (ECM) signaling which are essential to cellular functions, cell differentiation, and proliferation (Breslin and O'Driscoll 2013). Another preclinical analysis tool is animal models that are applied as *in vivo* studies to test drug efficacy. However, it also has some drawbacks which are ethical issues, requirement of a higher budget for experiments, and the need for a long-time period to get results. Moreover, it is not warranted to result with the same response as the human body response because chemical compounds are generally metabolized specifically in every species (Park et al. 2017; Bracken 2008). On the other hand, 3D cell culture mimics the natural environment of cells as *in vivo*. In the other words, the cell-cell and cell-ECM signaling

occur in *vitro* 3D cell culture environment. (Bissell and Radisky 2001). Also, recent studies show that 3D cell culture is more similar and predictive to *in vivo* environment than 2D cell culture has shown that it is more suitable for use in drug research and development (Lovitt, Shelper, and Avery 2014; Blomme 2016; Brancato et al. 2020). Moreover, Hou *et al*. described an high-throughput screening (HTS)-compatible method that enables the consistent production of organoids to perform cytotoxicity screen of 3300 approved drugs and compare in both 2D and 3D assays, also they showed a technique that supported large-scale drug screening relying on 3D tumor models (Hou et al. 2018). Wen *et al*. presented a study which is spheroid-based, 3D culture of pancreatic cancer cells for pancreatic drug testing by using acid phosphatase assay and drug efficacy testing showed that spheroids had much higher drug resistance compared to monolayers (Wen et al. 2013).

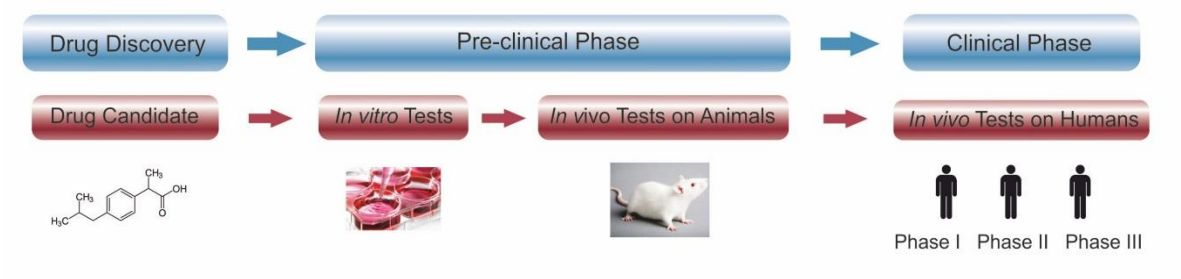

Figure 1.1. Drug discovery and development phases (Source: Onbas, Bilginer, and Arslan Yildiz 2021)

1.4. Three-dimensional cell culture models

3D cultured cells have features that are closer to the complex in vivo conditions (Ravi et al. 2015). Cells grow in 3D physical shape and this allows better cell-to-cell contact and intercellular signaling (Saji Joseph, Tebogo Malindisa, and Ntwasa 2019). Three-dimensional cell culture models are broadly categorized into non-scaffold and scaffold-based techniques, as well as hybrid 3D culture models as seen in Figure 1.2

(Jensen and Teng 2020). Scaffold-free 3D cell culture techniques are used to generate spheroids, and cell aggregates that do not rely on solid supports. Hanging drop, low attachment plate, magnetic levitation are commonly used methods. In scaffold-based cultures, scaffolds are used as convenient supports for 3D cell culture, biological and synthetic hydrogels are used as scaffolds for 3D cell culture. An ideal 3D culture model should be chosen for specific application and the model should mimic a tissue-specific physiological microenvironment which is important for proliferation, aggregation, and differentiation of cells (Anton et al. 2015). Also, cell-cell and cell-ECM interactions, tissue-specific stiffness, oxygen, nutrient and metabolic waste gradients, scaffold, and cells combination should be provided by the model (Griffith and Swartz 2006). At this point, selecting the appropriate 3D cell culture model has great importance for the study .

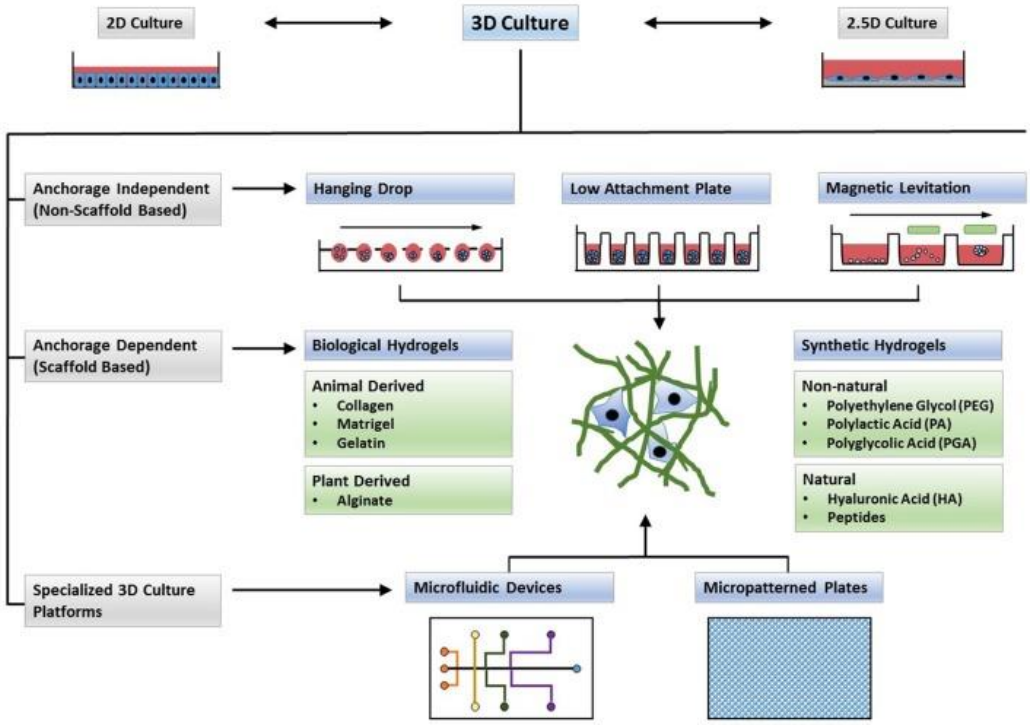

Figure 1.2. Types of 3D culture methods (Source: Langhans 2018)

1.4.1. Non-scaffold based 3D cell culture models

Scaffold-free 3D cell culture systems primarily rely on the self-aggregation of cells and development of multi-cellular aggregates commonly referred as spheroids. Spheroids can be developed from a wide variety of cell types and cells form their extracellular matrix components which are important for cell-cell contact and cell-matrix interactions (Sutherland 1988). The size of the spheroid depends on the primary number of cells seeded and it can grow until oxygen and nutrient gradients resemble the target tissue (Ekert et al. 2014). Spheroids have many characteristic properties such as (i) naturally mimicking solid tissues and ideal physiological cell-to-cell interactions (ii) formation of ECM components and cell-ECM interactions (iii) convenient gradient for diffusion growth factors and removal of metabolic waste (Breslin and O'Driscoll 2013; Saji Joseph, Tebogo Malindisa, and Ntwasa 2019). Also, spheroid analysis can be performed by imaging using light fluorescence, and confocal microscopy and that is another advantage of spheroids (Wen et al. 2013). There are different procedures to develop spheroid cultures such as hanging drop microplates, low adhesion plates with ultra-low attachment coating that encourages spheroid formation, magnetic levitation and magnetic bioprinting.

1.4.1.1. Hanging drop

Hanging drop technique is a well-recognized 3D culture method based on the self-aggregation of cells into spheroids (Saji Joseph, Tebogo Malindisa, and Ntwasa 2019; Langhans 2018). In hanging drops, cells are cultured in a small volume of media in a drop and suspended on the lid of a cell culture dish (Shri et al. 2017). After seeding the cells, the lid is carefully inverted and placed on top of the dish containing media to keep a humid environment. Surface tension provides the cells concentrate at the tip of the drop and remain in place. After several hours or days of culture, cells in hanging drop come together and form spheroids (Rimann and Graf-Hausner 2012). The hanging drop method is cost-effective and allows formation of multi-cellular spheres by co-suspending various cell

types. Also, spheroid size can be determined by the initial number of cells that are suspended in the drops (Langhans 2018). Moreover, it has been reported that the hanging drop method has 100% reproducibility for producing one spheroid per drop for various cell lines (Thoma et al. 2014). However, in hanging drop, only a limited volume of droplets can be generated because the surface tension no longer holds the droplet, also it is difficult to maintain spheroids, change the medium and is a laborious technique (Matak et al. 2017). After all, hanging drop cultures have multiple applications such as toxicity testing in hepatocytes (Shri et al. 2017), engineering cardiac spheroids (Polonchuk et al. 2017). In addition, Matak *et al*. used the hanging drop and colony formation methods with human primary renal cell carcinoma (RCC) cell lines, metastatic RCC cell lines, human kidney cancer stem cells and human healty epithelial cells. In the hanging drop assay, they showed the potential of various cancer cell lines to create solid aggregates in hypoxic and normoxic conditions (Matak et al. 2017).

1.4.1.2. Low attachment plate

Low adhesion plates support the self-aggregation of cells to form spheroids with the liquid overlay technique which is a highly reproducible culture procedure and encourages 3D spheroids (Carlsson and Yuhas 1984). Moreover, low adhesion plates are available with round, tapered or v-shaped bottoms and through low attachment, surfaces promote aggregation of cells and spheroid formation (Langhans 2018; Saji Joseph, Tebogo Malindisa, and Ntwasa 2019). Plates are fabricated from polystyrene treated with hydrophilic and hydrophobic coatings which decrease cells from attaching to the surface and cells aggregate with each other to form spheroids. Low adhesion plates produce one spheroid per well and this makes it well suited for medium throughput screening as well as multicellular culture (Saji Joseph, Tebogo Malindisa, and Ntwasa 2019). Also, it is an important advantage that these plates have a higher initial volume than hanging drops so that there is no need to manipulate the spheroids. Recently, a study reported a comparative analysis of 3D spheroids which were fabricated by ultra-low attachment plates and hanging

drop, also the RT4 human-bladder cancer cell line was used as a model to compare dose response of doxorubicin with both method (Amaral et al. 2017).

1.4.1.3. Magnetic levitation

Magnetic levitation is a rising method for the generation of spheroids (Souza et al. 2015). There are two approaches to fabricate spheroids: using magnetic nanoparticles and paramagnetic agents. In the prior approach, cells are incubated in a medium which is composed of bacteriophage plus magnetic iron oxide and gold nanoparticles that self-assemble into hydrogel to generate spheroids (Souza et al. 2010). Also, the nanoparticles are nontoxic, do not affect proliferation, and do not induce an inflammatory cytokine response by cells (Tseng et al. 2013). The magnetized cells are suspended in the culture medium while simultaneously manipulated by the external magnetic field. When a magnetic field is applied above the petri dish or multiwell plate, cells are levitated to the air-liquid interface where they interact and aggregate together into larger 3D cellular structures by inducing the formation of ECM and cell-cell interactions (Haisler et al. 2013; Souza et al. 2015). Also, these 3D cellular structures synthesize their ECM proteins like collagen, fibronectin, and laminin (Tseng et al. 2013). The magnetic levitation method is performed using varied cell types such as human glioblastoma (Tseng et al. 2013), adipose stem cells (Daquinag, Souza, and Kolonin 2013), breast cancer cells (Jaganathan et al. 2014). For instance, magnetically levitated human glioblastoma cells demonstrated greater proliferation and recapitulated *in vivo* protein expression observed in human glioblastoma tumor xenografts (Souza et al. 2015). Also, the method has been used to develop co-culture models of the bronchiole by assembling multiple 3D cultures in a layer (Tseng et al. 2013). In addition, magnetic levitation has been studied with stem cells to differentiate them in 3D; 3T3-L1 adipose stem cells were differentiated into adipocytes and formed an adiposphere in co-culture with endothelial cells (Daquinag, Souza, and Kolonin 2013). On the other hand, the latter approach is to levitate cells with paramagnetic agents instead of magnetic nanoparticles to fabricate 3D spheroid models. Türker *et al*. reported the formation of 3D cellular structures via magnetic levitation based on anti-helmholtz

configuration. Cells were levitated in the presence of Gadolinium (III) chelates which lead to assembly of cells at certain levitation height that induce intercellular interactions by using a setup that had a low working volume (30µl) (Türker, Demirçak, and Yildiz 2018). This setup had some limitations such as limited working volume, it is not possible to change medium and optical components are neded to observe spheroids. For that reason, a new high volume maglev setup (800µl) was fabricated by Onbas *et al*. to obtain 3D cellular structures based on magnetic levitation in the presence of Gadobutrol as a paramagnetic agents. By using this setup they demonstrated the fabrication of 3D cellular structures of NIH/3T3 cells with tunable size. Moreover, tumor models by using varied cancer cells and 3D co-culture models were formed in high-volume and low magnetic fields (Onbas and Yildiz 2021). As a result, the magnetic levitation method is a simple and requires low-cost set-up components that can perform basic and complex *in vitro* tisuue models in 3D environment.

1.4.2. Scaffold-based 3D cell culture models

Scaffold-based culture technologies provide physical support to basic mechanical structures and to ECM-like matrices on which cells can aggregate, proliferate, and migrate (Hayward et al. 2013). In scaffold-based 3D techniques, the chemical and physical properties of the scaffold material which affects cell characteristics are important (Kapałczyńska et al. 2018). Cells are embedded into the matrix and the matrix provides native cell function within the ECM. Scaffolds can be fabricated by using biological materials such as collagen, matrigel, gelatin, alginate, or synthetic origin-based materials such as polyethylene glycol, polylactic acid, hyaluronic acid (Langhans 2018). Natural biomaterials used for scaffold composition are various components of the ECM such as collagen, fibrin, and hyaluronic acid (Willerth et al. 2006; Gerecht et al. 2007). Also, naturally derived materials such as silk, gelatin and alginate can be used in scaffold synthesis (Awad et al. 2004). These materials have many advantages for tissue engineering applications. They are biocompatible, contain cell adhesion sites to support cell adhesion and cell-biomaterial interaction. On the other hand, synthetic materials are engineered to

mimic key characteristics of ECM such as stiffness, charge or adhesive moieties (Langhans 2018). Synthetic materials used in scaffolds contain biomaterials such as polymers, titanium, ceramic-based materials such as bioactive glasses and peptides (Gunatillake, Adhikari, and Gadegaard 2003; Van Den Dolder, Spauwen, and Jansen 2003; Lu et al. 2003). Synthetic materials also have many advantages. They have defined chemical formulation and adjustable mechanical properties. For instance, hormones, growth factors or biologically active molecules can be encapsulated in some synthetic scaffolds to affect cell differentiation, cell adhesion or proliferation (Hayward et al. 2013). So, the properties of the material are critical for the fabrication of scaffolds. Porosity, biodegradability, pore size, stiffness, and stability as well as cell compatibility or adhesiveness are features that should be considered (Caliari and Burdick 2016). However, some synthetic materials may lack cell adhesion sites and require coating with ECM proteins to mimic the environment in which cells normally live.

1.4.2.1. Biological hydrogels

Hydrogels are highly hydrated hydrophilic polymer networks formed from dilute polymer chains that make cross-link junctions or hydrogen bonding (Lian et al. 2017). Hydrogels are unique because they mimic ECM and allow travelling of soluble factors such as growth factors and cytokines through the tissue-like gel (Jensen and Teng 2020). So, they are one of the most used scaffolds materials. The hydrophilic structure of hydrogels facilitates the absorption and holding of a large amount of water (Hamidi, Azadi, and Rafiei 2008). Therefore, they are a powerful option for 3D culture in tissue engineering. Hydrogels are also versatile, and more suitable substitutes for natural tissues since they have features such as high water content, low surface tension, soft and rubbery consistency (Hamidi, Azadi, and Rafiei 2008). A variety of synthetic, natural, and mixture of both (hybrid) materials can be used to form hydrogels with a wide range of chemical and mechanical properties. Hybrid hydrogels are developed to obtain new physical and biological properties (Zhu 2011). Natural hydrogels are commonly derived from natural polymers such as collagen (Borlak, Singh, and Rittelmeyer 2015), matrigel (Catoira et al.

2019), gelatin, fibrinogen, hyaluronic acid (Gerecht et al. 2007), chitosan (Jong 2005), and alginate (Tibbitt and Anseth 2009). Natural hydrogels have natural adhesive properties, high cell viability, controlled proliferation, and differentiation (Drury and Mooney 2003). Collagen is a commonly used natural material for hydrogel preparation (Lian et al. 2017).

1.4.2.1.1. Collagen

Collagen is one of the most commonly used materials in 3D cell culture (Achilli, Lagueux, and Mantovani 2010; Lian et al. 2017; Desai et al. 2006; Borlak, Singh, and Rittelmeyer 2015; Lu et al. 2003). Collagen is the main ECM protein and primary organic component of native tissue. There are 29 identified types of collagen in the human body (Caliari and Burdick 2016). Type I collagen is the most abundant form and major structural component of many tissues. Therefore, it is an attractive material for biological studies. Collagen hydrogels generally consist of type I collagen, although there are types II and III, and other components such as glycosaminoglycans. Moreover, the basic structure of collagen consists of three polypeptide chains that wrap around each other to form a three-stranded rope structure (Drury and Mooney 2003). There are hydrogen and covalent bonds between strands. In natural tissues, the mechanical properties of collagen are ideal. However, collagen-based biomaterials lack covalent crosslinking, and because of this, mechanical strength is insufficient (Catoira et al. 2019). Therefore, their mechanical properties are improved by physical, chemical, and biological crosslinking methods (Achilli, Lagueux, and Mantovani 2010). Generally, NaCl is added into collagen solution to prepare a hydrogel with better optical performance and mechanical properties (Catoira et al. 2019). Also, increasing the temperature and pH can improve linear viscoelastic properties and transparency (Lian et al. 2017). Collagen has many advantages as a biomaterial. It presents low antigenicity, low inflammatory response, biocompatibility, and biodegradability. Collagen can be degraded by collagenase and proteases naturally (Drury and Mooney 2003). Its degradation can be locally controlled by cells present in engineered tissue. It is amenable to cell adhesion through integrin receptors without any modification and presents a natural viscoelastic environment to cells (Caliari and Burdick 2016). Integrin

receptors induce activation of cell signaling pathways that are important for cell survival, growth, and differentiation. Also, it can regulate the reaction to therapeutic approaches such as chemotherapy, immunotherapy (Langhans 2018). For example, breast, prostate, and lung cancer cell lines were grown in collagen and compared to 2D culture for drug response profiles and they showed completely different results in dose-response curves to docetaxel and fulvestrant (Stock et al. 2016). Nevertheless, collagen has some important drawbacks that contain limited long-term stability, low stiffness, and batch-to-batch variability. Collagen hydrogel mechanics can be dictated by altering collagen concentrations or gelation temperature that help to change hydrogel stiffness (Caliari and Burdick 2016).

1.4.2.1.2. Matrigel

Matrigel is a collagen-containing hydrogel that is also used in cell studies (Dolega et al. 2015; Fan et al. 2016; Jang et al. 2015). Matrigel is composed primarily of laminin, type IV collagen and entactin which is a basement membrane glycoprotein as well as several growth factors and proteoglycans (Caliari and Burdick 2016). Moreover, Matrigel matrix preparation extracted from the Engelbreth-Holm-Swarm (EHS) mouse sarcoma since tumor rich for ECM proteins as laminin, collagen IV, proteoglycans, entactin, and several growth factors (Caliari and Burdick 2016). Matrigel has many of the advantages of natural hydrogels like collagen. It has been used to analyze cell migration, tumor development and in drug screening studies (Caliari and Burdick 2016). For example, to make preclinical testing of chemotherapeutics, multiple myeloma cells are grown in a Matrigel-based human bone marrow-like microenvironment and it provided a screening system (Kirshner et al. 2008). Matrigel is obtained from natural sources and some drawbacks are arising from this. It is a complex scaffold that includes various components besides their main constituents and is chemically not well defined. Also, it has a tumorigenic origin and batch-to-batch variability in respect of mechanical properties (Caliari and Burdick 2016). Collagen and matrigel provide increased interaction of cells with ECM proteins, but cells cultured with collagen or Matrigel can show different phenotypes due to their different composition (Borlak, Singh, and Rittelmeyer 2015).

1.4.2.1.3. Gelatin

Gelatin is a natural, water-soluble peptide and its properties, such as biocompatibility, biodegradability makes it a multifunctional biopolymer (Foox and Zilberman 2015). It is commonly utilized in cosmetic (Cheng et al. 2009), pharmaceutical (Foox and Zilberman 2015), food (Karim and Bhat 2008), and medical applications (Jaipan, Science, and Carolina 2017). Also, it has been used as a coating agent in tissue regeneration to enhance cell attachment due to its unique mechanical properties (Santander et al. 2007; Othman et al. 2020; Awad et al. 2004). This polymer is obtained from acid, alkaline, or enzymatic hydrolysis of collagen. It is the main protein component of the bone and connective tissues of animals also fish and insects. There is two types of gelatin obtained through denaturing the triple-helical conformation of collagen: gelatin A processed by acids such as hydrochloric acid or sulfuric acid and gelatin B processed with alkaline solutions (Catoira et al. 2019; Foox and Zilberman 2015). Moreover, gelatin, needs to increase its mechanical properties and modulate its solubility and degradation rate in an aqueous solution (Foox and Zilberman 2015). Therefore, gelatin requires a physical, chemical, or biological crosslinking process. Environmental triggers such as pH, temperature, or ionic strength can be used for physical crosslinking. Additionally, formaldehyde, glutaraldehyde, glyceraldehyde are the chemical agents that can be used in the chemical crosslinking process (Foox and Zilberman 2015).

1.4.2.1.4. Alginate

Alginate is a linear polysaccharide obtained from brown algae that has been used in a variety of medical applications including pharmaceuticals, drug stabilization and delivery, cell encapsulation (Augst, Kong, and Mooney 2006). The polymer chain consists of β-D-mannuronic acid M units and α-L-guluronic acid G units that able to compose each other in long sequences of M-Blocks, G-Blocks, and alternating MG-Blocks as seen in Figure 1.3. The amount and distribution of these blocks depends on the origin of alginate. Alginate has

many advantages due to its ability to form physical hydrogels via ionic crosslinking. This process occurs when divalent cations are combined with alginate solution. Divalent cations are calcium, magnesium, strontium, or barium that interact with G units to promote the formation of ionic bridges between G blocks (Vicini et al. 2017). Therefore, the gelling capacity and crosslinking density are entirely related to the number of G blocks present along the chain (Drury and Mooney 2003). The G-units of the polymer create binding sites for the bivalent cations and G blocks are cross-linked with cations through interaction with the carboxylic groups in the sugars, which provide the formation of a gel network called "egg-box" as seen in Figure 1.3 (Vicini et al. 2017). Also, other mechanical properties and pore size of the ionically crosslinked hydrogel can be adjusted by altering the M to G ratio and molecular weight of the polymer chain. Ozawa *et al*. developed a method to fabricate microwell arrays from alginate gels and this alginate gel microwells are used for 3D cell culture (Ozawa et al. 2013). Also, alginate used as a cell scaffold after functionalized by the covalent attachment of a variety whole proteins to obtain sites for cell attachment (Frampton et al., n.d.). The fibronectin-derived adhesion peptide arginine glycine aspartic acid (RGD) is commonly used and coupled easily to alginate (Augst, Kong, and Mooney 2006). For instance, myoblast cells can adhere, proliferate, and fuse when adhered to RGD-modified alginate gels (Augst, Kong, and Mooney 2006). In this study, Mg-alginate hydrogel is used to fabricate 3D cellular structures by using characteristic gelation properties of Mg-alginate hydrogel with bio-patterning technique. Mg-alginate used as a carrier material for cells and nanoparticles also allowed cells to attach to surface while providing appropriate viscosity and porosity.

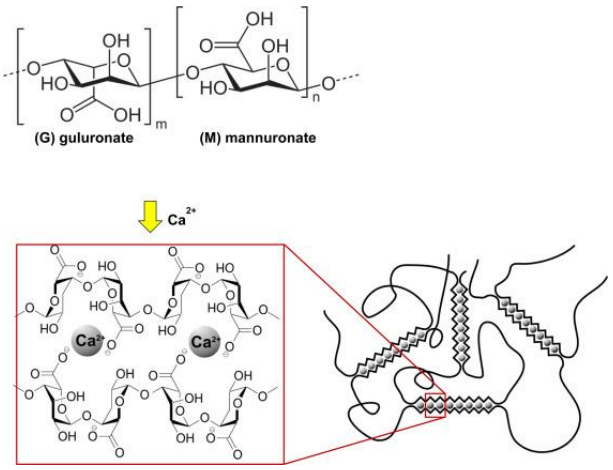

Figure 1.3. Structure of alginate and its binding of calcium cations in egg-box model (Source: GRANT et al. 1973)

1.4.2.2. Synthetic hydrogels

Synthetic hydrogels are ideal constituents to use as 3D cell culture scaffold since they can mimic the biological properties of ECM (Worthington, Pochan, and Langhans 2015). Synthetic hydrogels have many advantages through the well-defined structure (Zhang and Khademhosseini 2017). Moreover, they can be functionalized with adhesive moieties, proteolytic sites, and encapsulated growth factors (Zhu 2011). Also, their well-defined structure allows tunable mechanical properties to achieve an appropriate stiffness or porosity. The main unnatural polymers are polyethylene glycol (PEG), polylactic acid (PA), polyglycolic acid (PGA) that used to formulate hydrogels. Additionally, they are inexpensive, relatively inert and have high water absorption capacity and reproducible material features. However, unnatural polymers lack adhesive sites which are important in cell culture studies. Therefore, they require crosslinking of biological peptides that improve functionality of scaffold. Morever, poly(ethylene glycol)-fibrinojen were reported as a suitable biosynthetic hydrogel for 3D culture of three breast cancer cells: MCF-7, SK-BR-3 and MDA-MB-231 (Pradhan et al. 2017). Also, Ibuprofen releasing scaffold was designed

to reduce inflammation in wounds by using polylactide and polyglycolide polymers (Canton et al. 2010).

1.4.2.3. Bio-printing/bio-patterning

There are varied cell patterning and manipulation techniques to fabricate 3D cell culture models which are lithography (Liang et al. 2021), soft lithography techniques (Li et al. 2016), inkjet cell printing (Knowlton et al. 2017), acoustic force manipulation (Matai et al. 2019), magnetic cell bioprinting/patterning (Mishriki et al. 2019). Lithography-based 3D bioprinting does not utilize high temperatures or exert shear stress, so it gentle on cells and bioactive agents (Liang et al. 2021). Stereolithographic 3D printing also has some advantages which include avoidance of thermal degradation, higher accuracy and improved resolution (Robles-Martinez et al. 2019). Inkjet-based printing is a widely understood bioprinting method derived from conventional 2D desktop inkjet printers (Matai et al. 2019). Low-viscosity suspension of living cells, biomolecules, or growth factors can be used as biomaterials and it has the ability to introduce concentration gradients in 3D constructs (Li et al. 2016). Acoustic or sound waves can fabricate 3D patterns by moving cells in different directions and it is a nozzle-free technology that eludes clogging issues and protect cells from detrimental shear stress, heat, and pressure (Knowlton et al. 2017). Magnetic 3D bio-printing provides assembly of micro-tissues. It is possible to fabricate 3D models while contactless manipulation of cells into different shapes (Min et al. 2018). This technique has several advantages such as synthesis of ECM without needing any substrate, spatial control and the ability to print different cell lines rapidly (Matai et al. 2019). There are two procedures used in this setup. First, in the label-free diamagnet phoretic printing, cell-medium is mixed with paramagnetic buffer and then an external magnetic field is applied to form cell aggregates (Matai et al. 2019). When an external magnetic field is applied, cells behave as diamagnetic materials that migrates toward the region of the lower magnetic field (Abdel Fattah et al. 2016). Tseng *et al.* performed a study to investigate novel spheroid assay which is based on magnetic 3D bio-printing and using magnetized cells with a cylindrical magnet to attract cells to form a spheroid (Tseng et al. 2015a). Then,

the cells organize themselves to create a 3D environment that mimics many characteristics of native tissue especially cell-cell and cell-ECM interactions. Similar methods have been used to simulate different tissues like fat, lung, blood vessels and tumor microenvironments such as breast cancer and glioblastoma (Daquinag, Souza, and Kolonin 2013; Tseng et al. 2013, 2014; Jaganathan et al. 2014). In the second approach, cells were incubated with a biocompatible nanoparticle assembly including gold, iron oxide, and poly-L-lysine (Tseng et al. 2016). So, the cells become magnetized. Once magnetized the cells can be rapidly printed into 3D patterns using magnetic forces generated by a magnet. Patterning of cell aggregates into desired morphology can be controlled by the shape of magnet used. Mishriki *et al*. performed a contactless label-free method with MCF-7 cells that are suspended in a culture medium with a paramagnetic salt which diethylenetriaminepentaacetic acid gadolinium (III) dihydrogen salt hydrate (Gd-DTPA) was added (Mishriki et al. 2019). When magnetic field was applied, the main fluid which was containing paramagnetic salt is attracted towards the region of high magnetic field, displacing the MCF-7 ink towards region with low gradient. After that, 3D structures were printed on ultra-low attachment (ULA) surfaces (Mishriki et al. 2019).

CHAPTER 2

MATERIALS AND METHODS

2.1. Preparation and characterization of Mg-alginate hydrogel

Viscosity measurements were performed with Thermo Scientific HAAKE Viscotester 550. Since the viscosity measurement device requires at least 13 ml of sample, Mg-alginate hydrogels were prepared as 15 ml. The hydrogels were fabricated using low (Sigma, A1112) and high (Sigma, 71238) viscosity alginate, and $MgCl_2$ (Carlo Erba Reagents $MgCl_2.6H_2O$, FW: 203.31) was added as Mg^{2+} ion source. Both types of alginate concentrations were kept as 3 and 5% while $MgCl_2$ concentrations were used 400 mM for each alginate concentration. To obtain hydrogels, 7.5 mL of alginate solution and 7.5 mL $MgCl_2$ solution were mixed and homogenized in a falcon, then incubated for 22h at room temperature.

2.2. Theoretical calculations to compare Ca and Mg-alginate gelation process

To examine the interactions of Ca^{2+} and Mg^{2+} ions with alginate, first-principles density functional theory (DFT) calculations were carried out using Vienna *ab-initio* Simulation Package (VASP) with the implemented plane-wave projector-augmented wave (PAW) potentials (Physik, Wien, and Hauptstrasse 1993; Blochl 1994). Perdew-Burke-Ernzerhof form of generalized gradient approximation (GGA) was used for the exchange-correlation functional (Perdew, Burke, and Ernzerhof 1996). OptB86b-vdw functional was used in order to include the van der Waals interactions (Éamonn and David 2010; Bowler and Michaelides 2011). The plane-wave basis set cutoff energy was taken as 500 eV, and

the electronic and ionic convergency criteria are set as 10^{-5} and 10^{-4} eV. Large enough vacuum space was taken to avoid interactions between adjacent cells. Structural optimizations were carried until the pressures in each direction become less than 1kB. Charge transfer was calculated using the Bader technique (Henkelman, Arnaldsson, and´nsson 2006).

2.3. Cell culture

HeLa (human epithelial cervix adenocarcinoma, ATCC-CCL-2), SH-SY5Y (human bone marrow neuroblastoma, ATCC CRL-2266), SaOS-2 (human bone osteosarcoma ATCC HTB-85) cells were cultured in high glucose DMEM (GIBCO, Thermo Fischer Scientific) containing L-glutamine and supplemented with 1% penicillin/streptomycin (GIBCO, Thermo Fischer Scientific) and 10% fetal bovine serum (FBS) (GIBCO, Thermo Fischer Scientific). For 500 mL complete medium, 445 mL high glucose DMEM (Gibco, Thermo Fischer Scientific), 50 mL fetal bovine serum (FBS,10%) and 5 mL penicillin/streptomycin (1%) were mixed gently and stored +4ºC. It was heated in water bath at 37ºC. Frozen HeLa cell, SaOS-2 and SH-SY5Y stock taken from -80 °C and thawed in water bath at 37ºC. Dissolved cells were slowly added in 10mL, 10% complete medium and centrifuged for 5 min at 1000 rpm. Supernatant was removed, and precipitated cells were resuspended in 1 mL 10% medium. Then it was added in 75 cm^2 cell culture flask and completed with 10 mL 10% complete medium. Cells were incubated under 5% CO_2 at 37°C while cells reach 80-90% confluency, and then they were harvested and passaged to a new cell culture flask. Cells were expanded until reaching desired cell number for further experimental steps.

2.4. Fabrication of PMMA magnet holder for bio-patterning experiments

Polymethylmethacrylate (PMMA) magnet holder was prepared by using a laser cutter (Versa Laser VLS 2.30, Universal Laser) in the size of well plate. N35 Neodymium disc magnets with the dimensions 7×18 mm were obtained from Mıknatıs Teknik company (TR). Magnets were placed in PMMA holder as shown in Figure 2.1. Experiments were performed on 48 well plates (Tissue culture treated, Thermo Scientific) which was combined with PMMA magnet holder and magnets.

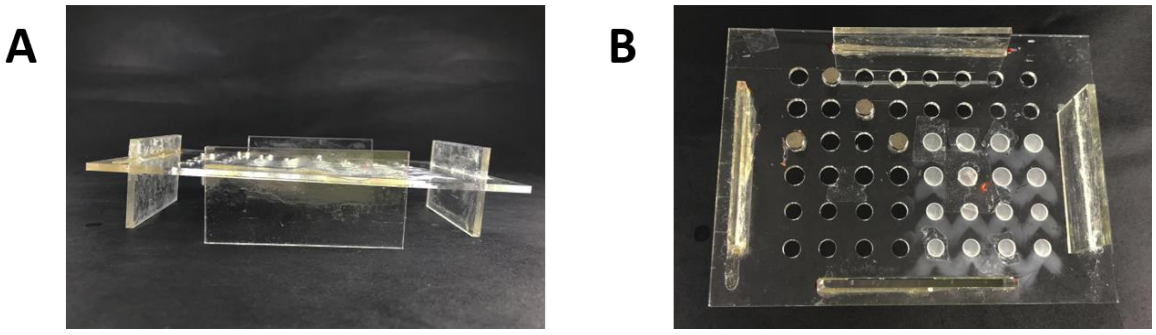

Figure 2.1. Image of PMMA holder for 7×18 mm N35 neodymium magnets A) side view of PMMA holder B) top view of PMMA holder

2.5. Optimization of Mg-alginate hydrogel bio-ink parameters to develop 3D cellular structure

The schematic of newly developed Mg-Alginate bio-patterning methodology was given in Figure 2.2. Initially, 48-well plate (Tissue culture treated, Thermo Scientific) was placed on the PMMA holder which has disc magnets and 350 µl of 10% complete medium was added to the wells. After that, a bio-ink was added to the wells with the optimized formulation comprised of Mg-alginate, magnetic nanoparticles, and cells, then cultured in a

5% CO_2, 37°C for 4 hours. Finally, patterned structure was obtained on the well surface as the shape of the disc magnet by applying an external magnetic field and after the washing step magnetically patterned 3D cellular structures were observed.

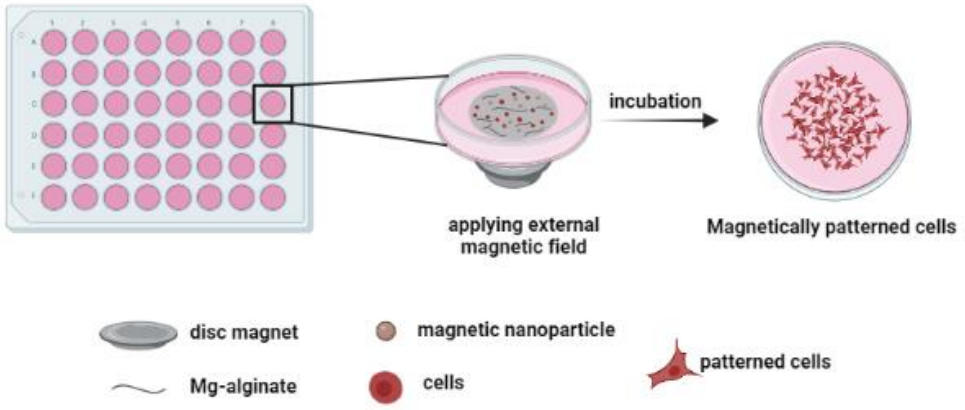

Figure 2.2. Schematic of newly developed Mg-alginate based bio-patterning method, created with BioRender.com

Experimental design is the most appropriate method to determine the effect of individual and interaction factors, simultaneously detecting the optimum setting of each factor at the same time. The set of experiments included in the design of parameters are known as an experimental matrix (Narenderan, Meyyanathan, and Karri 2019). The Plackett-Burman (P-B) design provides data on the single factor but not on the interaction. In addition, the Box-Behnken design (BBD) was three-level fractional factorial design and used to issues having three or more factors. It has three levels that can be coded as low, medium, and high, thus creating an independent quadratic design. This provides an easy way to organize and interpret results. To obtain an optimized formulation of Mg-Alginate hydrogel bio-ink for the patterned 3D cellular model with HeLa cell line, need to consider six parameters. These parameters were Mg-alginate concentration, $MgCl_2$ concentration, magnetic nanoparticle (MNP) concentration, cell number, Mg-alginate volume and MNP volume. To simplify optimization steps for bio-patterning method, the Plackett-Burman

design tool was used to eliminate some of these parameters and determine the most effective ones. Plackett-Burman design is a two-level fractional factorial design that enables the elimination of independent variables according to their significance (Narenderan, Meyyanathan, and Karri 2019). For this aim, low and high concentrations of each parameter were tested with 12 runs in total: alginate (low viscosity, A1112, Sigma) concentration (3 and 5 w/v%), $MgCl_2$ concentration (400 mM and 800 mM) MNP concentration (400 and 800 µg/ml), cell number (1×10^6 and $2\times10^{6)}$, Mg-alginate volume (4 µl and 8 µl) and MNP volume (2 µl and 4 µl). Bio-ink incubation kept as 4h during both 12 runs. To determine the most effective parameters, each run was scored in the response section by considering the attachment rate and density of the cells, the presence of patterned bio-ink and the absence of patterned cells after the wash step. After that, three most effective parameters were selected, and these parameters needed to be optimized with a suitable response surface method. For that reason, the Box-Behnken design model which provides an easy way to organize and interpret results was used to obtain optimized parameters of bio-patterning method (Gündoğdu et al. 2016). In this three-level factorial Box-Behnken experimental design model, 16 experimental runs were applied with 4 replicates on center points. Experimental runs were formed by MNP concentration (400, 600 and 800 µg/ml), cell number (1×10^6-1.5×10^6 -2×10^6), and Mg-alginate gel volume (4, 6 and 8 µl) while other parameters kept constant as alginate (5%), $MgCl_2$ (400 mM) and MNP volume (2µl). HeLa cells were used to fabricate patterned 3D cellular structure during optimization steps. After that, the applicability of the bio-patterning method was investigated by using SaOS-2 and SH-SY5Y cell lines with optimized parameters; 5% of alginate, 400 mM of $MgCl_2$, 600 µg/ml of MNP, 2×10^6 of cell number in 4 µl , 6 µl of Mg-alginate gel volume , 2 µl of MNP volume and 4 hour incubation of bio-ink. Design-Expert 7.0.0 (2005, Stat-Ease, Inc.) was used to generate experimental runs for both Plackett-Burman design and Box-Behnken design. Alginate and $MgCl_2$ solutions were prepared with the various concentrations and they were filtered (single filter unit, 0.2 µm, Minisart) for sterilization. Fe_3O_4 MNPs were synthesized (Patil et al. 2015) and sterilized with 30 min of UV light exposure, then the stock solution was prepared 1 mg/ml.

2.6. Cell viability analysis of bio-patterned 3D cellular structures

Cell viability analysis was performed with live/dead and Alamar blue assays. Live/dead assay solution contains two fluorescent dyes; propidium iodide (PI) labels dead cells as red and CytoCalcein™ Green labels viable cells as green. To conduct the live/dead assay on bio-patterned 3D cellular structure, PI and CytoCalcein™ Green were added at equal proportions in buffer solution. Complete medium of 3D cellular structure was replaced with 50 µL of fresh cell medium and 50 µL live/dead solution, then incubated for 30 min at 37°C. Then each well was examined by a fluorescence microscope (Zeiss Axio Observer). Alamar blue assay was used as a colorimetric method. It is a fluorometric analysis, which can be also used for absorbance analysis to examine proliferation profile of cells. Non-fluorescent blue resazurin metabolites by viable cells into resorufin and change the culture media to pink. As the number of viable cell number increased, proportionally resorufin production increases as well. Final concentration of alamar blue was 0.01% where 2 µL alamar blue and 198 µL complete medium was added over 3D cellular structure. Complete medium including alamar blue was used as a blank and incubated for 2-4 hours. After incubation, solutions were transferred into clean wells and measured at 570-600 nm by using Multiskan™ GO Microplate Spectrophotometer (Thermo Fischer Scientific). Proliferation percentage of viable cells were calculated based on absorbance values.

2.7. Characterization of bio-patterned 3D cellular structures

To characterize patterned 3D cellular structures; nucleus, cytoskeleton, and collagen immunostaining was performed for short (1 day) and long term (5 days) culturing time. Patterned 3D cellular structures were fixed with 4% paraformaldehyde prepared in 1X PBS for 15-20 minutes at room temperature and permeabilization was done by the addition of 1% Triton-X-100 prepared in 1X PBS and kept at room temperature for 1-5 minutes Then, blocking solution (1% BSA in 1X PBS) was applied and kept at room temperature for 30 minutes. Wash buffer (0.05% Tween 20 in PBS) was applied among these steps.

After these steps, TRITC-conjugated Phalloidin (Merck-Milipore) was performed for 60 minutes at room temperature to label F-actin of cell cytoskeleton. Then, wash buffer was applied three times for 5-10 minutes. After that, to label collagen I of extracellular matrix, anti-collagen Type I-FITC (Sigma-Aldrich) was added onto the samples and incubated for 60 minutes. After washing step, DAPI (AAT BIOQUEST) staining was carried out at room temperature for 1-5 minutes and rinsed three times for 5-10 minutes with wash buffer. Finally, patterned 3D cellular structures were visualized under a fluorescence microscope (Zeiss Axio Observer).

2.8. Drug screening study

Drug screening study was performed with doxorubicin (DOX) (HY-15142-100, Doxorubicin hydrochloride, MEDCHEM) which is an anticancer drug. Varied DOX concentrations which were 0.5, 1, 2.5, 5, 10, 20, 50, 100 μM for HeLa and SaOS-2 cell lines, 0.05, 0.1, 2.5, 5, 10, 20, 50 μM for SH-SY5Y cell line prepared from 10 mM of stock solution to investigate dose-response in 2D and 3D cell culture. For 2D cell culture, HeLa and SaOS-2 cells were seeded as 5000 cells per well and SH-SY5Y were seeded 30.000 cells per well in 96-well plate, and incubated overnight with varied DOX concentrations at 37 °C and 5% CO_2. In 3D cell culture, drug response of patterned 3D cellular structures was formed in 48-well plate and incubated with varied DOX concentrations overnight at 37 °C and 5% CO_2. Subsequently, MTT assay (Sigma Aldrich) was performed to test cell viability both 2D and 3D cultured cells. MTT reagent was prepared in PBS at 5 mg/mL of concentration then, added to wells (final concentration is 0.5 mg ml^{-1}). Samples were incubated 4 hours during incubation MTT reagent was reduced into purple formazan crystals by viable cells. After the incubation, MTT reagent was removed, and non-water-soluble formazan crystals were dissolved with DMSO. Absorbances were measured at 565 and 650 nm by Multiskan™ GO Microplate Spectrophotometer (Thermo Fischer Scientific). Later on, IC_{50} values of 2D cultures and 3D cellular structures were calculated with the GraphPad Prism software.

2.9. Statistical analysis

All values are expressed as the standard error of mean (±SEM). Statistical analysis for MTT assay was performed with unpaired two-tailed t-test by the GraphPad Prism software with a confidence interval of 95%. Significance was defined as $p<0.05$.

CHAPTER 3

RESULTS AND DISCUSSION

3.1. Preparation of Mg-alginate hydrogel

Alginate has a wide range of applications such as; technical utilization (Kurt Ingar Draget, Smidsrùd, and Skjåk-brñk 2005), foods, biomedicine (Nunamaker, Otto, and Kipke 2011), tissue engineering (Jiaa et al. 2014) through its ability to form a physical hydrogel (Kurt Ingar Draget, Smidsrùd, and Skjåk-brñk 2005; Augst, Kong, and Mooney 2006). The polymer chain for alginate hydrogel is composed of (1,4)-linked β-D-mannuronic acid (M), and its C-5 epimere, α-L- guluronic acid (G), able to connect in long sequences of M-Blocks, G-Blocks, and MG-Blocks in different sequential arrangements and proportions (Vicini et al. 2017). The gelation properties of alginate depend on its specific ion-binding characteristics (Kurt Ingar Draget, Smidsrùd, and Skjåk-brñk 2005). Alginate gels can be prepared by two methods: lowering the pH below the pK_a value of the uronic acid residues leading to alginic acid gels or in the presence of multivalent ions like Ba^{2+}, Sr^{2+}, Ca^{2+}, and Co^{2+} ions through ionotropic gelation (Topuz et al. 2012; Mørch et al. 2006). α-L-guluronic acid (G) part is the most important part that contributes to the gelling capacity of alginate because G blocks form cavities that act as a binding site for the multivalent cations and form ionic bridges between chains (Topuz et al. 2012). Mostly, the alginate hydrogels have been prepared with various divalent ions except for Mg^{2+} due to lack of strong polymer-ion interactions. Recently, Donati and co-workers showed that alginate favorably interacts with Mg^{2+} ions along the sequence guluronan > polyalternating > mannuronan and identified Mg^{2+} ions weakly bound by diffusion effect instead of strong binding like Ca^{2+} (Donati, Asaron, and Paoletti 2009). After the definition of magnesium ion interaction mechanism, Topuz *et al*. reported the gelation of alginate with Mg^{2+} ions and showed that gelation occurs in a slow process (Topuz et al. 2012). However, high concentrations of magnesium and alginate were required due to weak polymer-ion interaction. This situation

leads to faster gelation and the formation of stronger gels compared to low concentrations of magnesium and alginate (Topuz et al. 2012). Also, Topuz *et al*. showed that Mg-alginate gels are not stable and dissociate fast by themselves in the water. Thus, using high concentrations of magnesium and alginate extended the de-gelation time. The possible mechanism behind the de-gelation of alginate gels is the weak interactions between Mg^{2+} ions and alginate chains and the slow exchange of this cation with other ions. This may cause increased osmotic pressure within the hydrogel, gel swelling, and subsequent rupture (Topuz et al. 2012). When compared to the commonly used Ca-alginate system, calcium ions must be removed to dissociate the Ca-alginate gel (Mørch et al. 2006). Additional chemical such as ethylene glycol-bis (-aminoethyl ether) -N, N, N ', N' tetra acetic acid (EGTA), lactate, citrate, and phosphate is needed in this step for the exchange of Ca^{2+} ion (Gombotz and Wee 2012). In this study, two alginate sources which are low viscosity (Sigma, A1112) and high viscosity (suitable for immobilization of micro-organisms, Sigma, 71238) with different compositions were used to fabricate Mg-alginate hydrogel. Figure 3.1 shows hydrogels that were prepared by using low viscosity (3-5 w/v %) and high viscosity (3-5 w/v %) alginate sources with 400 mM of $MgCl_2$ concentration at room temperature for 22 hours. The difference was clearly seen between the two alginate sources. The hydrogels represented in Figure 3.1A (low, 3 w/v%) and Figure 3.1B (high, 3 w/v%) were prepared in the same concentration with different alginate sources similarly as in Figure 3.1C (low, 5 w/v%) and Figure 31.D (high, 5 w/v%). As seen in Figure 3.1B and Figure 3.1D, high viscosity alginate formed more stiff hydrogels. Also, similar behavior was observed for different concentrations of alginate. The hydrogels showed in Figure 3.1B (high, 3 w/v%) and Figure 3.1D (high, 5 w/v%) were prepared from high viscosity alginate in different concentration and they showed similar gelation behavior. Low viscosity alginate, which is alginic acid sodium salt from brown algae contains approximately 61% mannuronic acid and 39% guluronic acid. Also, high viscosity alginate which is suitable for immobilization of micro-organisms contains approximately 25-35% mannuronic acid and 65-70% guluronic acid. The amount and distribution of these blocks depend on the origin of alginate. The gelling capacity and crosslinking density are related to amount of gluronic acids and low viscosity alginate has lower gluronic acid content compared to high viscosity alginate. For that reason, Mg-alginate hydrogel prepared with

low viscosity alginate formed a loose, fluid-like structure. This loose structure provided an advantage for Mg-alginate hydrogel, which can be removed easily from the environment by self-dissociation without any additional chemicals (Topuz et al. 2012).

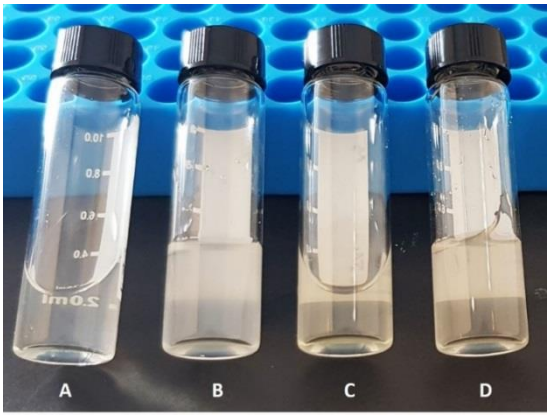

Figure 3.1. Representative picture of Mg-alginate hydrogels obtained by two different alginate (low and high viscosity), A) Hydrogel of low viscosity 3% alginate with 400 mM $MgCl_2$ B) Hydrogel of high viscosity 3% alginate with 400 mM $MgCl_2$ C) Hydrogel of low viscosity 5% alginate with 400 mM $MgCl_2$ D) Hydrogel of high viscosity 5% alginate with 400 mM $MgCl_2$

3.2. Viscosity analysis of Mg-alginate hydrogel

In this study, two different Mg-alginate hydrogels were prepared using different alginate sources low (Sigma, A1112) and high (Sigma, 71238) viscosity of alginate in two different concentrations 3 and 5 w/v % with 400 mM $MgCl_2$ under the same conditions. Polymer solutions generally behave as non-Newtonian fluids, for that reason, the viscosity is dependent on the shear rate at which it is measured (Kruse et al. 2018). The viscosity (Pa·s) of Mg-alginate hydrogels was measured at shear rates between 12.2 and 20 1/s as seen in Figure 3.2. The highest viscosity was observed for High 5 w/v % hydrogel which decreased with increasing shear rate from 2.13 to 1.5 Pa.s. The rest of the Mg-alginate hydrogels behaved similarly where their viscosity values were changing between 0.08-2.13 Pa.s. Among them the lowest viscosity was obtained for Low 3% and increased slightly

with increasing shear rate from 0.08 to 0.11. Pa.s. The viscosity results of Mg-alginate hydrogels are strongly related to amount of guluronic acid they contain. Low viscosity alginate has lower gluronic acid content as explained previously. The gelling capacity and crosslinking density are entirely related to the number of G blocks present along the chain (Drury and Mooney 2003). The G-units of the polymer create binding sites for the bivalent cations and G blocks are cross-linked with cations through interaction with the carboxylic groups in the sugars, which provide the formation of a gel network (Vicini et al. 2017). In this study, the loose structure of the hydrogel was used for bio-patterning application because the Mg-alginate hydrogel, which was used as a bioink keeps cells and MNPs together without dispersion at the same time while it allows cells to attach to the well surface. Therefore, low viscosity alginate (Sigma, A1112) was used during bio-patterning studies considering these features.

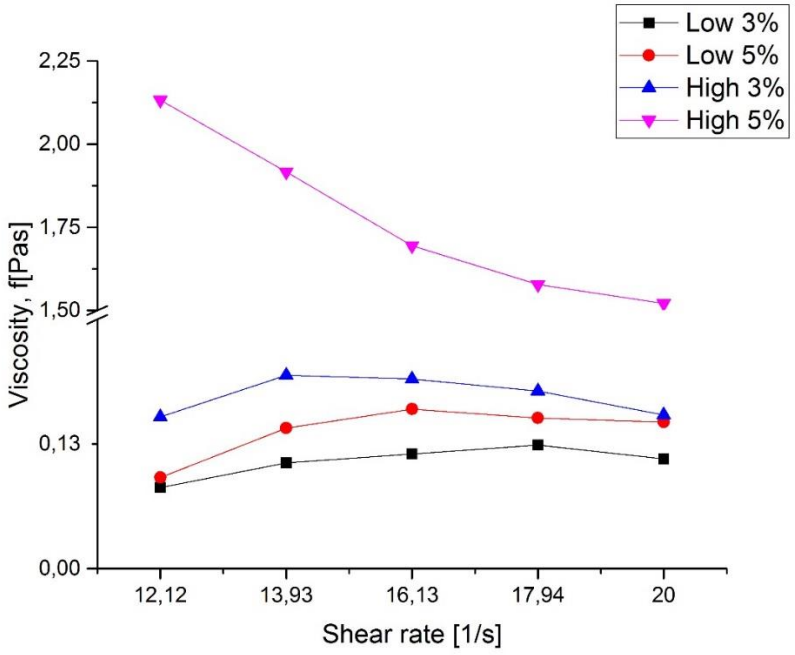

Figure 3.2. Viscosities of the Mg-alginate hydrogels (Pa.s) relation to the shear rate (1/s), samples are low viscosity 3-5% alginate with 400 mM $MgCl_2$ and high viscosity 3-5% alginate with 400 mM $MgCl_2$

3.3. Density functional theory calculations for comparison Ca and Mg-alginate gelation

Alginate has a gelling characteristic based on ion-binding properties. The composition of alginate is important with its affinity for multivalent cations. As shown in Figure 1.3, poly-guluronate is the selective part of alginate for affinity and has an active role in the formation of crosslinks, but poly-mannurate is almost not considered (K I Draget, n.d.). For that reason, the gelling capacity of alginate correlated to the amount of G-blocks. Alkaline earth metals are the main contributor of the gelation process, and the affinity of alginates for these metals increase in the following order: Mg << Ca < Sr < Ba (Vicini et al. 2017). Based on the theoretical calculations the binding energy of Ca is extremely high while Mg has weak interaction. Ca-G interaction results in breaking of the ether bond and high energy interactions of Ca and surrounding O atoms. *d* orbitals in Ca atom hybridizes with *p* orbitals of the surrounding atoms. Also, Figure 3.3 represents the binding energy differences between Ca^{2+} and Mg^{2+} ions. Due to the lack of strong polymer-ion interaction of Mg ions, literature reports that the gelling process of Mg-alginate does not occur (Donati, Cesàro, and Paoletti 2006; Mørch et al. 2006). However, recently Topuz *et al*. showed that higher alginate and Mg^{2+} contents lead to gelation and formation of hydrogel structures. In their study, Mg-alginate hydrogel was achieved using high concentrations of $MgCl_2$ and alginate.

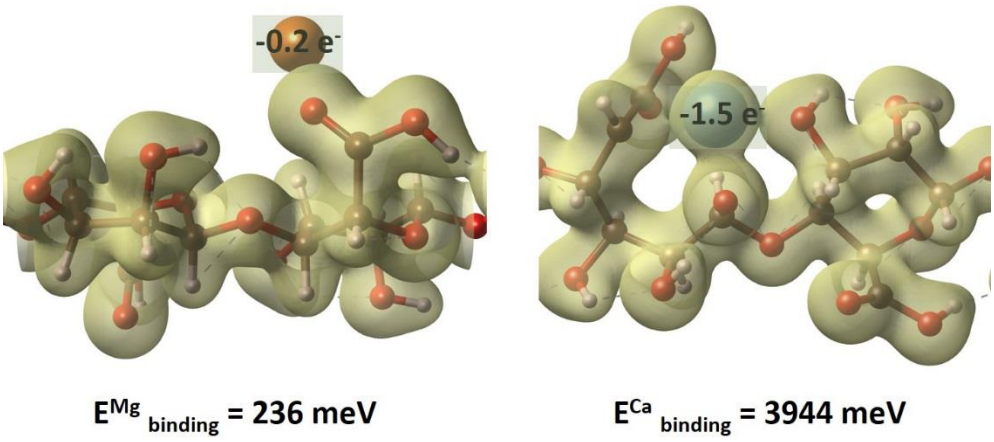

Figure 3.3. Computational calculations for comparison of Ca and Mg ion binding energy to G-block of alginate

3.4. Optimization of bio-patterning parameters by using experimental design models

In this study, six parameters were to considered for the optimization of bioink formulation. These parameters were; *(i)* alginate concentration, *(ii)* $MgCl_2$ concentration, *(iii)* MNP concentration, *(vi)* cell number, *(v)*Mg-alginate volume, and *(vi)* MNP volume. To simplify the optimization steps, initially Plackett-Burman experiment design model was used to identify which factors have a significant impact on the method. Plackett-Burman design model is frequently and effectively used for the elimination of independent variables according to their significance and contribution (Gündoğdu et al. 2016). The Plackett-Burman design with two levels (low and high values) of concentrations for six different variables was carried out according to the experimental matrix as shown in Table 3.1. Due to the weak polymer-ion interaction of magnesium, in this section magnesium-alginate hydrogel were only prepared by using high concentrations of $MgCl_2$ and alginate. As shown by Topuz *et al.*, Mg-alginate gel could not be successfully obtained at alginate concentrations below 3% (Topuz et al. 2012). Unlike Ca-alginate gel, which is generally prepared at lower alginate and Ca ion content, a loose hydrogel is obtained in a longer

period despite high concentrations. For that reason, the low and high value of alginate concentration was determined as 3% and 5% respectively for the Plackett-Burman design. As stated above, stronger ionic gels are obtained with high divalent ion content. In other words, the polymer affinity of magnesium which is lower than other ions requires high concentrations of magnesium source for the formation of Mg-alginate hydrogel. However, after a certain point, an excess amount of ions in the environment may cause destabilization (Topuz et al. 2012). For that reason, the low and high values of the $MgCl_2$ concentration were determined as 400 mM and 800 mM, respectively. The MNP was another important component of the bioink, because it helps for magnetic manipulation of the bio-ink and its content to obtain a patterned 3D cellular structures in the shape of the magnet. MNPs have been used in cell culture studies for manipulation of cells (Shimizu, Ito, and Honda 2006; Ito and Honda 2007) did not show any toxic effect for short-term incubation (Patil et al. 2015). For the optimization step, MNP concentrations were investigated with the low and high values as given 400 μg / ml and 800 μg / ml respectively. Extensive cell-cell interactions in 3D cellular structures promote the mimicking *in vivo* cell function (Lee et al. 2009). Also, cell-cell and cell-ECM interaction increases with high cell density which was important for bio-patterning study. For that reason, 1×10^6 and 2×10^6 cell number were used as the low and high values to investigate the effect of cell densities in the Plackett Burman design model. The last two parameters were the volume of the Mg-alginate gel (4 and 8 μl) and MNPs (2 μl and 4 μl). By using Plackett-Burman design model, 12 runs were created and light microscopy image evaluations of each run for gelation and de-gelation was shown in Figure 3.4 - Figure 3.15. Also, the response of cell patterning values were evaluated as percentage values in the response section by considering the success of patterned bio-ink, attachment rate of the cells, and the removal of patterned cells after the washing step as shown in Table 3.2.

Table 3.1. Plackett-Burman design matrix with low and high levels of factors

Name	Units	Low	High
Alginate concentration	%	3	5
$MgCl_2$ concentration	mM	400	800
MNP concentration	μg/ml	400	800
Cell number		1×10^6	2×10^6
Mg-alginate volume	μl	4	8
MNP volume	μl	2	4

The optimized Mg-alginate hydrogel bio-ink formulation was able to provide appropriate viscosity that keeps cells and MNPs without dispersion, and also favors cell adhesion on the surface. The highest scores were obtained for Run1 and Run6 as given Table 3.2. Also, a relatively high score was obtained for Run 4, where three parameters were similar with Run1; alginate concentration (5%), MNP concentrations (800 μg/ml), and Mg-alginate volume (4 μl). The main difference of those two runs were cell density; for Run 1 2×10^6 cells were used while 1×10^6 cells were used for Run 4 and the high cell density resulted in better patterned bio-ink to form 3D cellular structures as seen in Figure 3.7. Run2, Run5, and Run8 with a 3% alginate concentration of, and 800 mM $MgCl_2$ concentration were compared as given Figure 3.5, Figure 3.8, and Figure 3.11 respectively. 800 μg/ml of MNP concentration and 2×10^6 of cell containing formulation Run 2 had the highest score. On the other hand, 400 μg/ml of MNP containing formulation Run 5 resulted in patterning of the cells as the shape of magnet, but dispersion of some cells occurred during patterning and caused lower score than Run 2. That highlights MNP concentration was an important parameter for magnetic manipulation of bioink, where bioink and its content is patterned onto a surface by only applying external magnetic force. Therefore, MNP concentration had a critical effect to obtain successfully patterned 3D cellular structures. Also, unlike Run2 and Run5, Run8 was performed with 1×10^6 cells and has 800 mM of $MgCl_2$ and 800 μg/ml of MNP. The low number of cells caused the cells to

interact less with each other, and therefore, 3D pattern cellular structure did not occur as in the high cell density. These results suggested that, MNP concentration and cell number were the two most important parameters to fabricate 3D cellular structure via bio-patterning method. Moreover, hydrogel volume, MNP volume and total volume were critical parameters as well, since high total volume resulted bio-ink dispersion in the medium as it was shown in Figure 3.11 for Run 8.

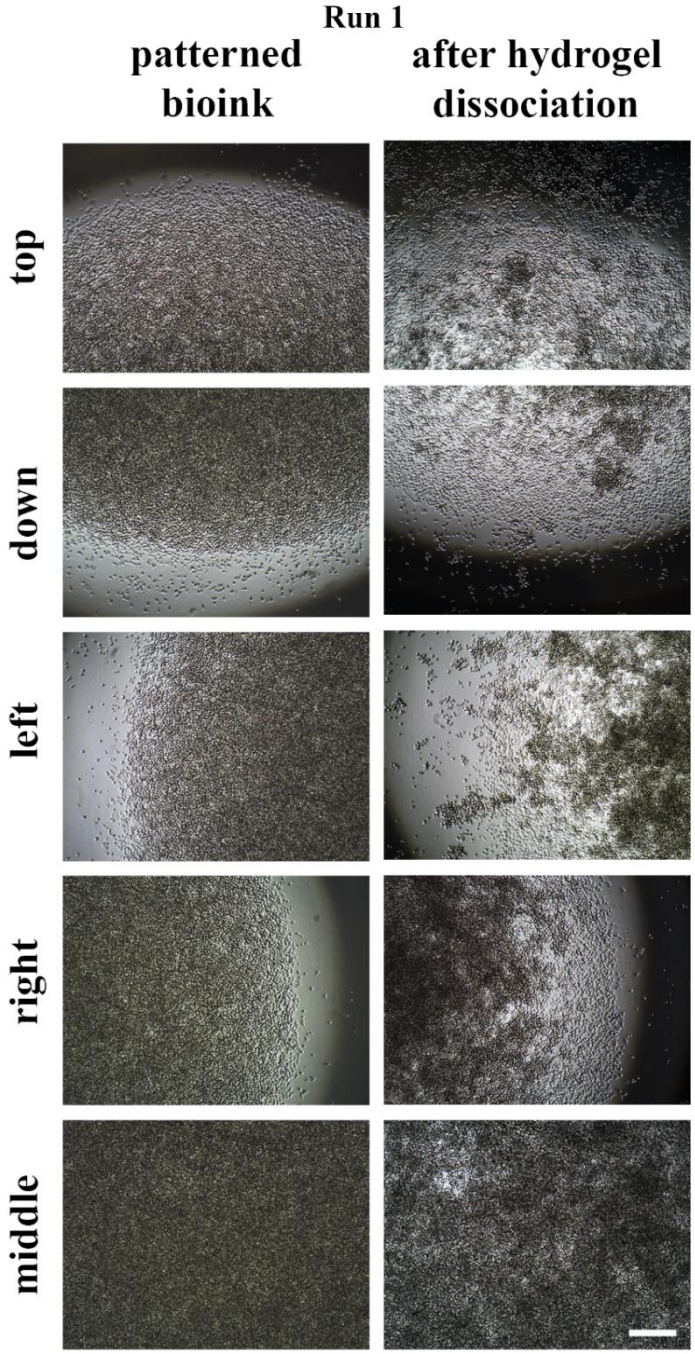

Figure 3.4. Light microscopy images of HeLa containing bio-ink for patterned and dissociated Mg-alginate hydrogel. **Run1** was performed with 5% alginate, 400 mM $MgCl_2$, 800 µg/ml MNP, 4 µl Mg-alginate volume, 4 µl MNP volume and 2×10^6 cells, scale bar: 200 µm

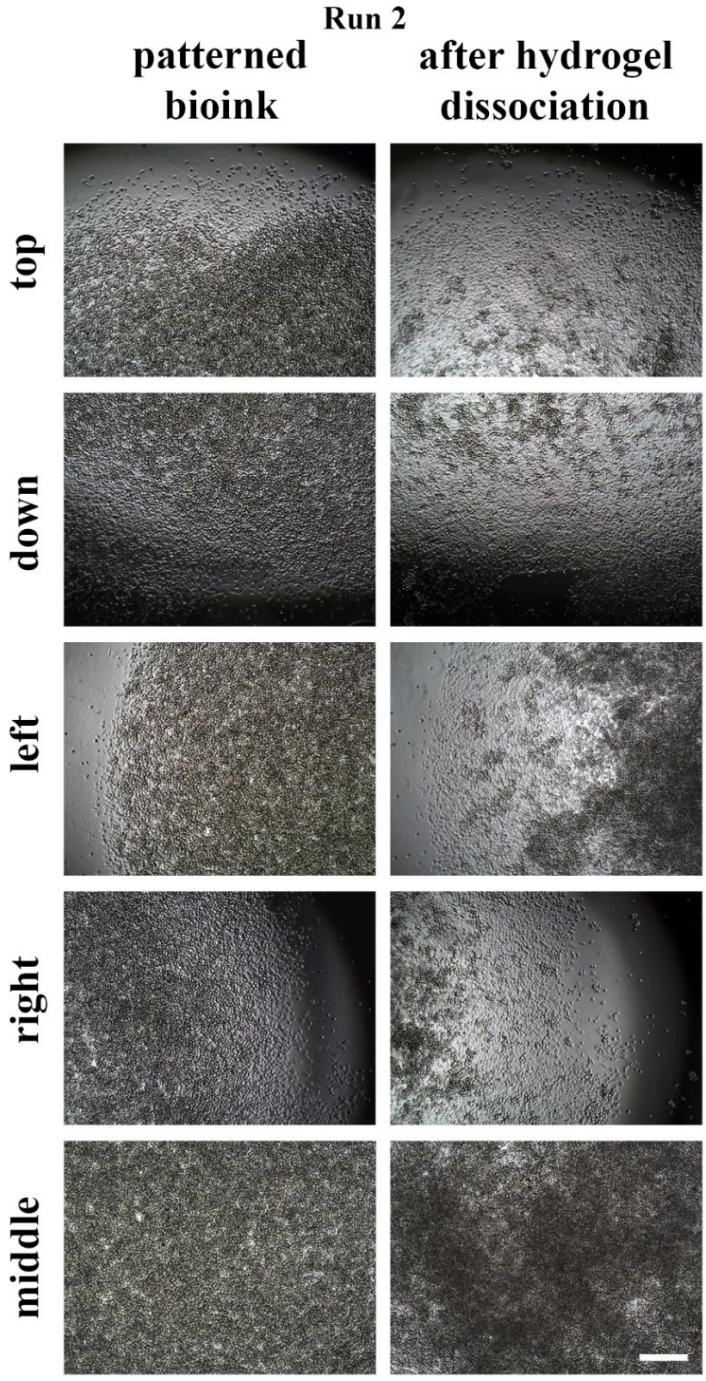

Figure 3.5. Light microscopy images of HeLa containing bio-ink for patterned and dissociated Mg-alginate hydrogel. **Run2** was performed with 3% alginate, 800 mM $MgCl_2$, 800 µg/ml MNP, 4 µl Mg-alginate volume, 2 µl MNP volume and 2×10^6 cells, scale bar: 200 µm

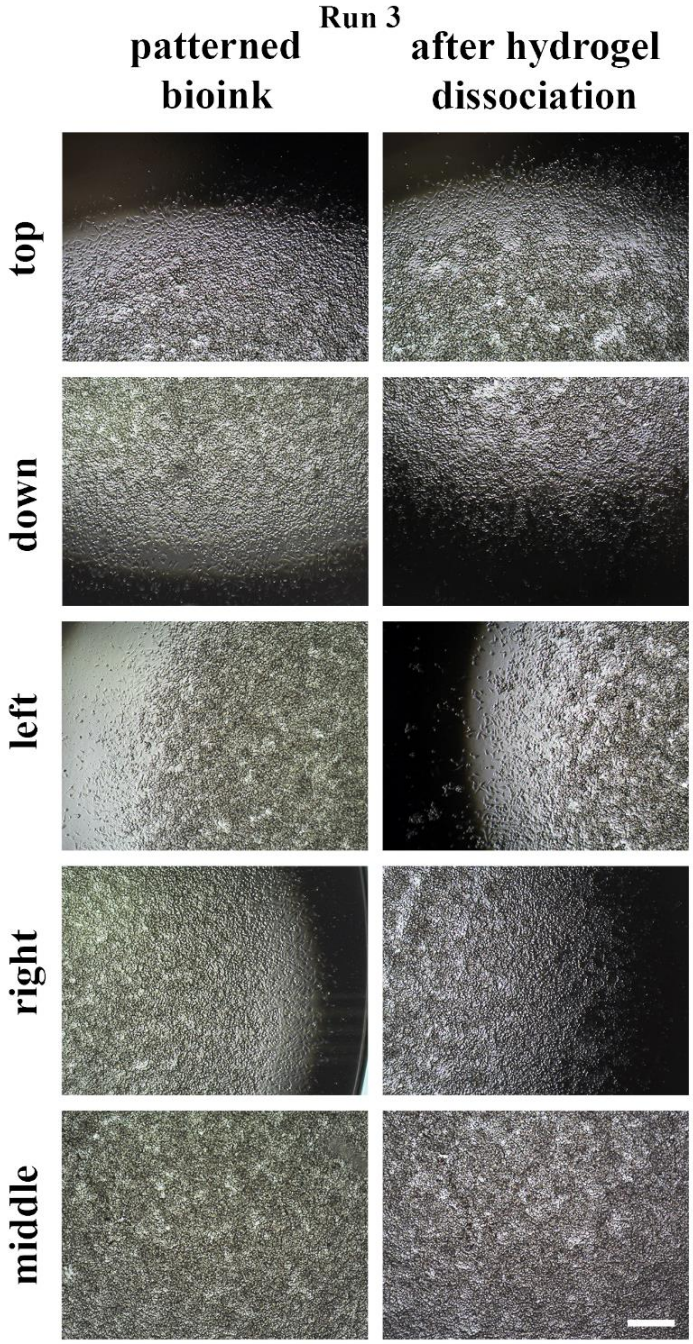

Figure 3.6. Light microscopy images of HeLa containing bio-ink for patterned and dissociated Mg-alginate hydrogel. **Run3** was performed with 3% alginate, 400 mM $MgCl_2$, 800 µg/ml MNP, 8 µl Mg-alginate volume, 4 µl MNP volume and 1×10^6 cells scale bar: 200 µm

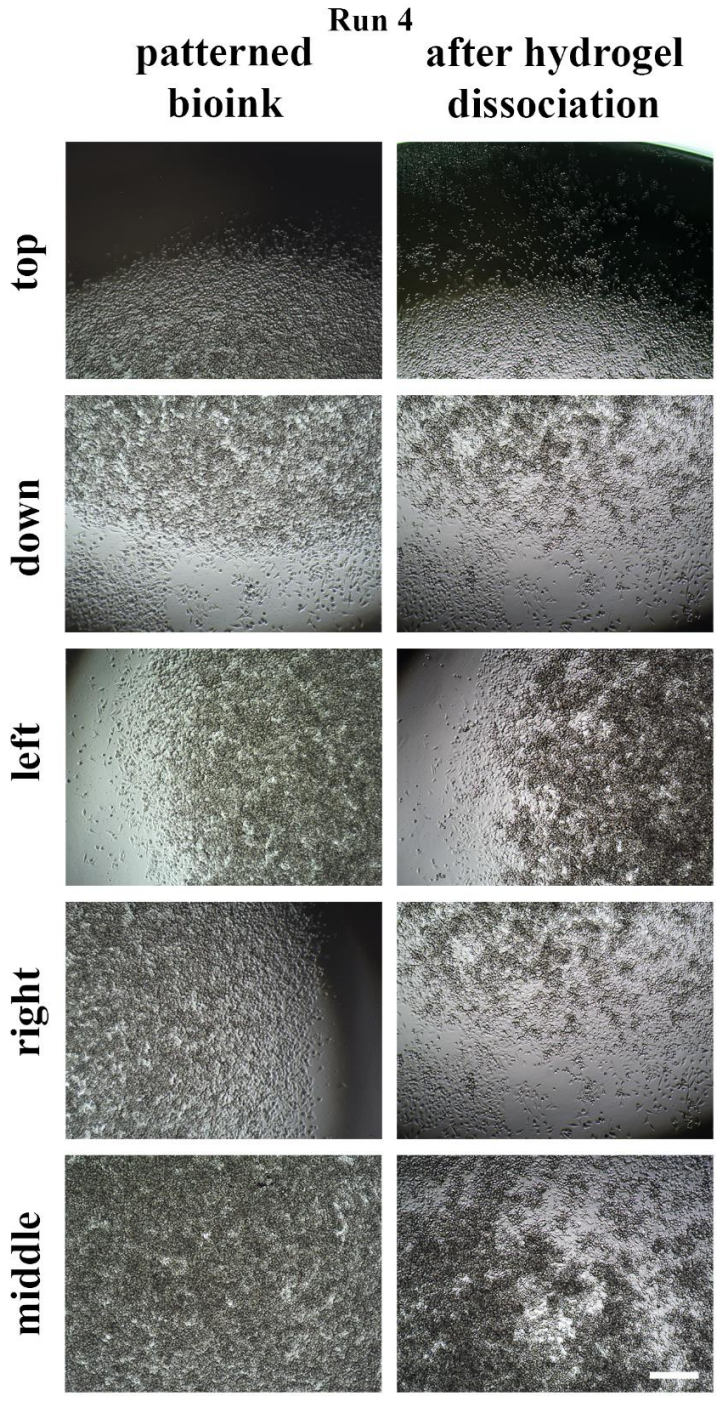

Figure 3.7. Light microscopy images of HeLa containing bio-ink for patterned and dissociated Mg-alginate hydrogel. **Run4** was performed with 5% alginate, 800 mM $MgCl_2$, 800 µg/ml MNP, 4 µl Mg-alginate volume, 2 µl MNP volume and 1×10^6 cells scale bar: 200 µm

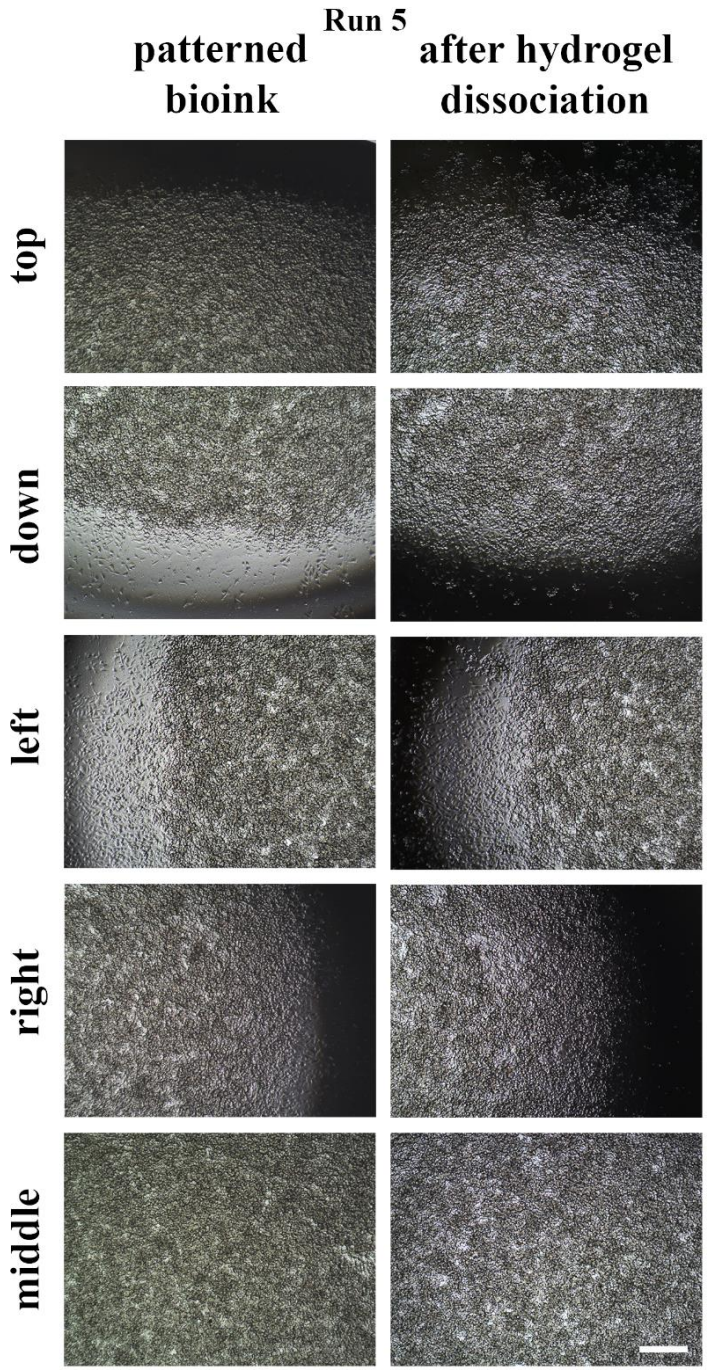

Figure 3.8. Light microscopy images of HeLa containing bio-ink for patterned and dissociated Mg-alginate hydrogel. **Run5** was performed with 3% alginate, 800 mM $MgCl_2$, 400 µg/ml MNP, 8 µl Mg-alginate volume, 2 µl MNP volume and 2×10^6 cells scale bar: 200 µm

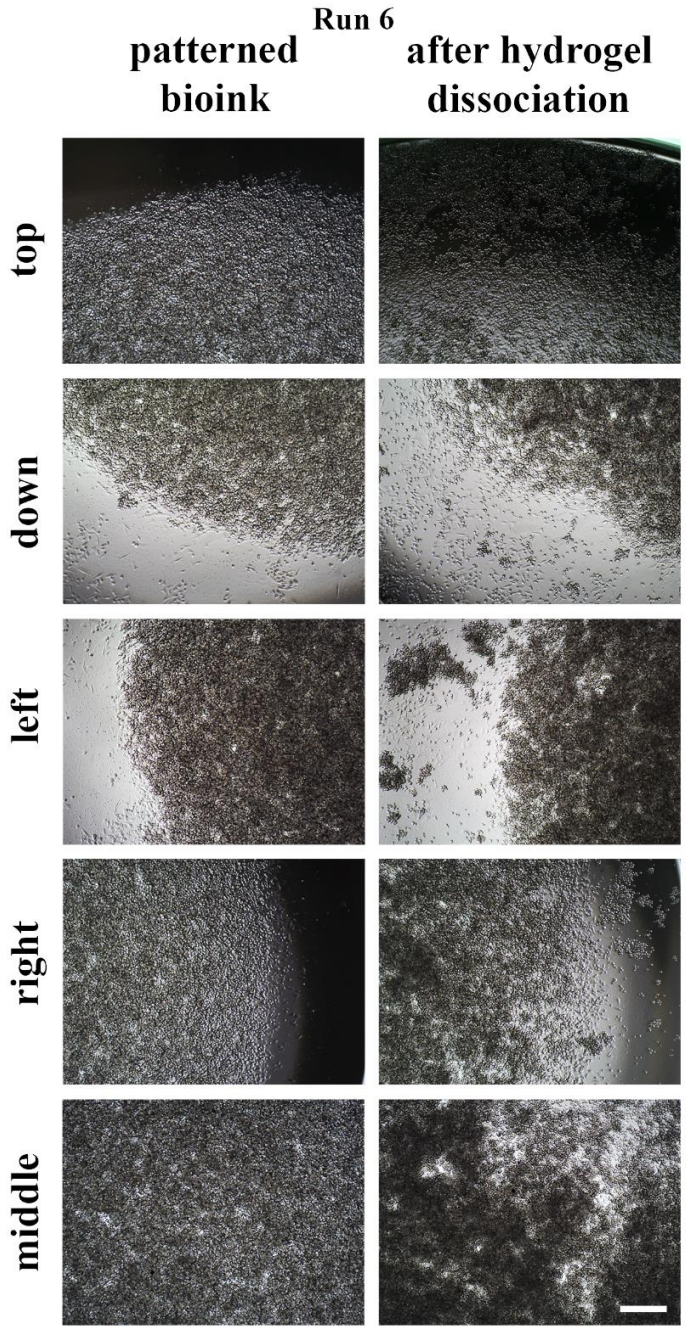

Figure 3.9. Light microscopy images of HeLa containing bio-ink for patterned and dissociated Mg-alginate hydrogel. **Run6** was performed with 5% alginate, 400 mM $MgCl_2$, 800 µg/ml MNP, 8 µl Mg-alginate volume, 2 µl MNP volume and 2×10^6 cells scale bar: 200 µm

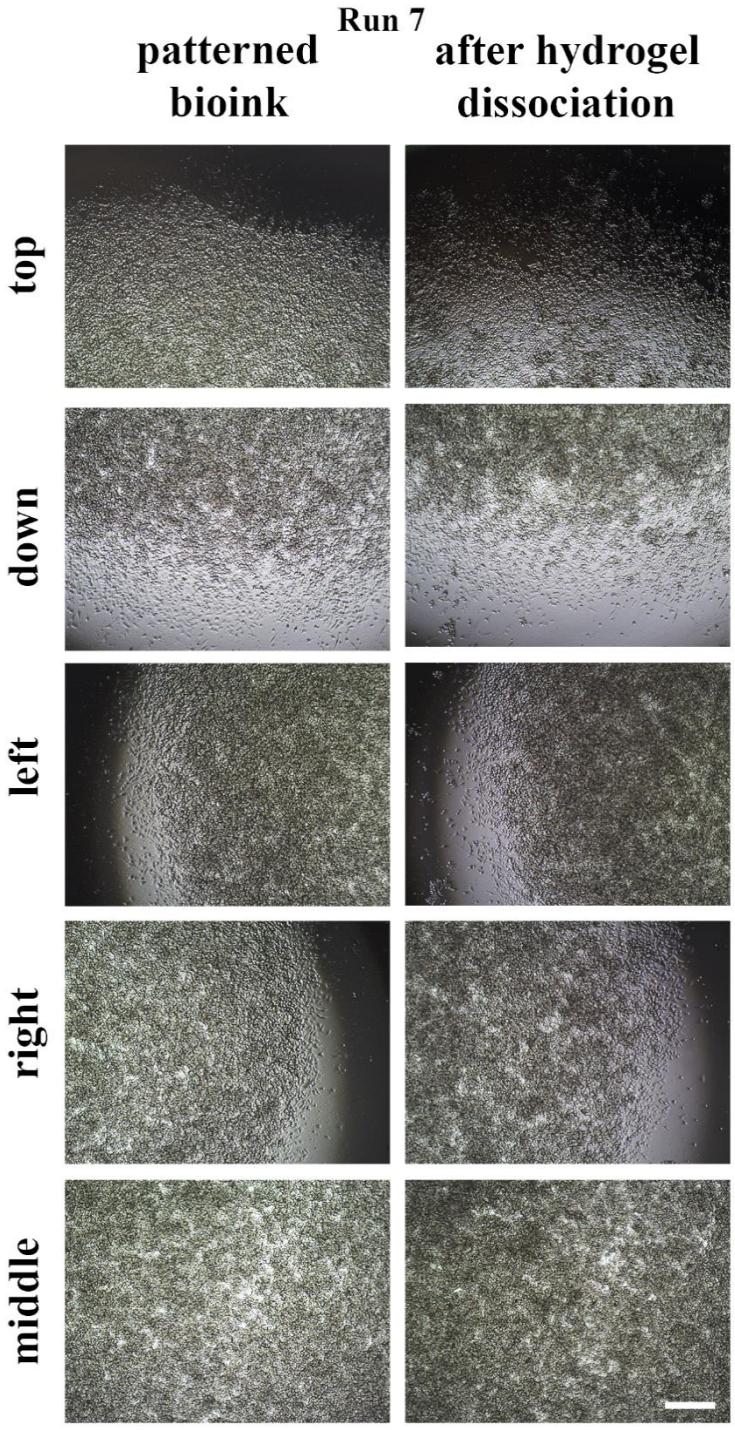

Figure 3.10. Light microscopy images of HeLa containing bio-ink for patterned and dissociated Mg-alginate hydrogel. **Run7** was performed with 5% alginate, 800 mM $MgCl_2$, 400 µg/ml MNP, 8 µl Mg-alginate volume, 4 µl MNP volume and 2×10^6 cells scale bar: 200 µm

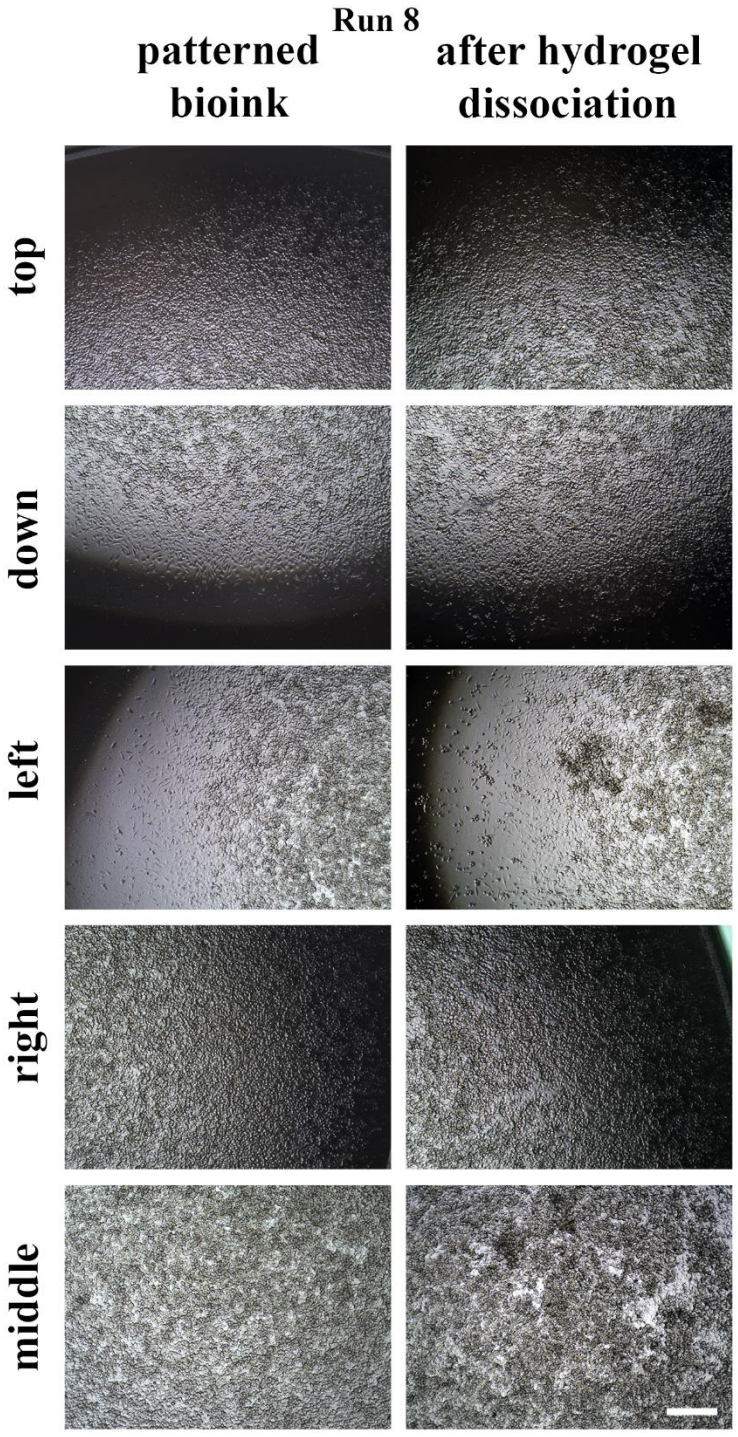

Figure 3.11. Light microscopy images of HeLa containing bio-ink for patterned and dissociated Mg-alginate hydrogel. **Run8** was performed with 3% alginate, 800 mM $MgCl_2$, 800 µg/ml MNP, 8 µl Mg-alginate volume, 4 µl MNP volume and 1×10^6 cells scale bar: 200 µm

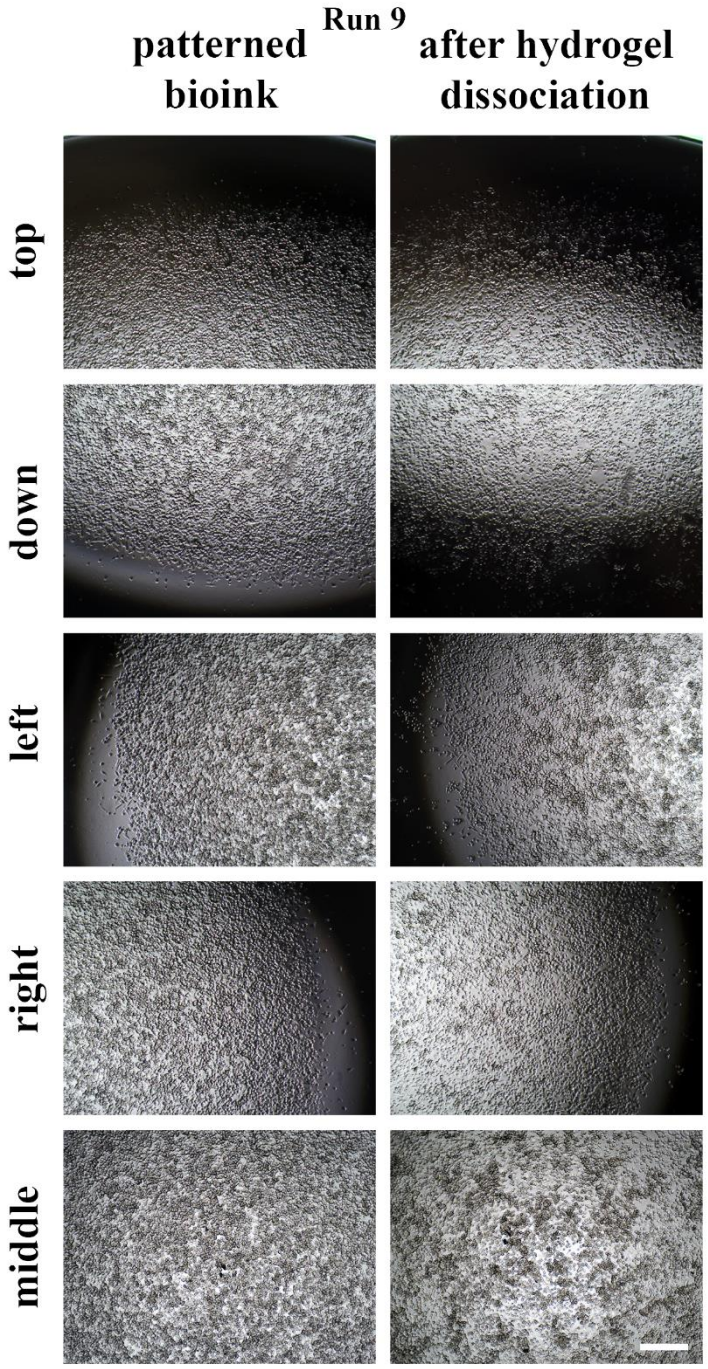

Figure 3.12. Light microscopy images of HeLa containing bio-ink for patterned and dissociated Mg-alginate hydrogel. **Run9** was performed with 5% alginate, 400 mM $MgCl_2$, 400 µg/ml MNP, 8 µl Mg-alginate volume, 2 µl MNP volume and 1×10^6 cells scale bar: 200 µm

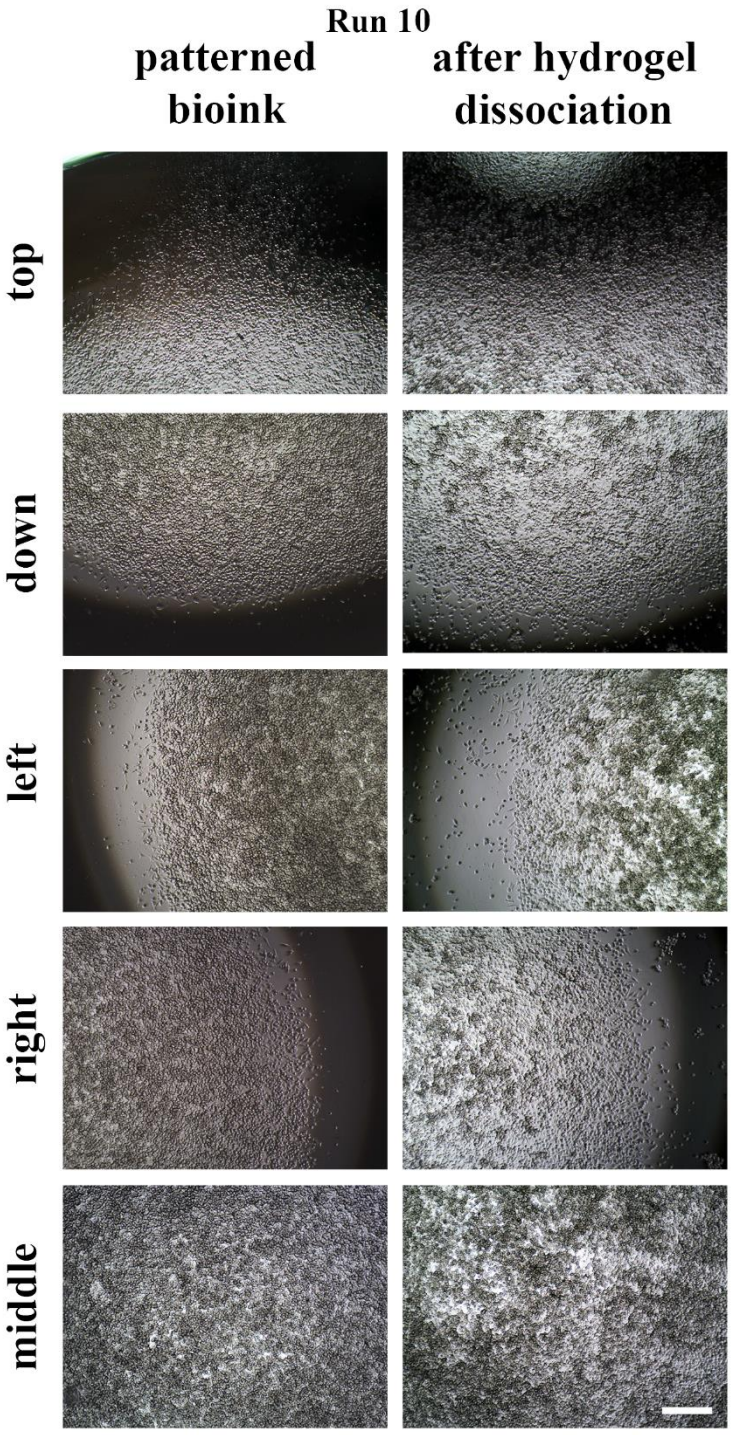

Figure 3.13. Light microscopy images of HeLa containing bio-ink for patterned and dissociated Mg-alginate hydrogel. **Run10** was performed with 5% alginate, 800 mM $MgCl_2$, 400 µg/ml MNP, 4 µl Mg-alginate volume, 4 µl MNP volume and 1×10^6 cells scale bar: 200 µm

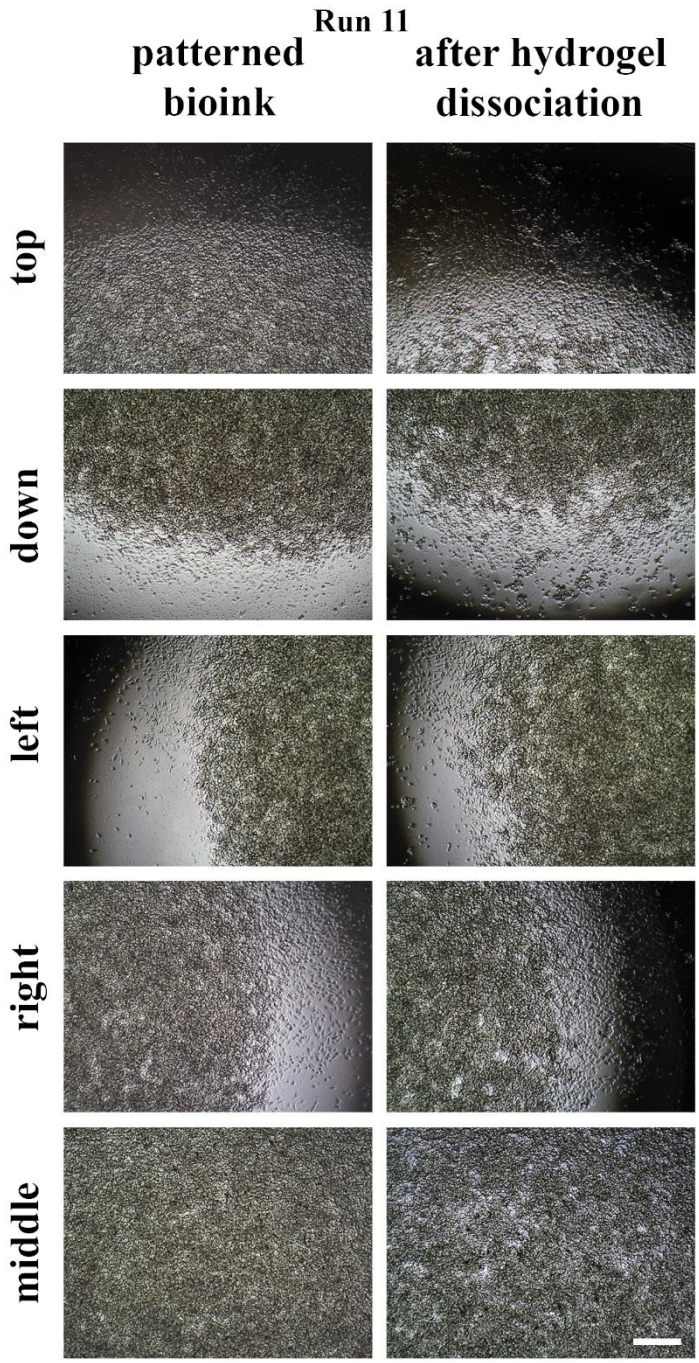

Figure 3.14. Light microscopy images of HeLa containing bio-ink for patterned and dissociated Mg-alginate hydrogel. **Run11** was performed with 3% alginate, 400 mM $MgCl_2$, 400 µg/ml MNP, 4 µl Mg-alginate volume, 4 µl MNP volume and 2×10^6 cells scale bar: 200 µm

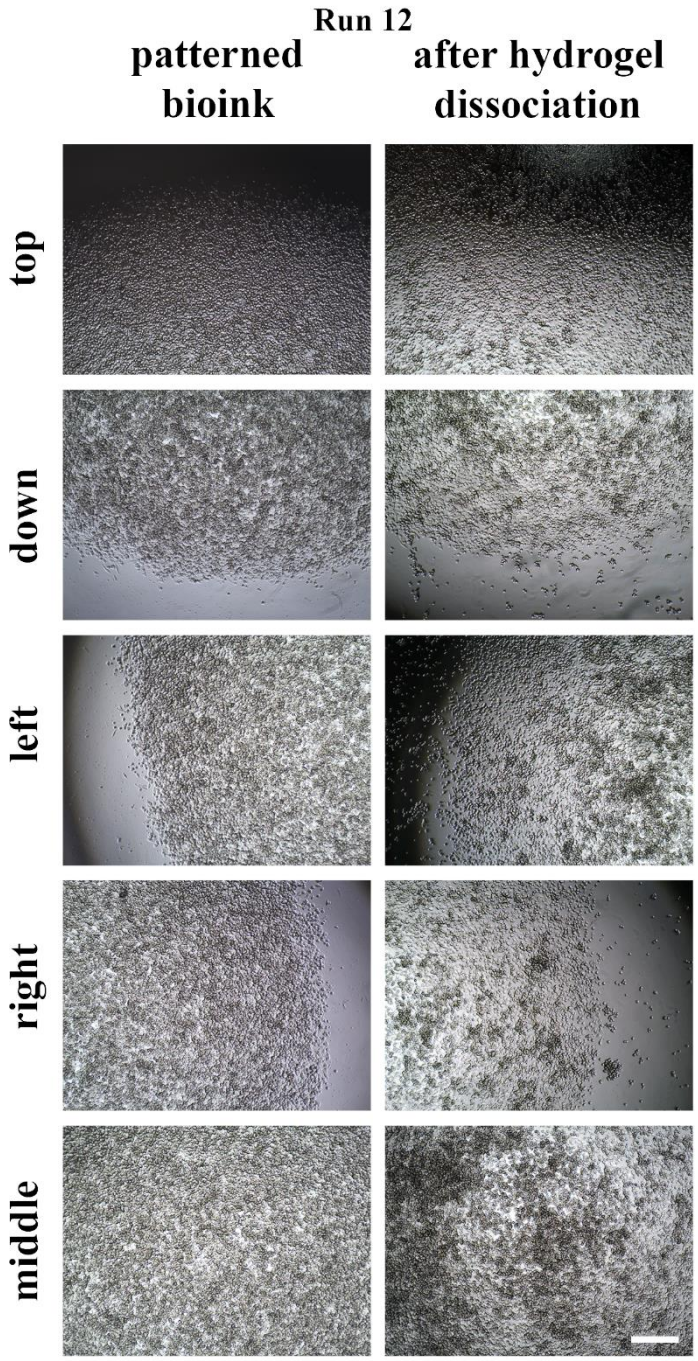

Figure 3.15. Light microscopy images of HeLa containing bio-ink for patterned and dissociated Mg-alginate hydrogel. **Run12** was performed with 3% alginate, 400 mM $MgCl_2$, 400 µg/ml MNP, 4 µl Mg-alginate volume, 2 µl MNP volume and 1×10^6 cells scale bar: 200 µm

Table 3.2. Plackett-Burman design model with 12 runs and their response values

Run	Alginate concentration %	$MgCl_2$ concentration mM	MNP concentration µg/ml	Cell number	Mg-alginate volume µl	MNP volume µl	Response
1	5.00	400.00	800.00	2×10^6	4	4	80
2	3.00	800.00	800.00	2×10^6	4	2	70
3	3.00	400.00	800.00	1×10^6	8	4	35
4	5.00	800.00	800.00	1×10^6	4	2	70
5	3.00	800.00	400.00	2×10^6	8	2	45
6	5.00	400.00	800.00	2×10^6	8	2	80
7	5.00	800.00	400.00	2×10^6	8	4	50
8	3.00	800.00	800.00	1×10^6	8	4	25
9	5.00	400.00	400.00	1×10^6	8	2	20
10	5.00	800.00	400.00	1×10^6	4	4	40
11	3.00	400.00	400.00	2×10^6	4	4	45
12	3.00	400.00	400.00	1×10^6	4	2	50

Table 3.3. Contribution (%) values of parameters were obtained from Plackett-Burman

Term	Contribution (%)
Alginate concentration	9.09
$MgCl_2$ concentration	0.19
MNP concentration	**22.45**
Cell number	**31.35**
Mg-alginate volume	**18.55**
MNP volume	6.68

The contribution (%) of the six parameters were evaluated by Plackett-Burman design model, for all 12 runs. As given in Table 3.3 the highest contributions were obtained as; cell number (31.35%), MNP concentration (22.45%) and Mg-alginate volume (18.55%).

According to ANOVA analysis F-value and p-value were obtained 6.30 and 0.03 respectively. When the p value is less than 0.05 it means that the model is significant.

Table 3.4. Box-Behnken design matrix with 3 variable levels of parameters

Name	Units	-1 Level	0	+1 Level
MNP concentration	µg/ml	400	600	800
Cell number		1×10^6	1.5×10^6	2×10^6
Mg-alginate volume	µl	2	4	6

As a result of Plackett Burman design model, optimization parameters were decreased to 3. These were considered for the Box-Behnken design model with 3 variable levels (low-medium-high) of parameters to obtain optimum values for the bio-patterning method as seen in Table 3.4. MNP concentration, cell number and Mg-alginate hydrogel volume which had the highest contribution to bio-patterning method were used to obtain Box-Behnken design model with their low, high and medium values, while Mg-alginate concentration, $MgCl_2$ concentration and MNP volume were kept constant as 5%, 400 mM and 2 µl respectively. Mg-alginate volume was applied between 2-8 µl in Plackt Burmen model, however in Box Behnken model it was reduced to 2-6 µl. Because high total volume increases the risk of cell dispersion in bio-patterning method. By using the Box Behnken design model, 16 runs were created and the response of cell biopatterning values was evaluated between 0-100 as shown in Table 3.5. Each run that was shown in Figure 3.16, 3.17, 3.18, 3.19, and 3.20 was scored in response section by considering the presence of patterned bio-ink, attachment rate of the cells, removal of patterned cells after the washing step.

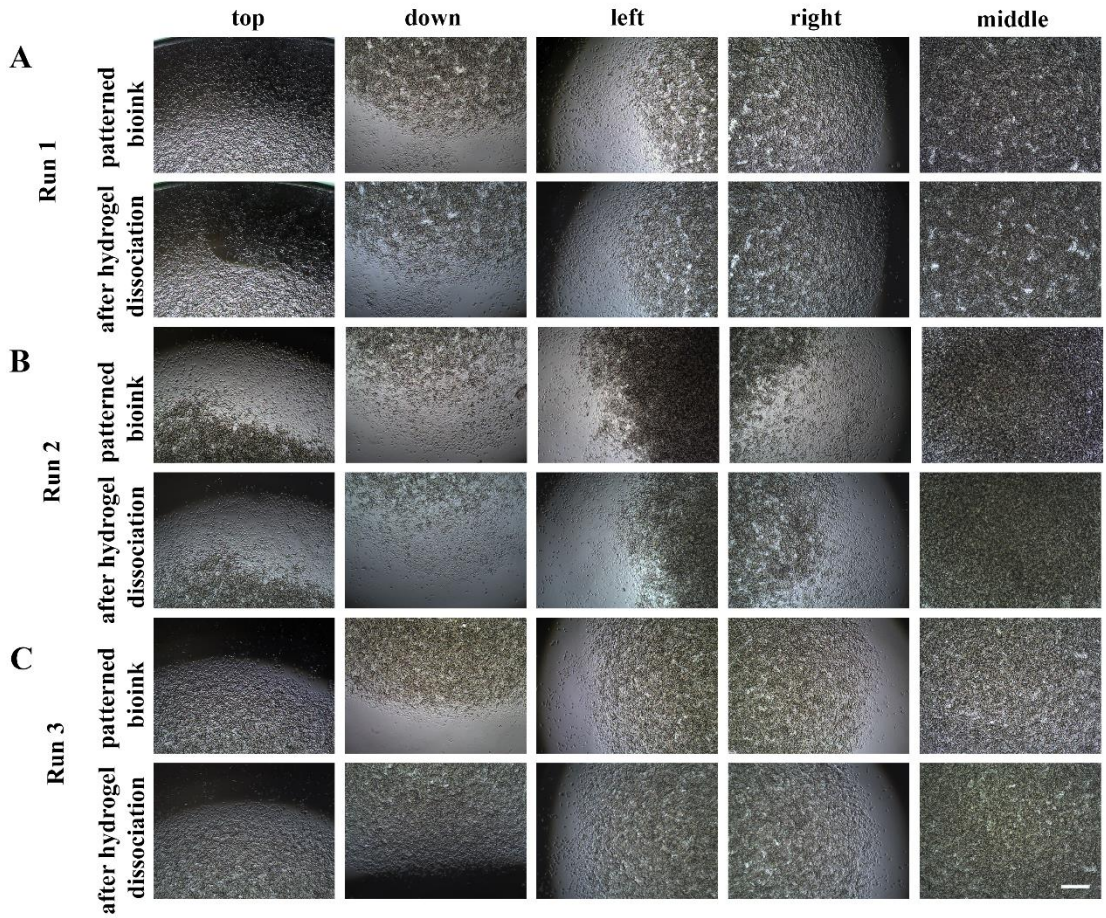

Figure 3.16. Light microscopy images of HeLa containing bio-ink for patterned and dissociated Mg-alginate hydrogel A) Run1, performed with 400 µg/ml MNP, 2×10^6 cells and 4 µl Mg-alginate B) Run2, performed with 800 µg/ml MNP, 1.5×10^6 cells and 2 µl Mg-alginate C) Run3 performed with 600 µg/ml MNP, 1.5×10^6 cells and 4 µl Mg-alginate scale bar: 200 µm

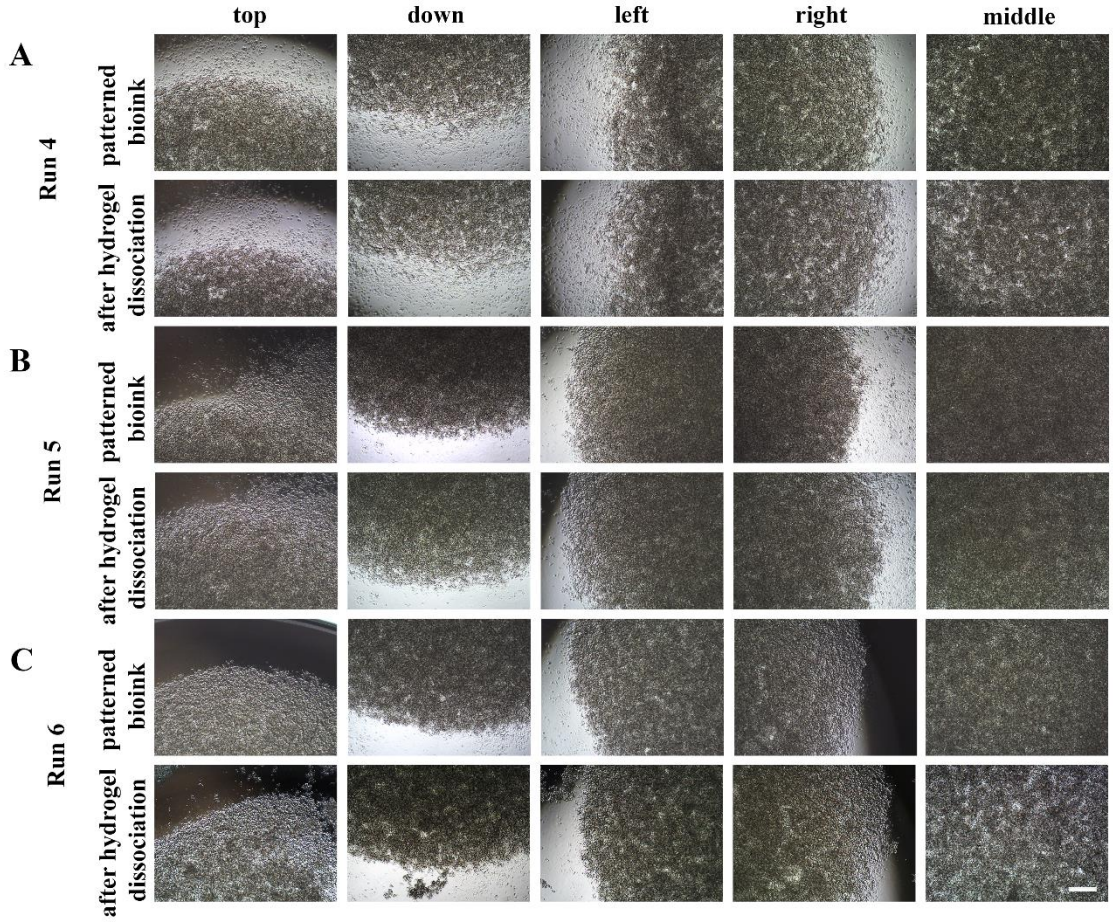

Figure 3.17. Light microscopy images of HeLa containing bio-ink for patterned and dissociated Mg-alginate hydrogel A) Run4, performed with 600 µg/ml MNP, 2×10^6 cells and 6 µl Mg-alginate B) Run5, performed with 600 µg/ml MNP, 2×10^6 cells and 2 µl Mg-alginate C) Run6 performed with 800 µg/ml MNP, 2×10^6 cells and 4 µl Mg-alginate scale bar: 200 µm

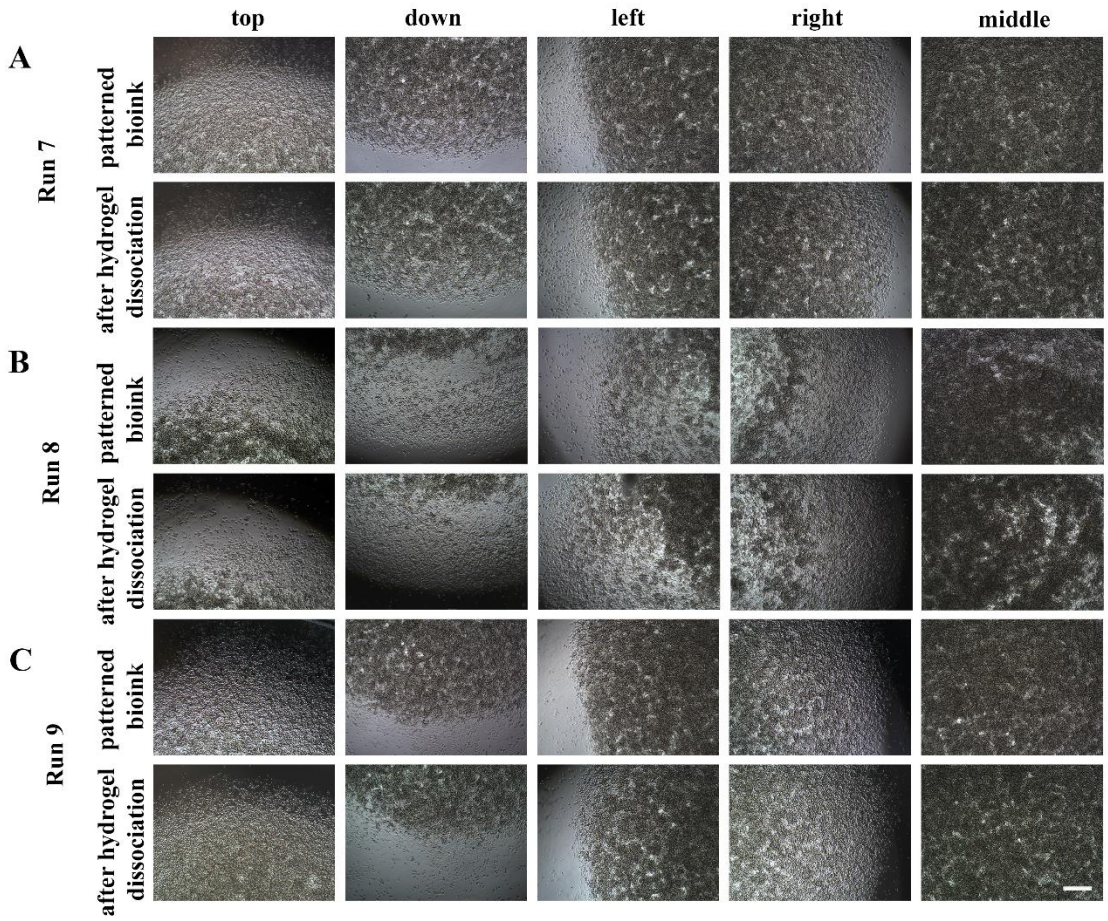

Figure 3.18. Light microscopy images of HeLa containing bio-ink for patterned and dissociated Mg-alginate hydrogel A) Run7, performed with 600 µg/ml MNP, 1.5×10^6 cells and 4 µl Mg-alginate B) Run8, performed with 800 µg/ml MNP, 1.5×10^6 cells and 6 µl Mg-alginate C) Run9 performed with 600 µg/ml MNP, 1.5×10^6 cells and 4 µl Mg-alginate scale bar: 200 µm

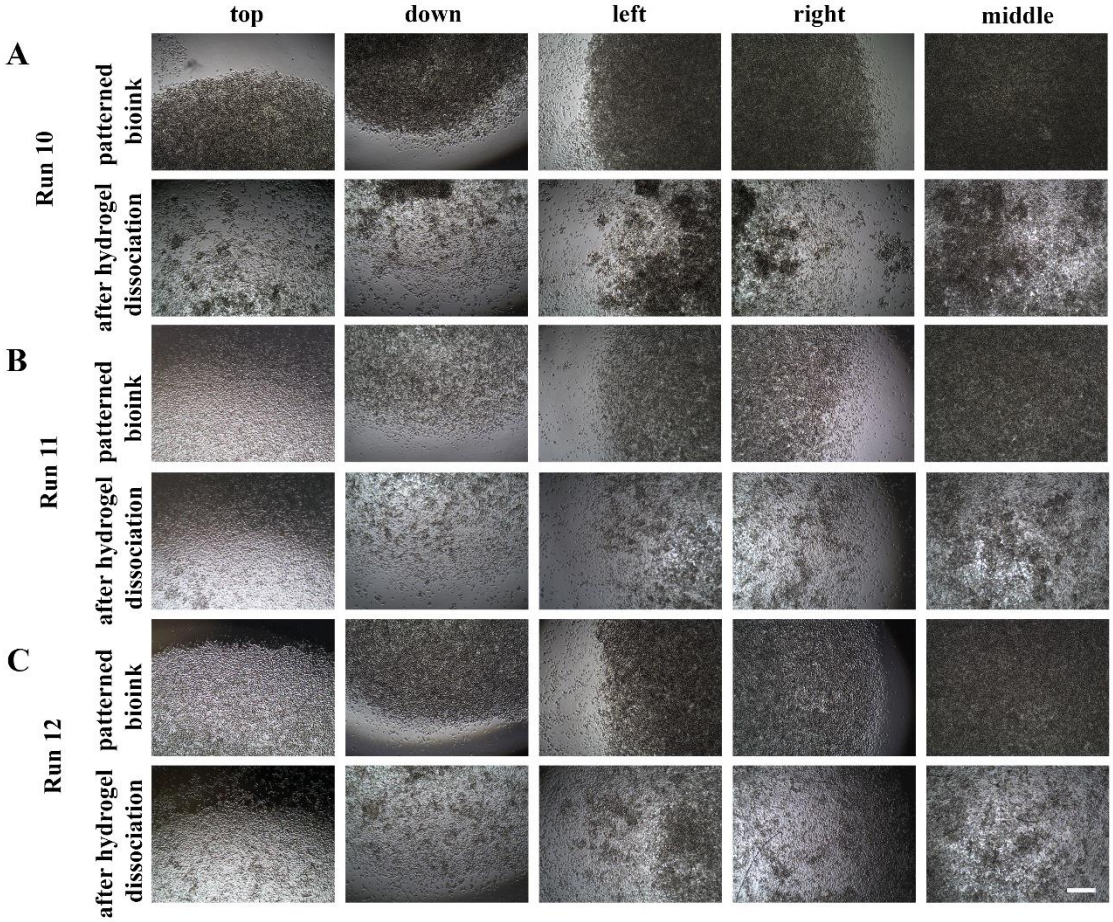

Figure 3.19. Light microscopy images of HeLa containing bio-ink for patterned and dissociated Mg-alginate hydrogel A) Run10, performed with 600 µg/ml MNP, 1×10^6 cells and 2 µl Mg-alginate B) Run11, performed with 600 µg/ml MNP, 1×10^6 cells and 6 µl Mg-alginate C) Run12 performed with 400 µg/ml MNP, 1.5×10^6 cells and 6 µl Mg-alginate scale bar: 200 µm

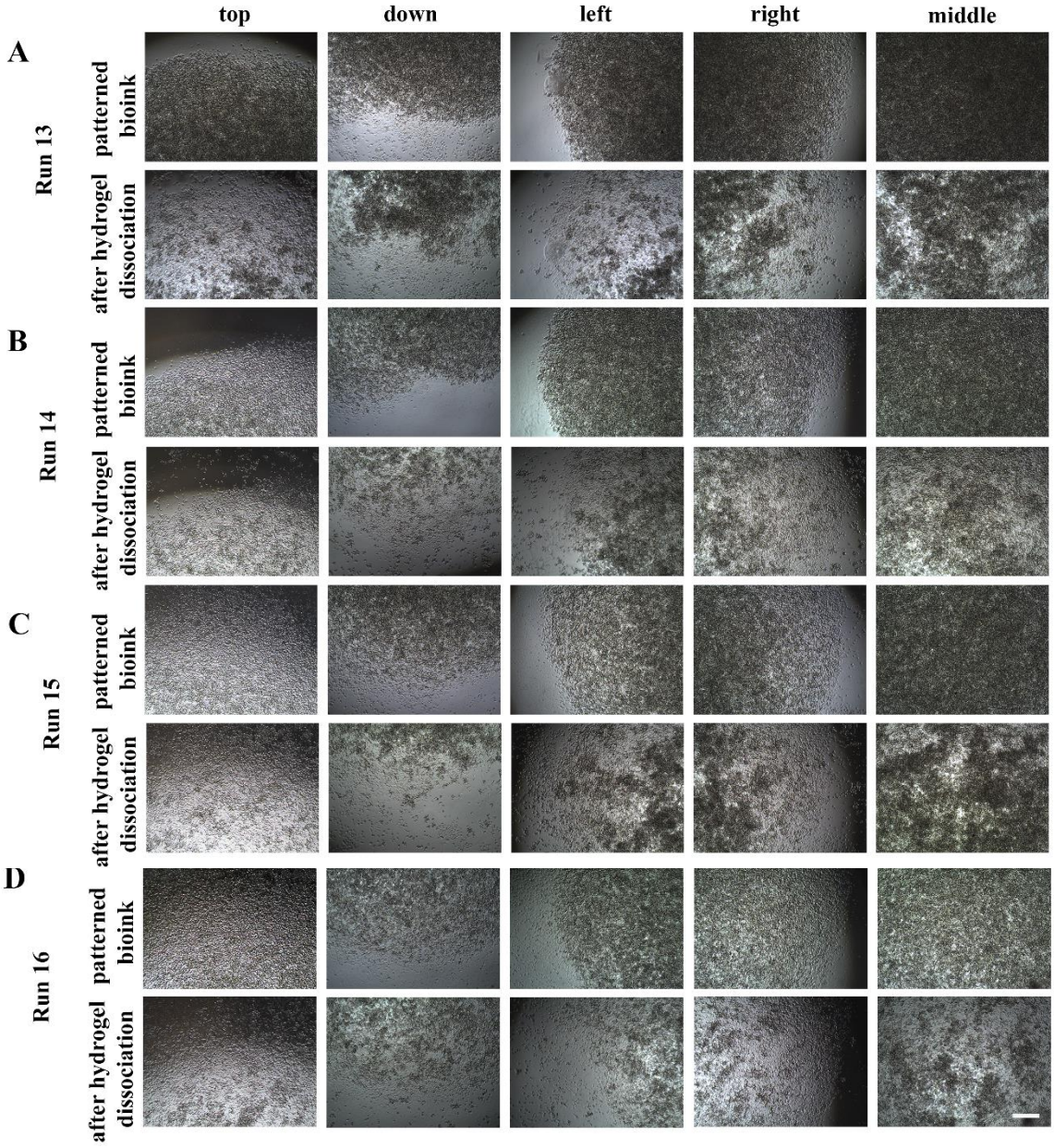

Figure 3.20. Light microscopy images of HeLa containing bio-ink for patterned and dissociated Mg-alginate hydrogel A) Run13, performed with 400 µg/ml MNP, 1.5×10^6 cells and 2 µl Mg-alginate B) Run14, performed with 400 µg/ml MNP, 1×10^6 cells and 4 µl Mg-alginate C) Run15 performed with 600 µg/ml MNP, 1.5×10^6 cells and 4 µl Mg-alginate D) Run16 performed with 800 µg/ml MNP, 1×10^6 cells and 4 µl Mg-alginate scale bar: 200 µm

Table 3.5. Box-Behnken design model with 16 runs and their responses to obtain optimum values for bio-patterning method by using 3 variables

Run	MNP concentration µg/ml	Cell number	Mg-alginate volume µl	Response
1	400.00	2×10^6	4	20
2	800.00	1.5×10^6	2	60
3	600.00	1.5×10^6	4	30
4	600.00	2×10^6	6	90
5	600.00	2×10^6	2	80
6	800.00	2×10^6	4	70
7	600.00	1.5×10^6	4	75
8	800.00	1.5×10^6	6	50
9	600.00	1.5×10^6	4	65
10	600.00	1×10^6	2	30
11	600.00	1×10^6	6	20
12	400.00	1.5×10^6	6	15
13	400.00	1.5×10^6	2	30
14	400.00	1×10^6	4	25
15	600.00	1.5×10^6	4	40
16	800.00	1×10^6	4	60

As shown in Figure 3.16, 3.17, 3.18, 3.19, and 3.20, each run in the Box-Behnken model was examined in detail and compared each other. Run12, Run13, and Run14 which had the lowest scores, performed with low MNP concentration (400 µg/ml) and cell number (1.5×10^6 and 1×10^6) as seen in Figure 3.19C, Figure 3.20A and Figure 3.20B respectively. Both low cell density and low MNP concentration resulted in dispersion of bioink and unpatterned cells. The Run4, Run5, and Run7 containing 600 µg/ml MNPs got the third-highest scores as given in Table 3.5. As seen in Figure 3.17A, patterned cell boundaries were clearly defined as the shape of disc magnet, and 3D cellular structure was

obtained very clearly for Run4, which had 2×10^6 cell, 6 µl Mg-alginate, and 600 µg/ml MNP. For that reason, parameters of Run4 which were 6 µl (5%) Mg-alginate, 400 mM $MgCl_2$ concentration, 2 µl (600 µg/ml) MNP, 2×10^6 of cell number, and 4h incubation, were selected as optimized formulation for futher bio-patterning parameters. Also, optimized total bio-ink volume was obtained as 12 µl for Run4. According to ANOVA analysis, this model was considered significant since the p-value of the model was obtained 0.01 ($p < 0.05$). Also, the "Lack of Fit F-value" of 0.66 implies the Lack of Fit is not significant relative to the pure error. Non-significant lack of fit means that the model fits well.

3.5. Formation of 3D tumor models with various cancer cells via Mg-alginate based biopatterning method

The behavior of long-term cultured 3D cellular structures of run 4 in terms of cell proliferation, migration, and viability was evaluated by using Live dead assay and Alamar blue assay. Live/dead assay was performed for 3D cellular structures of HeLa cells for day 1, 3, 5, and 7 culturing periods as shown in Figures 3.21, 3.22, and 3.23. Proliferation and migration of cells, and also high cell viability were observed starting from day1 as given in Figure 3.21C and Figure 3.21D. End of the day3, patterned HeLa cells covered all over the well surfaces with high cell viability according to live/dead assay as shown in Figure 3.22E and Figure 3.22F. As a result of the migration and proliferation of HeLa cells, 3D cellular structures with high cell density were observed on day 5 and day 7 as given in Figure 3.23F and Figure 3.23G. Based on over proliferation and diffusion limitations, low cell viability, especially in the middle area of 3D cellular structure was observed on day5 as shown in Figure 3.23F and that dead area increased and covered all the 3D cellular structure on day7 as seen in Figure 3.23G. The middle part of the 3D cellular structure behaves like necrotic core due to restricted oxygenation and nutrition environment in 3D cell culture (Edmondson et al. 2014). There are typical zones of cell proliferation and the distribution of diffused CO_2, oxygen, and nutrition in a 3D cell culture (Nath and Devi 2016; Mueller-Klieser 2000) outer layer comprises live and proliferative cells however middle area is called the necrotic core comprises hypoxic quiescent cells (Edmondson et al. 2014). For

that reason, a high number of living cells be observed in the outer parts since these parts have better oxygen and nutrition transfer. It is important to point out that the limited oxygenation and nutrition environment in 3D cellular structures mimics the microenvironment of *in vivo* tumor tissues (Lin and Chang 2008).

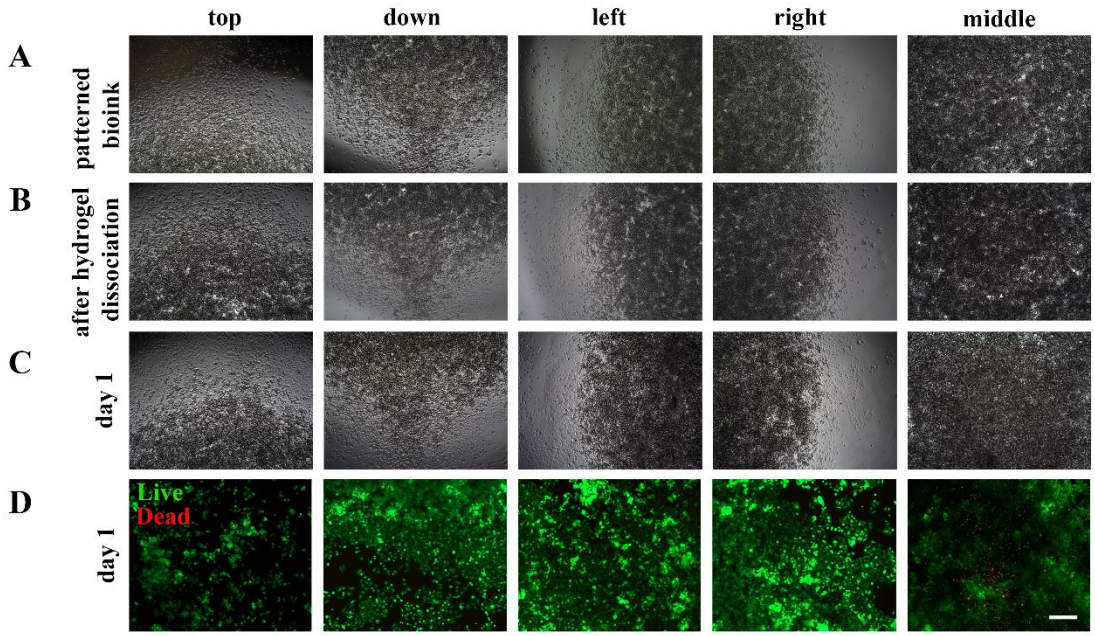

Figure 3.21. Light microscopy and fluorescent images of patterned HeLa cells A) Light microscopy images of patterned bio-ink B) Light microscopy images of patterned 3D cellular structure after dissociation of Mg-alginate hydrogel C) Light microscopy images of 1day cultured patterned 3D cellular structure D) Fluorescent microscopy images of 1day cultured patterned 3D cellular structure scale bar: 200 µm

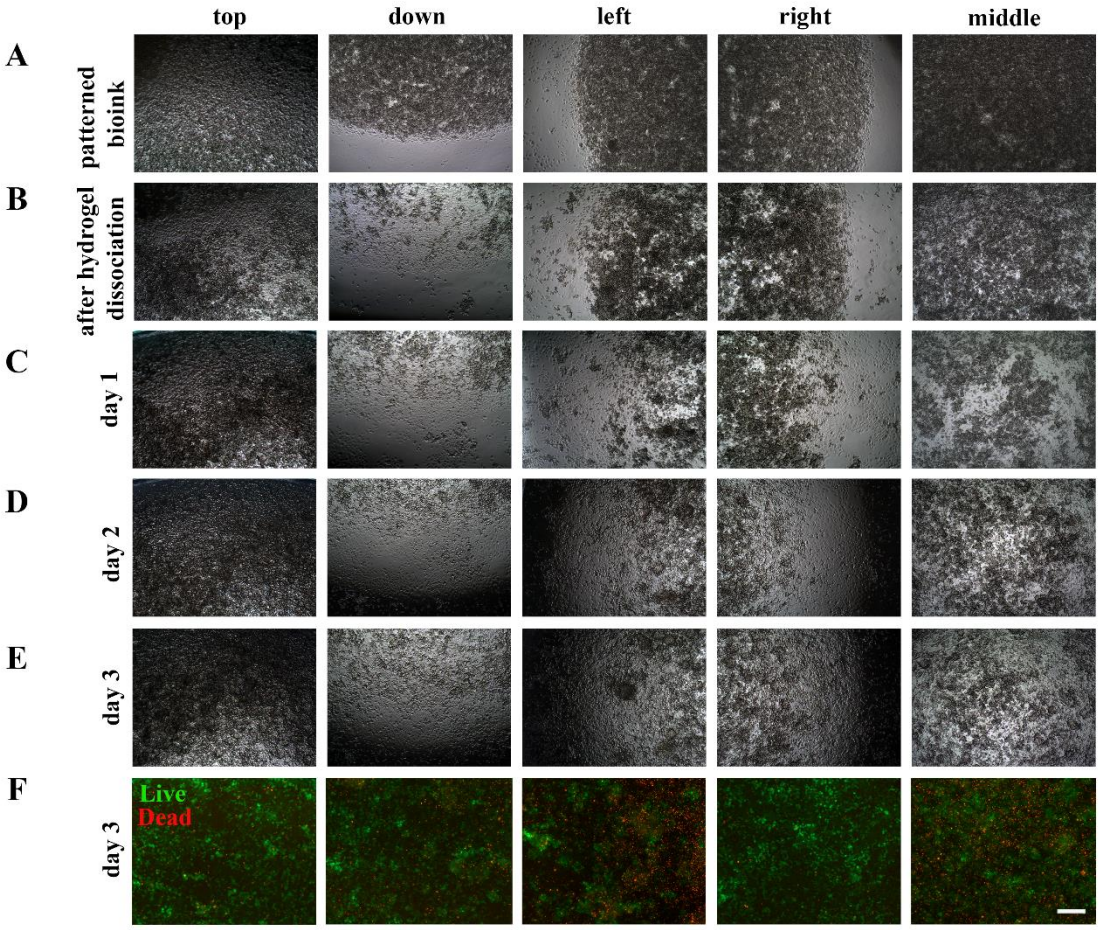

Figure 3.22. Light microscopy and fluorescent images of patterned HeLa cells A) Light microscopy images of patterned bioink B) Light microscopy images of patterned 3D tumor structure after dissociation of Mg-alginate hydrogel C) Light microscopy images of 1day cultured patterned 3D cellular structure E) Light microscopy images of 3day cultured patterned 3D cellular structure F) Fluorescent microscopy images of 3day cultured patterned 3D cellular structure, scale bar: 200 μm

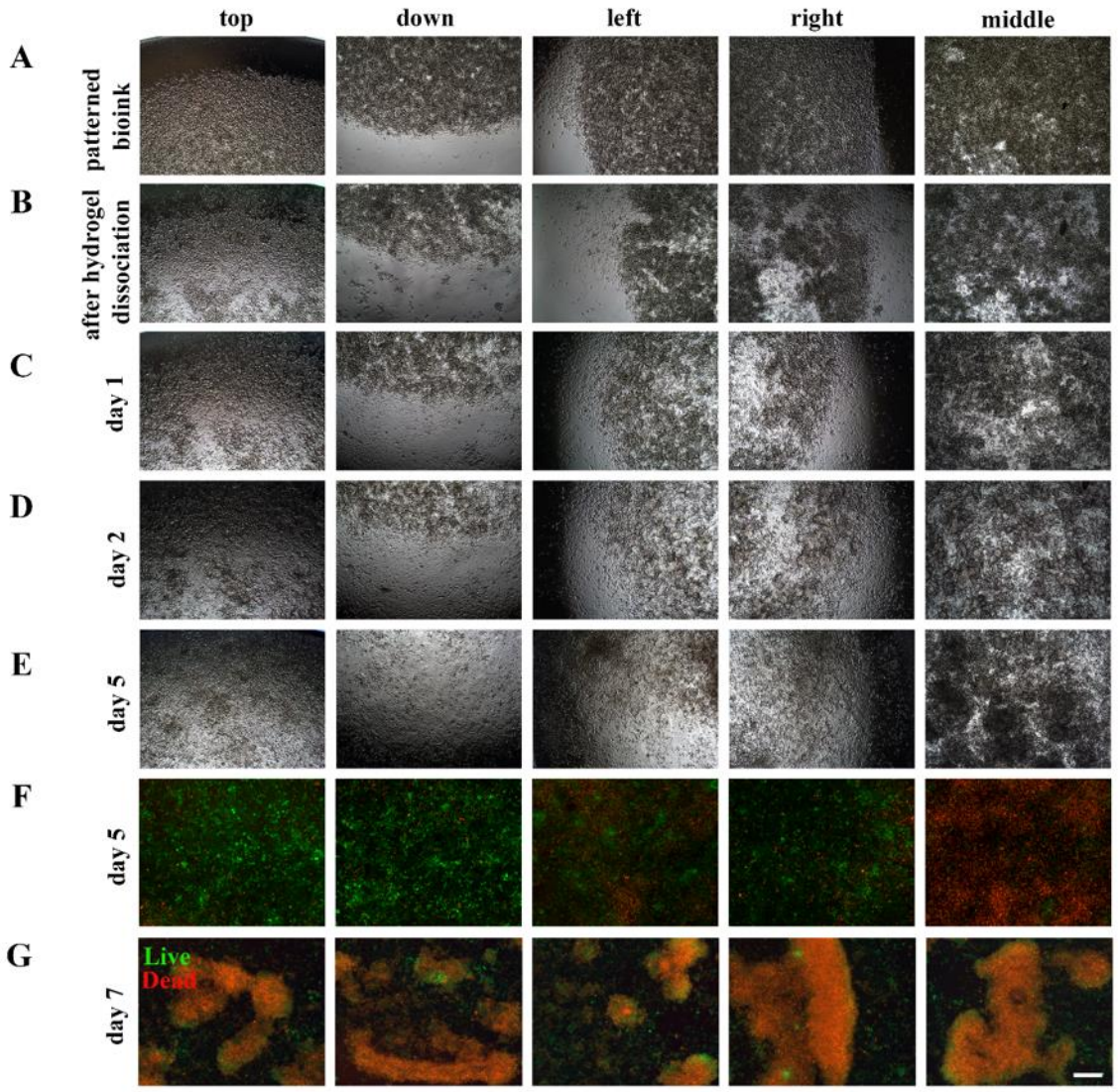

Figure 3.23. Light microscopy and fluorescent images of patterned HeLa cells A) Light microscopy images of patterned bioink B) Light microscopy images of patterned 3D tumor structure after dissociation of Mg-alginate hydrogel C) Light microscopy images of 1day cultured patterned 3D cellular structure E) Light microscopy images of 5day cultured patterned 3D cellular structure F) Fluorescent microscopy images of 5day cultured patterned 3D cellular structure G) Fluorescent microscopy images of 7day cultured patterned 3D cellular structure, scale bar: 200 µm

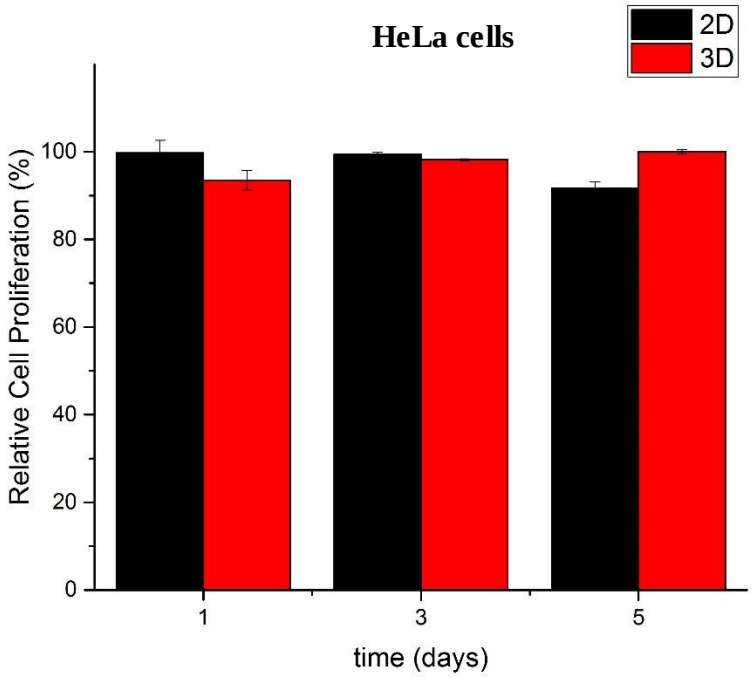

Figure 3.24. Relative cell proliferation of patterned 3D cellular structures of HeLa cells for 1, 3 and 5 day cell culture time obtained via Alamar blue assay

After live/dead analysis, Alamar blue assay was performed for patterned 3D cellular structure to see relative cell proliferation for 1, 3, and 5 day culture period as seen in Figure 3.24. The proliferation of 3D patterned HeLa cells was slightly lower than 2D cultured HeLa cells on the first day. On day 3 and day 5, cell proliferation rate increased to 98 and 99 % for 3D cellular structure while cell proliferation on standard 2D culture decreased to 98 % and 91 % respectively. Results from 3D studies show that 3D environments can significantly favor cell proliferation and cell survival (Duval et al. 2017; Jensen and Teng 2020). The reason for low cell proliferation compared to 2D control for day1 was related to the adaptation period of cells in a 3D cell culture environment. It is well known fact that, cells in 3D cell culture environment need a certain time to adapt to the environment to proliferate. When consider proliferation and migration behavior of long term cultured 3D cellular structure, newly developed method is very motivated to use for drug screening studies. HeLa cells were used in different studies to fabricate *in vitro* cervical tumor model such as 3D printing of Hela cells and gelatin/alginate/fibrinogen hydrogels were reported by Zhao *et al*, and Hela cells showed a higher proliferation rate in

the printed 3D environment compared to 2D monolayer culture (Zhao et al. 2014). Similarly, alginate-gelatin bio-ink was formulated and enabled high fidelity printing for the construction of 3D structure with Hela spheroids which was presented by Othman *et al* (Othman et al. 2020). The applicability of the newly developed Mg-Alginate based biopatterning method was investigated for the formation of 3D tumor models by using varied cancer cells which were SaOS-2 and SH-SY5Y cells in addition to HeLa cells. Same optimized parameters were applied, cell proliferation, migration, and viability of long-term cultured patterned 3D cellular structures were investigated by performing live/dead and Alamar blue analysis. Due to the formation of necrotic core, cell viability was very low in long-term analysis after 7 days for HeLa cells. That's why, live/dead assay was performed for Saos-2 and SH-SY5Y cells at the day 1, 3, and 5 of the 3D cell culturing periods with the bio-patterning method. Also, cell proliferation, migration, and viability of long-term cultured and patterned 3D SH-SY5Y models were examined by performing live/dead and Alamar blue analysis as seen in Figure 3.25, 3.26, 3.27, and 3.28. SH-SY5Y cells, , formed clusters while proliferating. Cell proliferation and migration observed on day 1 and day 3 with high cell viability as seen in Figure 3.25C, Figure 3.25D, Figure 3.25E and Figure 3.26F. End of the day3, patterned SH-SY5Y cells covered all over the well surface with high cell viability according to live/dead assay as shown in Figure 3.26F. However, necrotic core formation was observed from the middle to the outer part on day 5 as seen in Figure 3.27F.

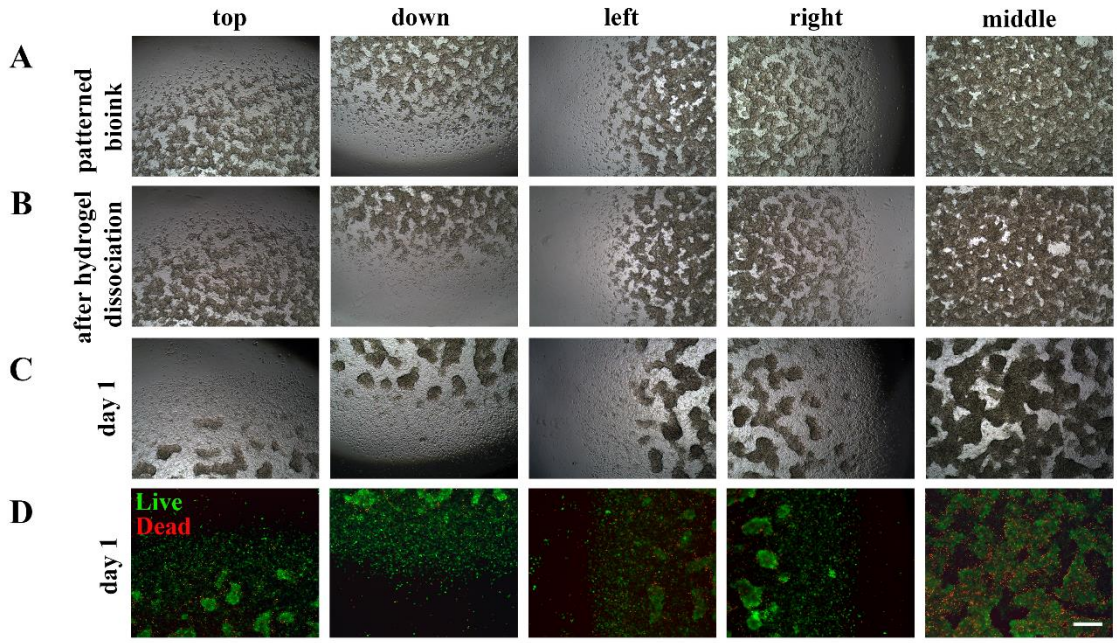

Figure 3.25. Light microscopy and fluorescent images of patterned SH-SY5Y cells A) Light microscopy images of patterned bioink B) Light microscopy images of patterned 3D tumor structure after dissociation of Mg-alginate hydrogel C) Light microscopy images of 1day cultured patterned 3D cellular structure, D) Fluorescent microscopy images of 1day cultured patterned 3D cellular structure scale bar: 200 µm

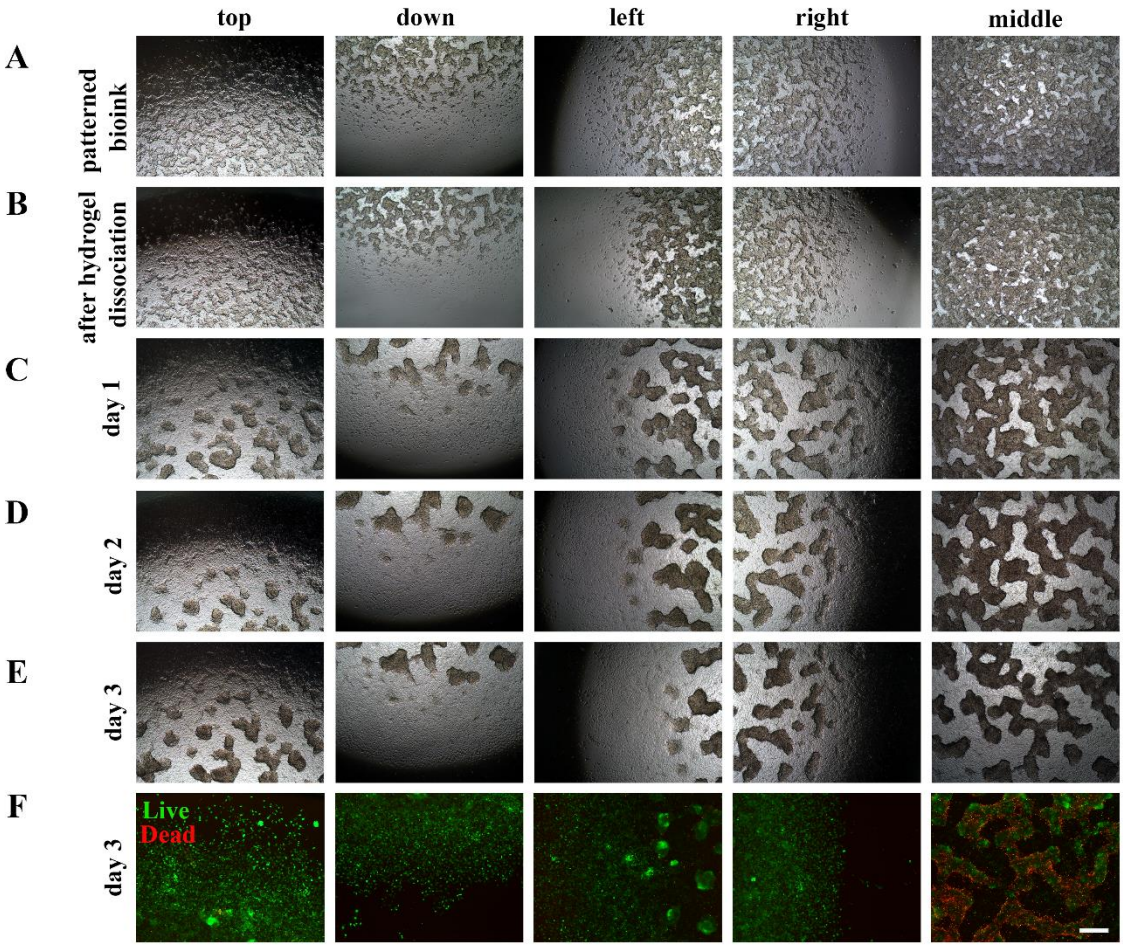

Figure 3.26. Light microscopy and fluorescent images of patterned SH-SY5Y cells A) Light microscopy images of patterned bioink B) Light microscopy images of patterned 3D tumor structure after dissociation of Mg-alginate hydrogel C) Light microscopy images of 1day cultured patterned 3D cellular structure E) Light microscopy images of 3day cultured patterned 3D cellular structure F) Fluorescent microscopy images of 3day cultured patterned 3D cellular structure, scale bar: 200 μm

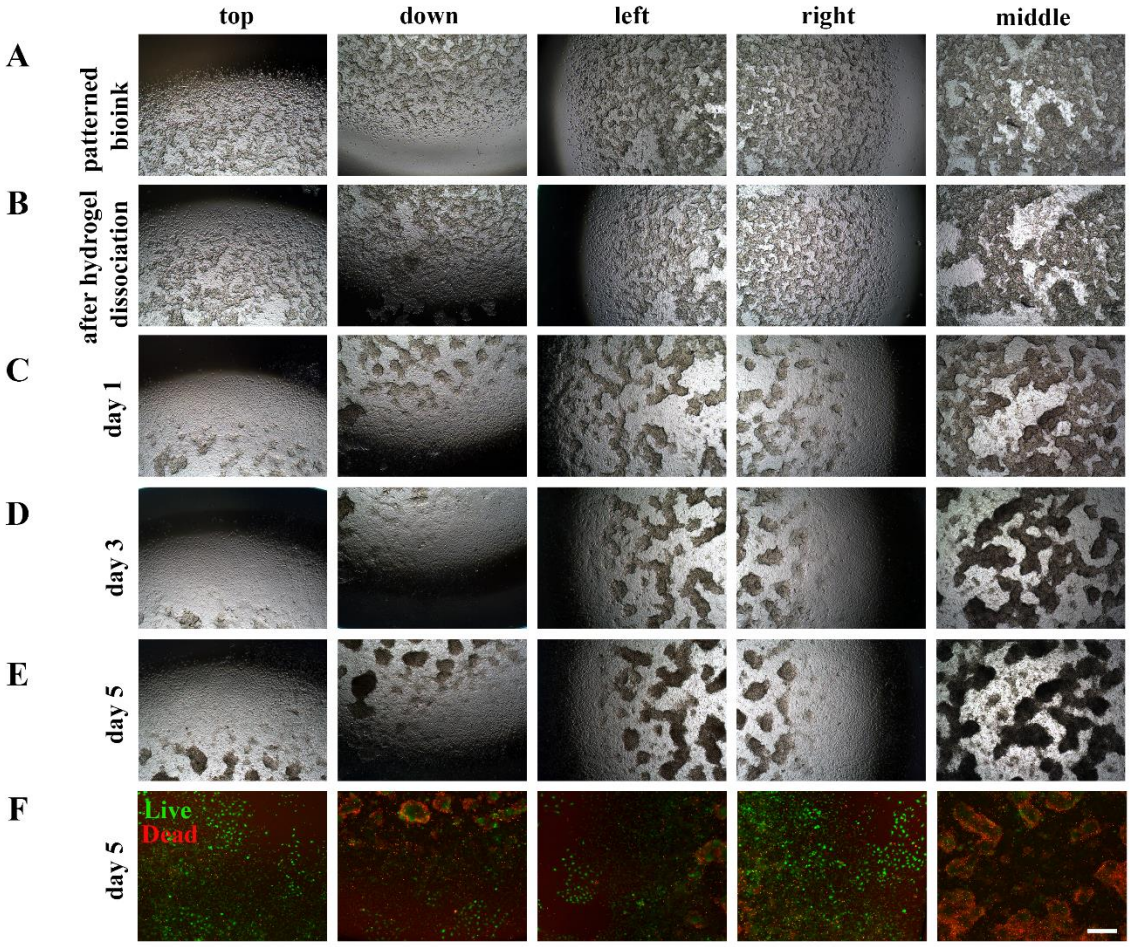

Figure 3.27. Light microscopy and fluorescent images of patterned SH-SY5Y cells A) Light microscopy images of patterned bioink B) Light microscopy images of patterned 3D tumor structure after dissociation of Mg-alginate hydrogel C) Light microscopy images of 1day cultured patterned 3D cellular structure E) Light microscopy images of 5day cultured patterned 3D cellular structure F) Fluorescent microscopy images of 5day cultured patterned 3D cellular structure, scale bar: 200 µm

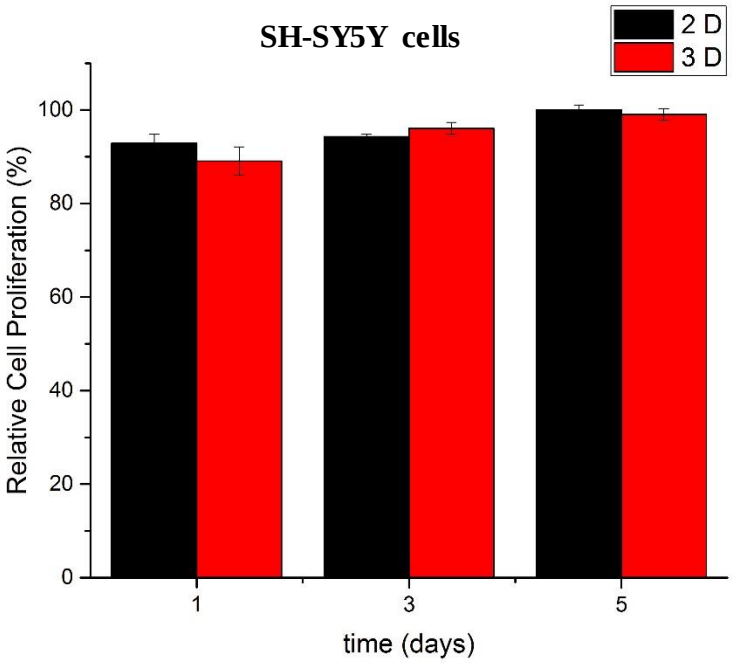

Figure 3.28. Relative cell proliferation of patterned 3D cellular structures of SH-SY5Y cells for 1, 3 and 5 day cell culture time obtained via Alamar blue assay

After live/dead analysis, Alamar blue assay was performed for SH-SY5Y cells in 2D and 3D cell culture system to investigate relative cell proliferation for 1, 3 and 5 day culture period as seen in Figure 3.28. The proliferation of 3D patterned SH-SY5Y cells was slightly lower than 2D cultured SH-SY5Y cells on the first day. Moreover, on day 3 and day 5, the cell proliferation rate reached to 96 and 99 % for 3D cellular structure. Also, cell proliferation on 2D increased to 94 and 100 % respectively. As a result of the proliferation rate, SH-SY5Y cells adapted in a short time to the 3D microenvironment. Deweerd *et al*. showed that neuroblastoma cells regulate their gene expression and change their morphology to respond to a 3D environment in which cells reside and function *in vivo*. Unlike conventional 2D culture, cells form adhesions and receive support on their ventral surfaces in 3D environment (Deweerd, Hoffman-kim, and Ph 2007). Additionally, SH-SY5Y is a human-derived neuroblastoma cell line widely used in neuroscience research. Also, it has the ability to differentiate into post-mitotic neurons using agents such as retinoic acid and brain-derived neurotrophic factors (Innala et al. 2014). Therefore, it was seen as a convenient model for studying Parkinson's and Alzheimer's diseases (Marrazzo, Angeloni, and Hrelia 2019). Neuroblastoma SH-SY5Y cells were also used in newly

synthesized drug screening studies for Alzheimer's disease treatment (Hroudová et al. 2016). Moreover, 3D culture of SH-SY5Y cells favorable more *in vivo*-like morphology and growth of these cells. Carbon nanotubes (CNT) and poly(3,4-ethylenedioxythiophene) (PEDOT) were used as a scaffold in 3D SH-SY5Y culture (Dominguez-Alfaro et al. 2020). Also, collagen hydrogel or porous collagen-based scaffolds were used to form 3D cultures of SH-SY5Y and neuronal cell lines (Desai et al. 2006). Various 3D culture models have been formed with SH-SY5Y cells in terms of cell aggregates, spheroids, or different scaffolds (Innala et al. 2014; Deweerd, Hoffman-kim, and Ph 2007).

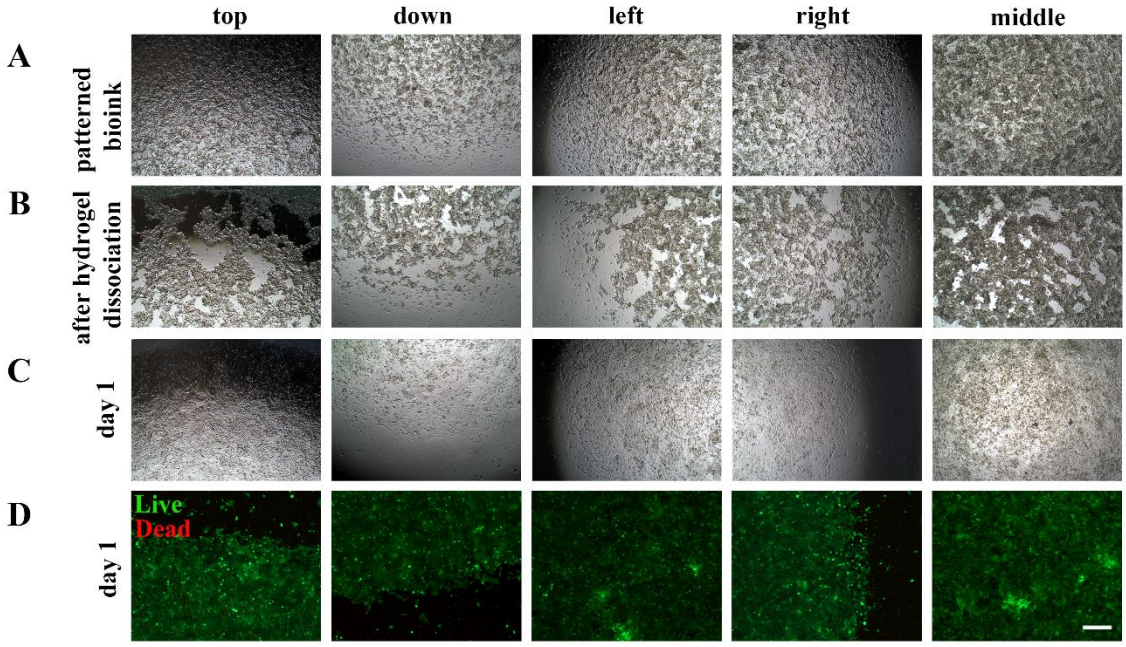

Figure 3.29. Light microscopy and fluorescent images of patterned SaOS-2 cells A) Light microscopy images of patterned bioink B) Light microscopy images of patterned 3D tumor structure after dissociation of Mg-alginate hydrogel C) Light microscopy images of 1day cultured patterned 3D cellular structure D) Fluorescent microscopy images of 1day cultured patterned 3D cellular structure, scale bar: 200 µm

In addition to the 3D neuroblastoma cellular structure, also SaOS-2 cells were used to form 3D osteosarcoma model which is the most common bone tumor that mainly affects children and adolescents (Rimann et al. 2014). Also, cell proliferation, migration and

viability of long term cultured SaOS-2 3D cellular structure was investigated by performing live/dead and Alamar blue analysis as seen in Figure 3.29, 3.30, 3.31 and 3.32. SaOS-2 cells showed similarity with HeLa cells in terms of proliferation and migration behavior. Proliferation and migration of cells were observed starting from day1 to day3 towards to the edges of the well with high cell viability as seen in Figures 3.29 and 3.30. After day 5, as a result of fast proliferation and and migration, entire well surface was covered as seen in Figure 3.31. On day 5, low cell viability was observed due to diffusion limitation as mentioned previously. Eventually, the results showed that Mg-alginate based bio-patterning method applicable to form 3D SaOS-2 cellular structure and it can be a suitable candidate for drug screening applications.

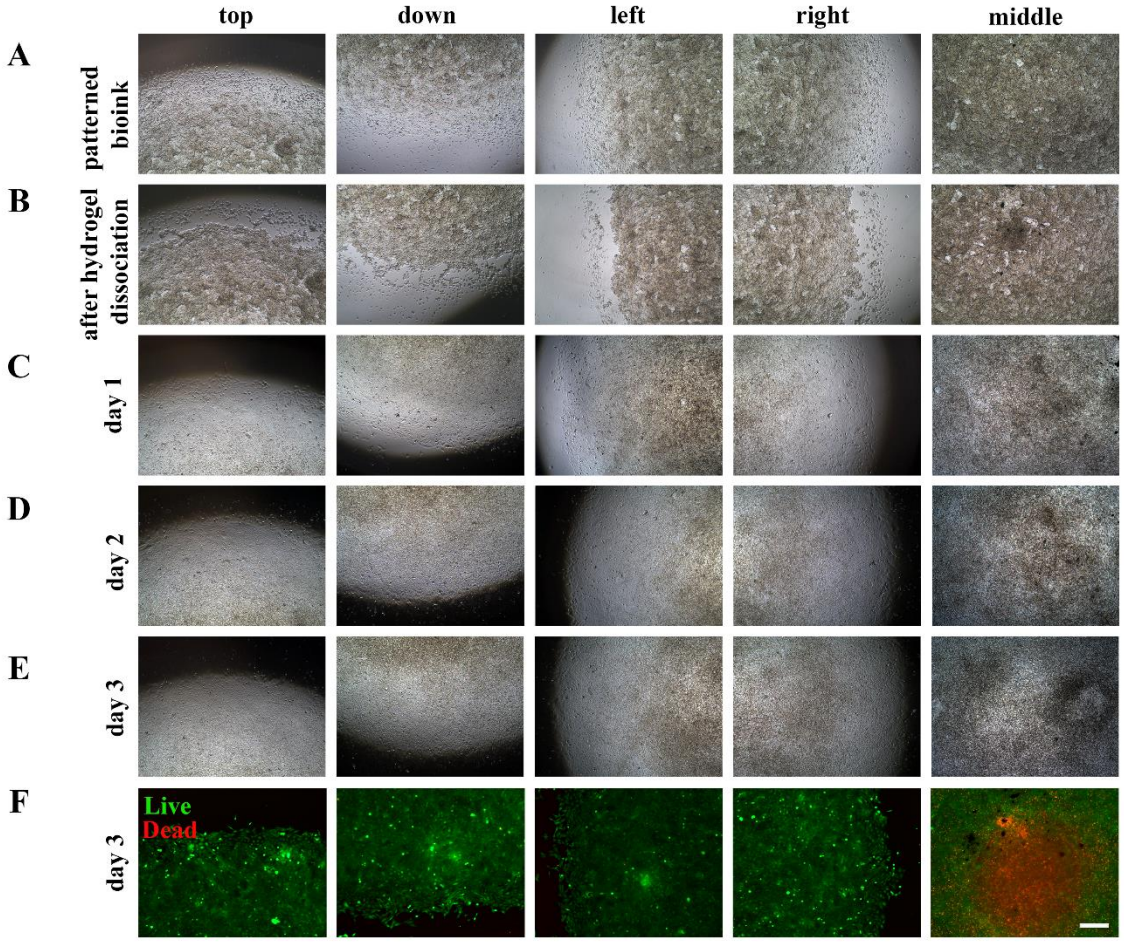

Figure 3.30. Light microscopy and fluorescent images of patterned SaOS-2 cells A) Light microscopy images of patterned bioink B) Light microscopy images of patterned 3D tumor structure after dissociation of Mg-alginate hydrogel C) Light microscopy images of 1day cultured patterned 3D cellular structure E) Light microscopy images of 3day cultured patterned 3D cellular structure F) Fluorescent microscopy images of 3day cultured patterned 3D cellular structure, scale bar: 200 μm

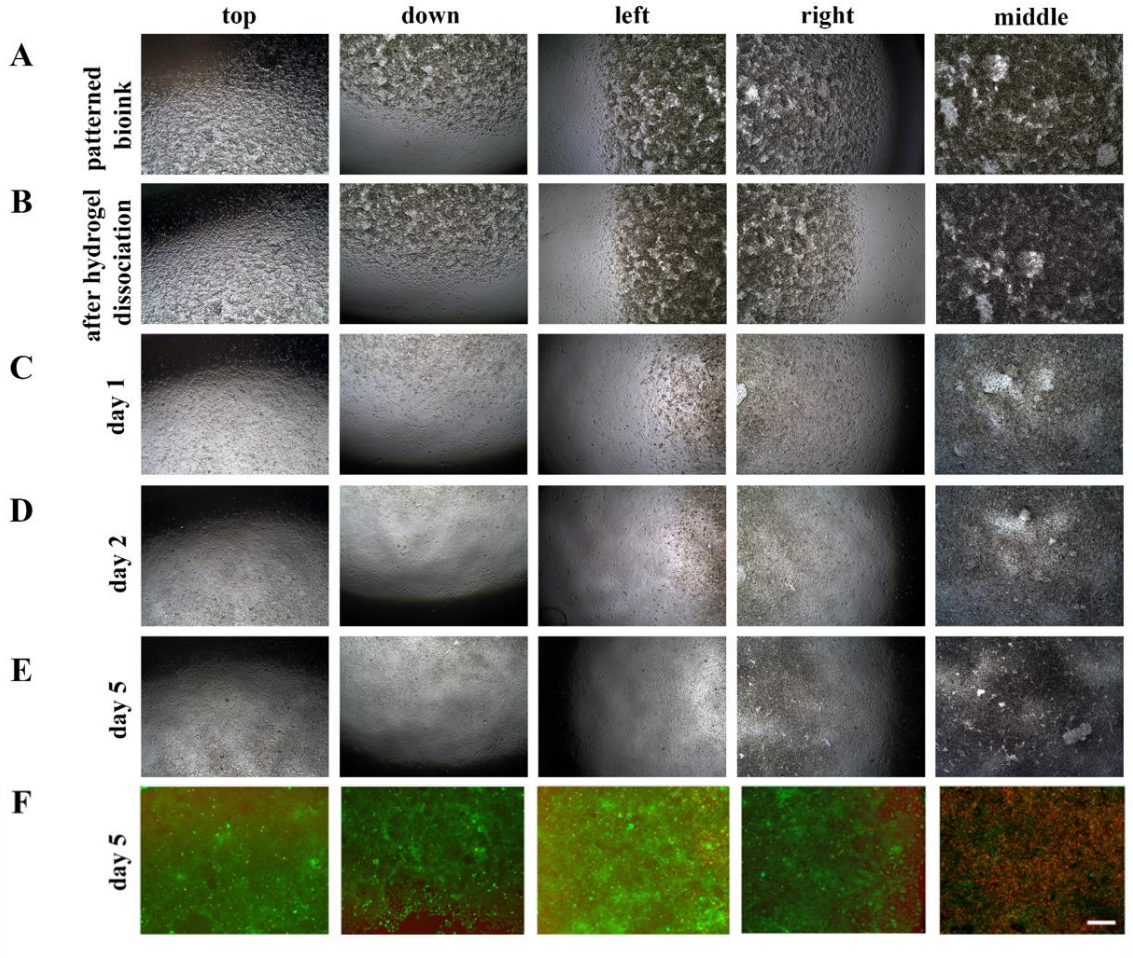

Figure 3.31. Light microscopy and fluorescent images of patterned SaOS-2 cells A) Light microscopy images of patterned bioink B) Light microscopy images of patterned 3D tumor structure after dissociation of Mg-alginate hydrogel C) Light microscopy images of 1day cultured patterned 3D tumor structure E) Light microscopy images of 5day cultured patterned 3D tumor structure F) Fluorescent microscopy images of 5day cultured patterned 3D tumor structure, scale bar: 200 µm

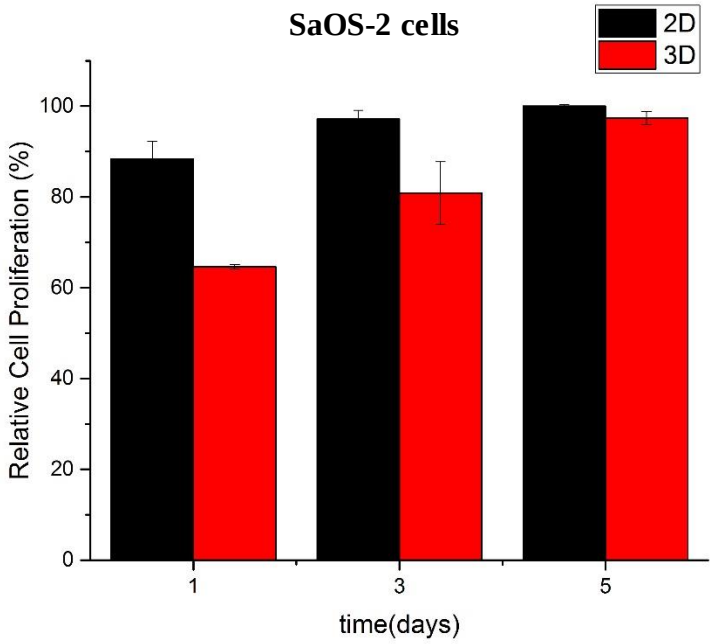

Figure 3.32. Relative cell proliferation of patterned 3D cellular structures of SaOS-2 cells for 1, 3 and 5 day cell culture time obtained via Alamar blue assay

After live/dead analysis, Alamar blue assay was performed for SaOS-2 cells in 2D and 3D cell culture system to evaluate relative cell proliferation for 1, 3 and 5 day culture periods as seen in Figure 3.32. The proliferation rate of 3D patterned SaOS-2 cells lower than 2D cultured SaOS-2 cells on day 1, day 3 and day5 but the gap between 2D and 3D cell culture was decreasing while increasing cell proliferation rate of 3D cellular structure with increasing culturing time. Cell proliferation rate reached to 63, 78, and 94 % for 3D cellular structure on day 1, 3, and 5 respectively which means cells adapted to 3D cell culture environment with increasing culturing time. In addition, cells cultured with hydrogel systems show differences in migration, proliferation behavior, or cell-matrix adhesion compared to the 2D situation (Greiner et al. 2015). Recently, Ojansivu *et al*. reported a bio-ink that was formed with gelatin-alginate and SaOS-2 cells for extrusion-based bioprinting with optimal biological and physicochemical properties (Santander et al. 2007). They evaluated the effect of wood-based cellulose nanofibrils (CNF) and bioactive glass (BaG) on the rheological properties of gelatin-alginate bioinks and the initial responses of bone cells embedded in these inks. Additionally, in another study, SaOS-2

cells were embedded into a alginate hydrogel and four different gelatinous hydrogel matrices were used for suspending SaOS-2 cells to decide whether the biocompatible polymeric silica/biosilica can serve active matrix suitable for 3D cell growth (Müller et al. 2015). The recent studies showed that various polymers can be combined with alginate hydrogels also used as a matrix for 3D cell culture.

3.6. Characterization of patterned 3D tumor models

The immunostaining analysis was performed for patterned 3D cellular structures of HeLa, SaOS-2, and SH-SY5Y cells both for short-term (day 1) and long-term (day 5) culturing time as seen in Figures 3.33, 3.34, and 3.35. The immunostaining analysis of collagen I, F-actin, and DAPI was done to identify cellular and extracellular components of 3D cellular structures. Collagen I secretion was observed clearly for 3D cellular structures of HeLa, SaOS-2, and SH-SY5Y cells for both short and long-term culturing time. Collagen is the main component of the ECM and 3D cellular structures provide more tissue-related environment with producing ECM, cell-matrix, and cell-cell interactions that were missing in standard 2D cultures (Page, Flood, and Reynaud 2013). In addition, immunofluorescent staining of F-actin was performed to indicate the cytoskeletal organization of the 3D cellular structures (Monteiro et al. 2020). F-actin staining of 3D cellular structures were observed clearly after short and long-term incubation for 3D cellular structures including HeLa, SaOS-2, and SH-SY5Y cells. Also, nucleus of cells were visualized via DAPI staining.

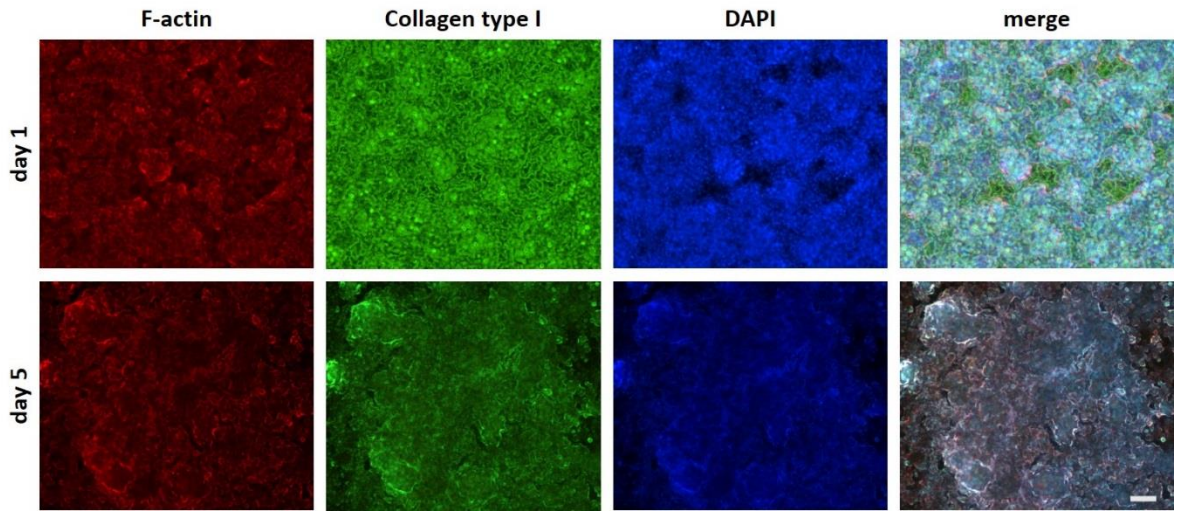

Figure 3.33. Immunofluorescence staining of F-actin, collagen type I and DAPI for 3D cultured HeLa cells for 1 and 5-day culturing time, scale bar: 100 µm

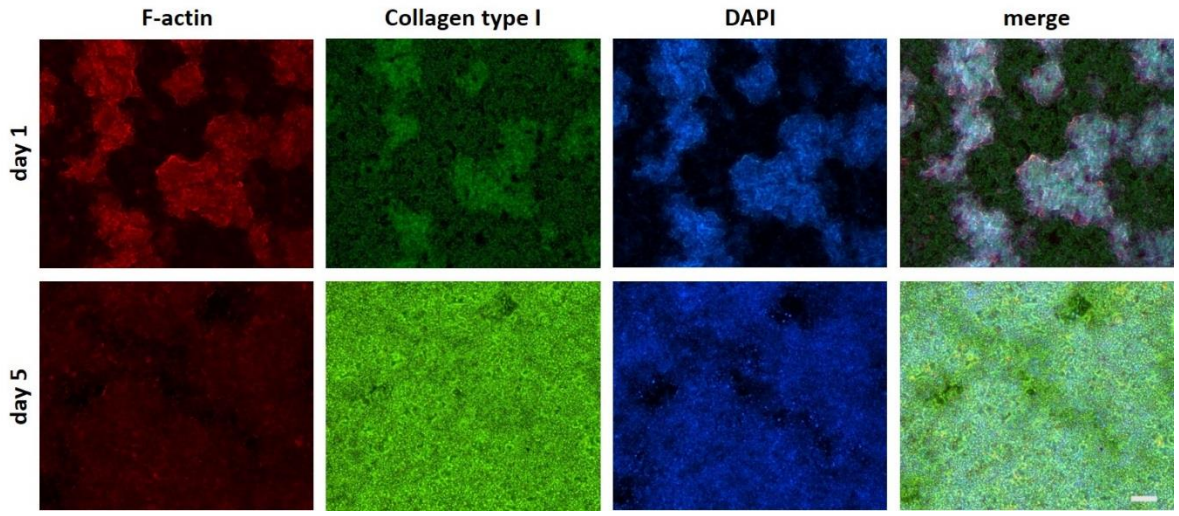

Figure 3.34. Immunofluorescence staining of F-actin, collagen type I and DAPI for 3D cultured SH-SY5Y cells, for 1 and 5-day culturing time, scale bar: 100 µm

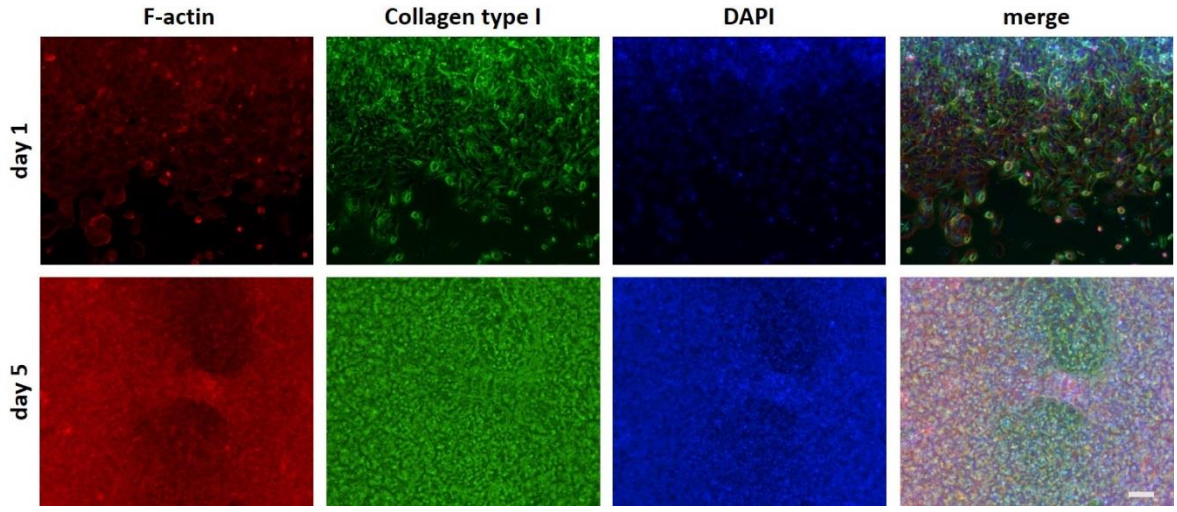

Figure 3.35. Immunofluorescence staining of F-actin, collagen type I and DAPI for 3D cultured SaOS-2 cells, for 1 and 5-day culturing time, scale bar: 100 µm

3.7. Drug screening of patterned 3D tumor models

To evaluate drug response of patterned 3D cellular structures which were fabricated by using HeLa, SaOS-2, and SH-SY5Y cancer cell lines, DOX was applied and cellular viability was screened. DOX is an anticancer agent and commonly used for the treatment of many carcinoma types. Also, it has several cytotoxic effect mechanisms which are intercalation into DNA, inhibition of topoisomerase II, generation of free radicals causing oxidative stress (Hanušová, Boušová, and Skálová 2011). Inhibition of topoisomerase II which is the main anti-proliferative effect result in growth arrest and programmed cell death (Arai et al. 2013). To investigate dose-response for DOX, varied concentration of DOX (0.5, 1, 2.5, 5, 10, 20, 50, 100 µM) was applied after 24h culturing time and MTT assay was performed to evaluate cell viability. IC_{50} values were calculated as 3.3 and 8.2 µM for 2D control and patterned 3D cellular structure for HeLa cells respectively by using GraphPad Prism software as seen in Figure 3.36. Moreover, t-test analysis was performed and resulted as dose-response of 2D control and patterned 3D cellular structure were

significantly different *(p<0.05)* and patterned HeLa cellular structure had significant resistance to DOX compared to standard 2D cell culture. The toxicity of drugs has been investigated for 2D and 3D cell culture models and comparing in terms of drug resistance (Baek et al. 2016; Tung et al. 2011; Godugu et al. 2013). Recently, Baek *et al*. formed 3D spheroids by using HeLa, SH-SY5Y and U2OS cell lines to observe the effect of increasing concentrations of DOX which was investigated based on the integrity and viability of spheroids. Afterward it was seen that HeLa and U2OS maintained their spheroid shape and resulted in higher IC_{50} values (11.2 and 9.7 μM respectively) compared to the 2D system (Baek et al. 2016). Similarly, 3D culture of HeLa cells resulting in higher IC_{50} values than the standard 2D cultures in both bio-patterned cellular structure and spheroid model, since they mimic the *in vivo* microenvironment with extensive cell-cell and cell-ECM interaction. Therefore, 3D tumor model of HeLa cells provide better understood for drug screening applications.

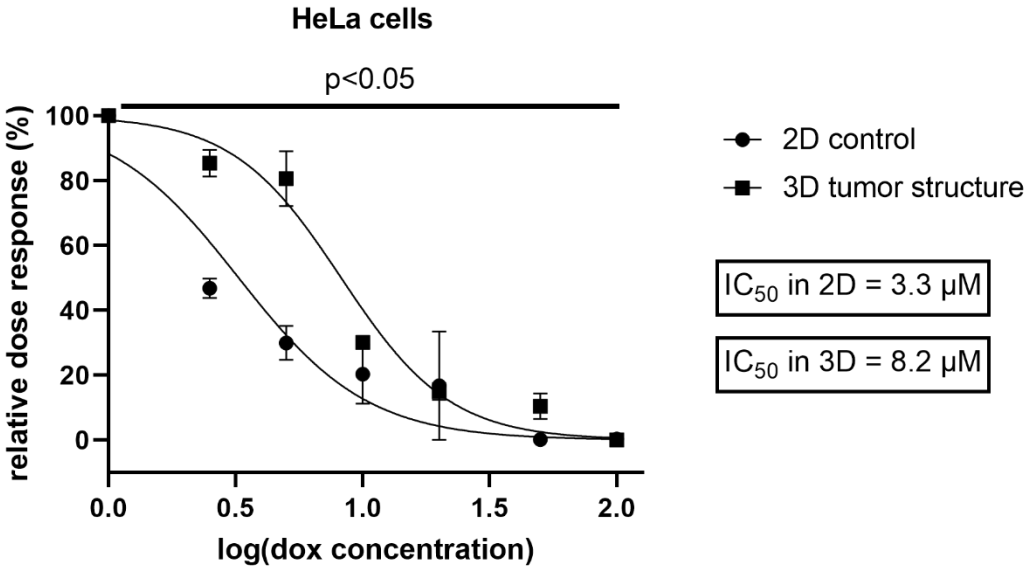

Figure 3.36. Dose response of patterned 3D cellular structure and 2D control for HeLa cells with fitted lines. Error bars represent standard error of mean, p<0.05 compared to control.

Also 3D osteosarcoma model was obtained using SaOS-2 cells via bio-patterning method for drug screening studies and dose response of the 3D tumor model was investigated for DOX. IC_{50} values were obtained for DOX applied 3D tumor model and 2D control as seen in Figure 3.37. IC_{50} values were calculated as 7.0 and 4.4 μM for 3D cellular structure and 2D control respectively. IC_{50} value of 3D cellular structure was significantly higher *($p<0.0001$)* for SaOS-2 compared to standard 2D cell culture according to t-test. Recently, Rimann *et al.* fabricated micro-tissues by the hanging drop method with the osteosarcoma cell lines SaOS-2, HOS, and MG-63. After that, SaOS-2 and HOS cell lines were exposed to doxorubicin, cisplatin, taurolidine, pemetrexed, and taxol, then the cell viability was performed by the Luminescent Cell Viability Assay. As a result, IC_{50} values of 3D cultures were all higher (1.7 to > 16,000-fold) for doxorubicin, cisplatin, taxol and taurolidine when compared to conventional 2D monolayer culture (Rimann et al. 2014). Moreover, Arai *et al.* fabricated spheroids with 11 osteosarcoma cell lines by using NanoCulture plates and they examined the cytotoxic effect of doxorubicin on 2D culture and spheroid conditions. The IC_{50} values were calculated between 0.05 μM and 0.78 μM under 2D culture conditions and between 0.15 μM and 2.62 μM under spheroid culture conditions (Arai et al. 2013). Similarly, 3D culture of SaOS-2 cells resulting in higher IC_{50} values than the standard 2D cultures in bio-patterned cellular structure, micro-tissues that fabricated by hanging drop and spheroids because these models are recapitulating the *in vivo* situation better than the standard monolayer cultures and gaining more significance for drug screening studies. Later on, 3D neuroblastoma model was also formed using SH-SY5Y cells via bio-patterning method for drug screening studies and dose response of the 3D tumor model was investigated for DOX. Unlike HeLa and SaOS-2 cells, drug screening in SH-SY5Y cells was performed at very low concentrations, as SH-SY5Y cells began to respond at very low DOX concentrations.

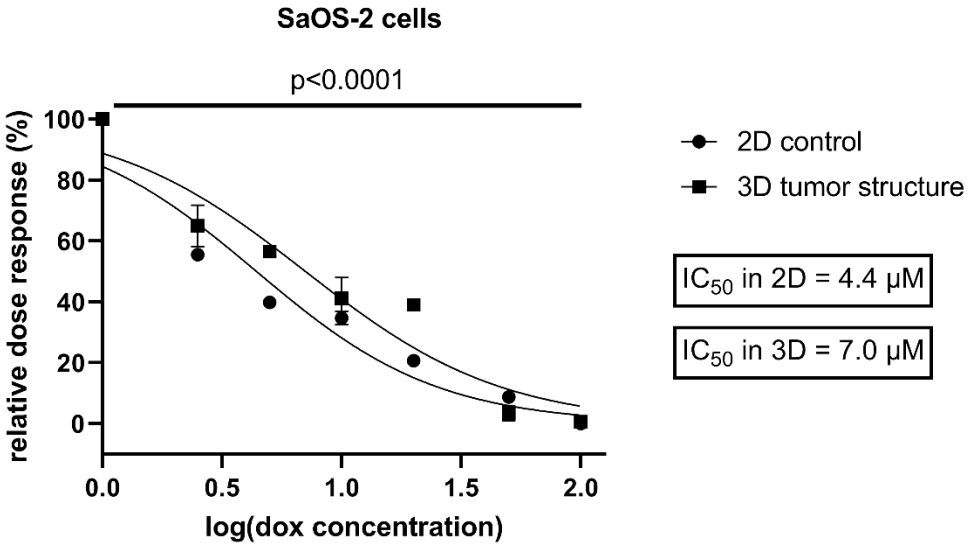

Figure 3.37. Dose response of patterned 3D cellular structure and 2D control for SaOS-2 cells with fitted lines. Error bars represent standard error of mean, $p<0.0001$ compared to control.

IC_{50} values were obtained for DOX applied 3D tumor model and 2D control as seen in Figure 3.38. Also, IC_{50} values were calculated 2.1 and 0.2 µM for 3D tumor model and 2D control respectively. IC_{50} value of 3D model was significantly higher *($p<0.0001$)* in SH-SY5Y compared to standard 2D cell culture according to t-test. Recently, the influences of curcumin and its combined effects with doxorubicin were investigated in SH-SY5Y cells by cell survival assay, flow cytometry and migration assays. 3D spheroid of SH-SY5Y cells were fabricated by hanging drop. The spheroids were exposed to curcumin together with doxorubicin for 24 h and this combined treatment significantly inhibited the spheroid migration (Namkaew et al. 2018). 3D tumor models have close similarity to the *in vivo* microenvironment of tumor tissues compared to monolayer cultures, in particular cell-cell interactions, gene expression profile, as well as the resistance to anticancer drugs. Therefore 3D tumor models have gained increasing interest for anticancer drug screening.

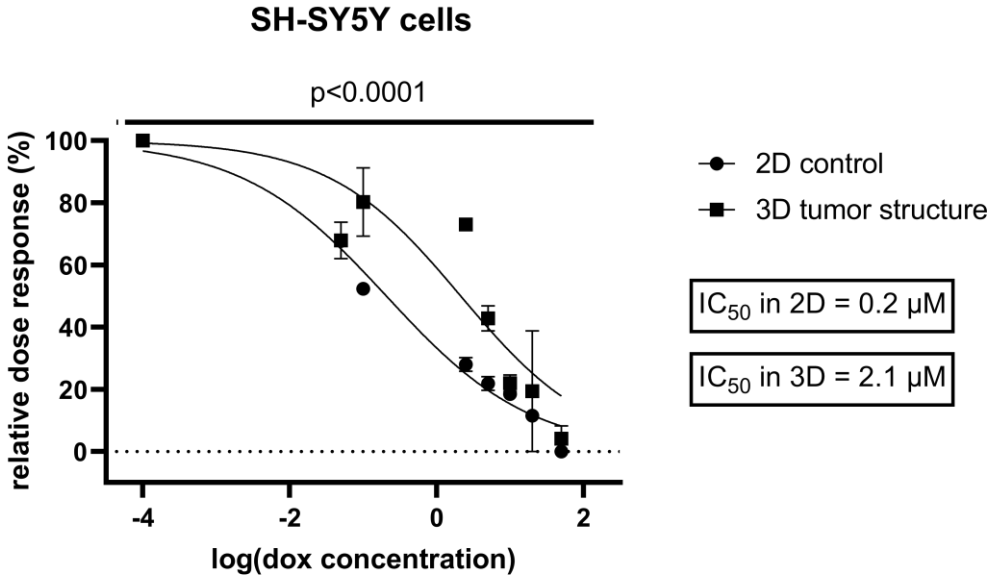

Figure 3.38. Dose response of 3D cellular structure and 2D control for SH-SY5Y cells with fitted lines. Error bars represent standard error of mean, $p<0.0001$ compared to control.

The reasons for the significant differences for 3D cell culture models and 2D cell culture models in terms of drug response related to the fact that 3D structures better mimic the natural cell structure. There is a limited correlation between 2D cultures and *in vivo* systems due to the absence of structural complexity and tissue microenvironment, and lack of cell-cell and cell-ECM interactions which are important for precise prediction of drug or candidate compound (Radhakrishnan et al. 2020). 3D cell culture models mimic the *in vivo* physiology by cell-cell and cell-ECM interactions which affect drug response and contribute to drug resistance unlike in 2D culture systems (Langhans 2018). Also, exposure of molecules between cells on the exterior and cells in the interior, which are completely different in 2D where cells have uniform exposure that is related to the cellular architecture of 3D and 2D cell culture models (Tseng et al. 2015b; Pampaloni, Reynaud, and Stelzer 2007). Likewise, to make straightforward and reliable drug testing, Tung *et al*. formed spheroids by using 384-well format hanging drop culture plate and obtained 3D cellular constructs which showed significant differences in drug responses and chemical resistance by following cell viability with alamarBlue analysis (Tung et al. 2011). Similarly, Wen *et*

al. developed a spheroid-based, 3D culture of pancreatic cancer model for pancreatic drug testing, by using acid phosphatase assay and the results showed that spheroids had higher drug resistance than conventional 2D culture (Wen et al. 2013). In another study, Nirmalanandhan *et al*. cultured cancer cells in 3D collagen gel model to observe the anti-proliferative activity of known lung cancer drugs which were Paclitaxel, Alimta, Zactima, Doxorubicin, Vinorelbine, Gemcitabine, 17AAg, Cisplatin with two lung cancer cell lines (A549 and H358). Their results showed that 3D cultures have significant differences in terms of drug response compared to 2D culture systems by using antiproliferative assay (Nirmalanandhan et al. 2010). The observed differences in the efficacy of anticancer drugs indicate that the biological implications of screening platforms have to be considered for drug candidates in preclinical studies.

CHAPTER 4

CONCLUSION

Cell culture is needed to study cell and tissue physiology. Standard 2D cell culture has been used for typical *in vitro* cell culture but growing cells on plastic surfaces could not mimic natural cell growth. In 3D cell culture, cells behave more natively and interact with their surroundings which represent the *in vivo* microenvironment. Hydrogels are crosslinked networks, commonly used for 3D cell culture with their ability to simulate the nature of most soft tissues. In this thesis a new methodology has been developed based on bio-patterning technique to fabricate 3D cellular structures by using the characteristic of Mg-alginate gelation and fabricated 3D cellular structures were utilized in drug screening studies. In this method, Mg-alginate was the important component of bio-ink because it was used as a carrier material for cells and nanoparticles also allowed cells to attach to surface while providing appropriate viscosity and porosity. In addition to this, it disappears in the environment with its self-dissociation/de-gelation property. Computational methodology was performed for comparison of Ca^{2+} and Mg^{2+}-alginate gelation and showed that the binding energy of Ca^{2+} is extremely high while Mg^{2+} has weak interaction. To obtain the optimum loose structure of Mg-alginate hydrogels, two different commercial alginates which have a different amount of gluronic acid content were characterized in terms of viscosity. Alginate with low viscosity was used for further cell culture studies since it had the lowest viscosity value among them. In bio-patterning method, the bio-ink was obtained by combining Mg-alginate, MNP and cells in optimized formulation, and then by applying external magnetic force, bio-ink was patterned onto the well surface as the shape of magnet. This part was performed in 4 hours incubation and during incubation, the hydrogel dissociates but the cellular structures remain on the surface, and magnetically patterned 3D cellular structures were obtained. Optimization of bio-patterning parameters were analyzed by using Plackett-Burman and Box-Behnken experimental design models by using HeLa cells. Plackett-Burman design was used to eliminate some of optimization

parameters and determine the most effective ones. After the three most effective parameters were selected, these parameters were optimized with Box-Behnken design model. As a result, the optimization steps, the optimized parameters were; 6 µl (5%) Mg-alginate, 400 mM $MgCl_2$ concentration, 2 µl (600 µg/ml) MNP, 2×10^6 of cell number, and 4h incubation of bio-ink. Also, the applicability of the bio-patterning method was investigated by using SaOS-2 and SH-SY5Y cells. Later, cell viability and characterization of bio-patterned 3D cellular structures were analyzed for short term (1 day) and long term (5 days). It was observed that cell viability was high in long term (day 5) after bio-patterning. In the last step, drug screening studies were carried out with DOX to observe dose response of patterned 3D cellular structures. MTT assay was performed to investigate cell viability. IC_{50} values were calculated to compare drug response of 3D cellular structures and 2D culture by using GraphPad Prism software. The IC_{50} values were calculated for 3D cellular structure of HeLa, of SaOS-2 and SH-SY5Y cells as 8.2, 7.8, and 2.1 µM respectively while IC_{50} values of 2D controls obtained as 3.2, 4.4, and 0.2 µM respectively. As a result, it was observed that the drug resistance of 3D tumor structures of HeLa, SaOS-2 and SH-SY5Y were significantly higher compared to standard 2D cell culture according to t-test statistical analysis. Finally, it is seen that 3D cellular structures fabricated by Mg-alginate based bio-patterning method are promising experimental platforms for drug screening studies. At the same time, it is important that the cells can be patterned in a short time and require no extra chemical to remove the hydrogel from environment. In addition, this developed methodology is easy to apply, cheap and time-saving.

REFERENCES

Abdel Fattah, Abdel Rahman, Elvira Meleca, Sarah Mishriki, Alina Lelic, Fei Geng, Rakesh P. Sahu, Suvojit Ghosh, and Ishwar K. Puri. 2016. "In Situ 3D Label-Free Contactless Bioprinting of Cells through Diamagnetophoresis." *ACS Biomaterials Science and Engineering* 2 (12): 2133–38. https://doi.org/10.1021/acsbiomaterials.6b00614.

Achilli, Matteo, Jean Lagueux, and Diego Mantovani. 2010. "On the Effects of UV-C and PH on the Mechanical Behavior, Molecular Conformation and Cell Viability of Collagen-Based Scaffold for Vascular Tissue Engineering." *Macromolecular Bioscience* 10 (3): 307–16. https://doi.org/10.1002/mabi.200900248.

Alhaque, Sharmin, Michael Themis, and Hassan Rashidi. 2018. "Three-Dimensional Cell Culture: From Evolution to Revolution." *Philosophical Transactions of the Royal Society B: Biological Sciences* 373 (1750). https://doi.org/10.1098/rstb.2017.0216.

Amaral, Robson L.F., Mariza Miranda, Priscyla D. Marcato, and Kamilla Swiech. 2017. "Comparative Analysis of 3D Bladder Tumor Spheroids Obtained by Forced Floating and Hanging Drop Methods for Drug Screening." *Frontiers in Physiology*. https://doi.org/10.3389/fphys.2017.00605.

Anton, Delphine, Hélène Burckel, Elodie Josset, and Georges Noel. 2015. "Three-Dimensional Cell Culture: A Breakthrough in Vivo." *International Journal of Molecular Sciences* 16 (3): 5517–27. https://doi.org/10.3390/ijms16035517.

Arai, Kazuya, Ruriko Sakamoto, Daisuke Kubota, and Tadashi Kondo. 2013. "Proteomic Approach toward Molecular Backgrounds of Drug Resistance of Osteosarcoma Cells in Spheroid Culture System." *Proteomics* 13 (15): 2351–60. https://doi.org/10.1002/pmic.201300053.

Augst, Alexander D, Hyun Joon Kong, and David J Mooney. 2006. "Alginate Hydrogels as Biomaterials." *Macromolecular Bioscience*, no. 6: 623–33. https://doi.org/10.1002/mabi.200600069.

Awad, Hani A., M. Quinn Wickham, Holly A. Leddy, Jeffrey M. Gimble, and Farshid Guilak. 2004. "Chondrogenic Differentiation of Adipose-Derived Adult Stem Cells in Agarose, Alginate, and Gelatin Scaffolds." *Biomaterials* 25 (16): 3211–22. https://doi.org/10.1016/j.biomaterials.2003.10.045.

Baek, Nam Huk, Ok Won Seo, Min Sung Kim, John Hulme, and Seong Soo A. An. 2016. "Monitoring the Effects of Doxorubicin on 3D-Spheroid Tumor Cells in Real-Time." *OncoTargets and Therapy* 9: 7207–18. https://doi.org/10.2147/OTT.S112566.

Bissell, Mina J., and Derek Radisky. 2001. "Putting Tumours in Context." *Nature Reviews Cancer* 1 (1): 46–54. https://doi.org/10.1038/35094059.

Blochl, P. E. 1994. "Projector Augmented-Wave Method." *The American Physical Society* 50 (24).

Blomme, Eric A. G. 2016. "Toxicology Strategies for Drug Discovery: Present and Future." *Chemical Research Toxicology*, no. 29: 473–504.

Borlak, Jürgen, Prafull Kumar Singh, and Ina Rittelmeyer. 2015. "Regulation of Liver Enriched Transcription Factors in Rat Hepatocytes Cultures on Collagen and EHS Sarcoma Matrices," 1–23. https://doi.org/10.1371/journal.pone.0124867.

Bowler, David R, and Angelos Michaelides. 2011. "Van Der Waals Density Functionals Applied to Solids." *American Physical Society* 195131: 1–13. https://doi.org/10.1103/PhysRevB.83.195131.

Bracken, Michael B. 2008. "Why Animal Studies Are Often Poor Predictors of Human Reactions to Exposure." *J R Soc Med* 101: 120–22.

Brancato, Virginia, Joaquim Miguel Oliveira, Vitor Manuel Correlo, Rui Luis Reis, and Subhas C. Kundu. 2020. "Could 3D Models of Cancer Enhance Drug Screening?" *Biomaterials* 232 (December 2019): 119744. https://doi.org/10.1016/j.biomaterials.2019.119744.

Breslin, Susan, and Lorraine O'Driscoll. 2013. "Three-Dimensional Cell Culture: The Missing Link in Drug Discovery." *Drug Discovery Today* 18 (5–6): 240–49. https://doi.org/10.1016/j.drudis.2012.10.003.

Caliari, Steven R., and Jason A. Burdick. 2016. "A Practical Guide to Hydrogels for Cell Culture." *Nature Methods* 13 (5): 405–14. https://doi.org/10.1038/nmeth.3839.

Canton, Irene, Robert Mckean, Mirren Charnley, Keith A. Blackwood, Calogero Fiorica, Anthony J. Ryan, and Sheila MacNeil. 2010. "Development of an Ibuprofen-releasing Biodegradable PLA/PGA Electrospun Scaffold for Tissue Regeneration." *Biotechnology and Bioengineering* 105 (2): 396–408.

Carlsson, J., and J. M. Yuhas. 1984. "Liquid-Overlay Culture of Cellular Spheroids." *Recent Results in Cancer Research. Fortschritte Der Krebsforschung. Progrès Dans Les Recherches Sur Le Cancer* 95 (Foa 4): 1–23. https://doi.org/10.1007/978-3-642-82340-4_1.

Catoira, Marta Calvo, Luca Fusaro, Dalila Di Francesco, Martina Ramella, and Francesca Boccafoschi. 2019. "Overview of Natural Hydrogels for Regenerative Medicine Applications." *Journal of Materials Science: Materials in Medicine*. https://doi.org/10.1007/s10856-019-6318-7.

Cheng, Shuk Y A N, Marcus Chun, W A H Yuen, C H I W A I Kan, Kevin Ka, Leung Cheuk, Chung H I N Chui, and K I M Hung Lam. 2009. "Cosmetic Textiles with Biological Benefits : Gelatin Microcapsules Containing Vitamin C." *International Journal Of Molecular Medicine* 24: 411–19. https://doi.org/10.3892/ijmm.

Choi, Sung-wook, Yi-chun Yeh, Yu Zhang, Hsing-wen Sung, and Younan Xia. 2010. "Uniform Beads with Controllable Pore Sizes for Biomedical Applications **," no. 14: 1492–98. https://doi.org/10.1002/smll.201000544.

Chung, Bong Geun, Kwang-Ho Lee, Ali Khademhosseini, and Sang-Hoon Lee. 2012. "Microfluidic Fabrication of Microengineered Hydrogels and Their Application in Tissue Engineering." *Lab on a Chip* 12: 45–49.

Daquinag, Alexes C., Glauco R. Souza, and Mikhail G. Kolonin. 2013. "Adipose Tissue Engineering in Three-Dimensional Levitation Tissue Culture System Based on Magnetic Nanoparticles." *Tissue Engineering. Part C, Methods* 19 (5): 336–44. https://doi.org/10.1089/ten.tec.2012.0198.

Desai, Anu, William S Kisaalita, Charles Keith, and Z Wu. 2006. "Human Neuroblastoma (SH-SY5Y) Cell Culture and Differentiation in 3-D Collagen Hydrogels for Cell-Based Biosensing." *Biosensors and Bioelectronics* 21: 1483–92. https://doi.org/10.1016/j.bios.2005.07.005.

Deweerd, Elizabeth S, Diane Hoffman-kim, and D Ph. 2007. "Genomic and Morphological Changes of Neuroblastoma Cells." *Tissue Engineering* 13 (5). https://doi.org/10.1089/ten.2006.0251.

Dolder, Juliette Van Den, Paul H.M. Spauwen, and John A. Jansen. 2003. "Evaluation of Various Seeding Techniques for Culturing Osteogenic Cells on Titanium Fiber Mesh." *Tissue Engineering* 9 (2): 315–25. https://doi.org/10.1089/107632703764664783.

Dolega, Monika E., Fabien Abeille, Nathalie Picollet-D'hahan, and Xavier Gidrol. 2015. "Controlled 3D Culture in Matrigel Microbeads to Analyze Clonal Acinar Development." *Biomaterials* 52: 347–57.

Dominguez-Alfaro, Antonio, Nuria Alegret, Blanca Arnaiz, Maitane Salsamendi, David Mecerreyes, and Maurizio Prato. 2020. "Toward Spontaneous Neuronal Differentiation of SH-SY5Y Cells Using Novel Three-Dimensional Electropolymerized Conductive Scaffolds." *ACS Applied Materials and Interfaces*. https://doi.org/10.1021/acsami.0c16645.

Donati, Ivan, Fioretta Asaron, and Sergio Paoletti. 2009. "Experimental Evidence of Counterion Affinity in Alginates: The Case of Nongelling Ion Mg2+." *Journal of Physical Chemistry B* 113 (39): 12877–86. https://doi.org/10.1021/jp902912m.

Donati, Ivan, Attilio Cesàro, and Sergio Paoletti. 2006. "Specific Interactions versus Counterion Condensation. 1. Nongelling Ions/Polyuronate Systems." *Biomacromolecules* 7 (1): 281–87. https://doi.org/10.1021/bm050646p.

Draget, K I. n.d. "Alginates." In *Handbook of Hydrocolloids*.

Draget, Kurt Ingar, Prof Olav Smidsrùd, and Prof Gudmund Skjåk-brñk. 2005. "Alginates from Algae," 1–30.

Drury, Jeanie L., and David J. Mooney. 2003. "Hydrogels for Tissue Engineering: Scaffold

Design Variables and Applications." *Biomaterials* 24 (24): 4337–51. https://doi.org/10.1016/S0142-9612(03)00340-5.

Duval, Kayla, Hannah Grover, Li Hsin Han, Yongchao Mou, Adrian F. Pegoraro, Jeffery Fredberg, and Zi Chen. 2017. "Modeling Physiological Events in 2D vs. 3D Cell Culture." *Physiology* 32 (4): 266–77. https://doi.org/10.1152/physiol.00036.2016.

Éamonn, D, and C David. 2010. "Higher-Accuracy van Der Waals Density Functional." *The American Physical Society* 82. https://doi.org/10.1103/PhysRevB.82.081101.

Edmondson, Rasheena, Jessica Jenkins Broglie, Audrey F. Adcock, and Liju Yang. 2014. "Three-Dimensional Cell Culture Systems and Their Applications in Drug Discovery and Cell-Based Biosensors." *Assay and Drug Development Technologies* 12 (4): 207–18. https://doi.org/10.1089/adt.2014.573.

Ekert, Jason E., Kjell Johnson, Brandy Strake, Jose Pardinas, Stephen Jarantow, Robert Perkinson, and David C. Colter. 2014. "Three-Dimensional Lung Tumor Microenvironment Modulates Therapeutic Compound Responsiveness in Vitro - Implication for Drug Development." *PLoS ONE* 9 (3): 1–14. https://doi.org/10.1371/journal.pone.0092248.

Fan, Rong, Marine Piou, Evan Darling, Denis Cormier, Jun Sun, and Jiandi Wan. 2016. "Bio-Printing Cell-Laden Matrigel–Agarose Constructs." *Journal of Biomaterials Applications* 31 (5): 684–92.

Foox, Maytal, and Meital Zilberman. 2015. "Drug Delivery from Gelatin-Based Systems," 8–10. https://doi.org/10.1517/17425247.2015.1037272.

Frampton, J P, M R Hynd, M L Shuler, and W Shain. n.d. "Fabrication and Optimization of Alginate Hydrogel Constructs for Use in 3D Neural Cell Culture" 015002. https://doi.org/10.1088/1748-6041/6/1/015002.

Gerecht, Sharon, Jason A. Burdick, Lino S. Ferreira, Seth A. Townsend, Robert Langer, and Gordana Vunjak-Novakovic. 2007. "Hyaluronic Acid Hydrogel for Controlled Self-Renewal and Differentiation of Human Embryonic Stem Cells." *Proceedings of the National Academy of Sciences of the United States of America* 104 (27): 11298–

303. https://doi.org/10.1073/pnas.0703723104.

Godugu, Chandraiah, Apurva R. Patel, Utkarsh Desai, Terrick Andey, Alexandria Sams, and Mandip Singh. 2013. "AlgiMatrix™ Based 3D Cell Culture System as an In-Vitro Tumor Model for Anticancer Studies." *PLoS ONE* 8 (1). https://doi.org/10.1371/journal.pone.0053708.

Gombotz, Wayne R., and Siow Fong Wee. 2012. "Protein Release from Alginate Matrices." *Advanced Drug Delivery Reviews* 64 (SUPPL.): 194–205. https://doi.org/10.1016/j.addr.2012.09.007.

GRANT, Gregor T., Edwin R. MORRIS, David A. REES, Peter J.C SMITH, and David THOM. 1973. "Biological Interactions between Polysaccharides and Divalent Cations: The Egg-Box Model." *FEBS LETTERS* 32: 195–98.

Greiner, Alexandra M., Franziska Klein, Tetyana Gudzenko, Benjamin Richter, Thomas Striebel, Bayu G. Wundari, Tatjana J. Autenrieth, Martin Wegener, Clemens M. Franz, and Martin Bastmeyer. 2015. "Cell Type-Specific Adaptation of Cellular and Nuclear Volume in Micro-Engineered 3D Environments." *Biomaterials*, no. 69: 121–32.

Griffith, Linda G., and Melody A. Swartz. 2006. "Capturing Complex 3D Tissue Physiology in Vitro." *Nature Reviews Molecular Cell Biology* 7 (3): 211–24. https://doi.org/10.1038/nrm1858.

Gunatillake, Pathiraja A., Raju Adhikari, and N. Gadegaard. 2003. "Biodegradable Synthetic Polymers for Tissue Engineering." *European Cells and Materials*. https://doi.org/10.22203/eCM.v005a01.

Gündoıdu, Tuıba Keskin, Ġrem Deniz, Gülizar Çalişkan, Erdem Sefa Şahin, and Nuri Azbar. 2016. "Experimental Design Methods for Bioengineering Applications." *Critical Reviews in Biotechnology* 36 (2): 368–88. https://doi.org/10.3109/07388551.2014.973014.

Haisler, William L., David M. Timm, Jacob A. Gage, Hubert Tseng, T. C. Killian, and Glauco R. Souza. 2013. "Three-Dimensional Cell Culturing by Magnetic Levitation."

Nature Protocols 8 (10): 1940–49. https://doi.org/10.1038/nprot.2013.125.

Hamidi, Mehrdad, Amir Azadi, and Pedram Rafiei. 2008. "Hydrogel Nanoparticles in Drug Delivery." *Advanced Drug Delivery Reviews* 60 (15): 1638–49. https://doi.org/10.1016/j.addr.2008.08.002.

Hanušová, Veronika, Iva Boušová, and Lenka Skálová. 2011. "Possibilities to Increase the Effectiveness of Doxorubicin in Cancer Cells Killing" 43 (May): 540–57. https://doi.org/10.3109/03602532.2011.609174.

Hayward, Adam S., Naoko Sano, Stefan A. Przyborski, and Neil R. Cameron. 2013. "Acrylic-Acid-Functionalized Polyhipe Scaffolds for Use in 3d Cell Culture." *Macromolecular Rapid Communications* 34 (23–24): 1844–49. https://doi.org/10.1002/marc.201300709.

Heberer, Michael, Ivan Martin, D Ph, and Marcel Jakob. 2021. "Three-Dimensional Cell Culture and Tissue Engineering in a T-CUP (Tissue Culture Under Perfusion) ¨" 13 (8). https://doi.org/10.1089/ten.2006.0158.

Henkelman, Graeme, Andri Arnaldsson, and Hannes Jo´nsson. 2006. "A Fast and Robust Algorithm for Bader Decomposition of Charge Density." *Computational Material Science* 36: 354–60.

Hou, Shurong, Hervé Tiriac, Banu Priya Sridharan, Louis Scampavia, Franck Madoux, Jan Seldin, Glauco R. Souza, Donald Watson, David Tuveson, and Timothy P. Spicer. 2018. "Advanced Development of Primary Pancreatic Organoid Tumor Models for High-Throughput Phenotypic Drug Screening." *SLAS Discovery* 23 (6): 574–84. https://doi.org/10.1177/2472555218766842.

Hroudová, Jana, Namrata Singh, Zdeněk Fišar, and Kallol K. Ghosh. 2016. "Progress in Drug Development for Alzheimer's Disease: An Overview in Relation to Mitochondrial Energy Metabolism." *European Journal of Medicinal Chemistry*. https://doi.org/10.1016/j.ejmech.2016.03.084.

Hu, Yuhang, Jin-Oh You, and Joanna Aizenber. 2016. "Micropatterned Hydrogel Surface with High-Aspect-Ratio Featuresfor Cell Guidance and Tissue Growth." *ACS Applied*

Materials and Interfaces 8: 21939–45.

Ikada, Yoshito. 2006. "Challenges in Tissue Engineering." *Journal of The Royal Society Interface* 3: 589–601.

Imamura, Yoshinori, Toru Mukohara, Yohei Shimono, Yohei Funakoshi, Naoko Chayahara, Masanori Toyoda, Naomi Kiyota, et al. 2015. "Comparison of 2D- and 3D-Culture Models as Drug-Testing Platforms in Breast Cancer." *Oncology Reports* 33 (4): 1837–43. https://doi.org/10.3892/or.2015.3767.

Inamdar, Niraj K, and Jeffrey T Borenstein. 2011. "Microfluidic Cell Culture Models for Tissue Engineering." *Current Opinion in Biotechnology* 22: 681–89.

Innala, Marcus, Ilse Riebe, Volodymyr Kuzmenko, Johan Sundberg, Paul Gatenholm, Eric Hanse, and Sara Johannesson. 2014. "3D Culturing and Differentiation of SH-SY5Y Neuroblastoma Cells on Bacterial Nanocellulose Scaffolds." *Artificial Cells, Nanomedicine, and Biotechnology* 42: 302–8.

Ito, Akira, and Hiroyuki Honda. 2007. "Magnetic Nanoparticles for Tissue Engineering." *Nanotechnologies for the Life Sciences* 9: 308–37. https://doi.org/10.1002/9783527610419.ntls0102.

Jaganathan, Hamsa, Jacob Gage, Fransisca Leonard, Srimeenakshi Srinivasan, Glauco R. Souza, Bhuvanesh Dave, and Biana Godin. 2014. "Three-Dimensional in Vitro Co-Culture Model of Breast Tumor Using Magnetic Levitation." *Scientific Reports* 4: 1–9. https://doi.org/10.1038/srep06468.

Jaipan, Panupong, Material Science, and North Carolina. 2017. "Gelatin-Based Hydrogels for Biomedical Applications." *MRS Communications* 7: 416–26. https://doi.org/10.1557/mrc.2017.92.

Jang, Jae Myung, Si-Hoai-Trung Tran, Sang Cheol Na, and Noo Li Jeon. 2015. "Engineering Controllable Architecture in Matrigel for 3D Cell Alignment." *ACS Applied Materials and Interfaces* 7: 2183–88.

Jensen, Caleb, and Yong Teng. 2020. "Is It Time to Start Transitioning From 2D to 3D Cell Culture?" *Frontiers in Molecular Biosciences*.

https://doi.org/10.3389/fmolb.2020.00033.

Jiaa, Jia, Dylan J. Richardsa, Samuel Pollarda, Yu Tan, Joshua Rodriguez, Richard P. Visconti, Thomas C. Trusk, et al. 2014. "Engineering Alginate as Bioink for Bioprinting." *Acta Biomaterialia*, no. 10: 4323–31.

Jong, Bin Kim. 2005. "Three-Dimensional Tissue Culture Models in Cancer Biology." *Seminars in Cancer Biology* 15 (5 SPEC. ISS.): 365–77. https://doi.org/10.1016/j.semcancer.2005.05.002.

Kapałczyńska, Marta, Tomasz Kolenda, Weronika Przybyła, Maria Zajączkowska, Anna Teresiak, Violetta Filas, Matthew Ibbs, Renata Bliźniak, Łukasz Łuczewski, and Katarzyna Lamperska. 2018. "2D and 3D Cell Cultures – a Comparison of Different Types of Cancer Cell Cultures." *Archives of Medical Science* 14 (4): 910–19. https://doi.org/10.5114/aoms.2016.63743.

Karim, A.A., and Rajeev Bhat. 2008. "Gelatin Alternatives for the Food Industry: Recent Developments, Challenges and Prospects." *Trends in Food Science & Technology* 19: 644–56.

Katt, Moriah E., Amanda L. Placone, Andrew D. Wong, Zinnia S. Xu, and Peter C. Searson. 2016. "In Vitro Tumor Models: Advantages, Disadvantages, Variables, and Selecting the Right Platform." *Frontiers in Bioengineering and Biotechnology* 4 (FEB). https://doi.org/10.3389/fbioe.2016.00012.

Kirkpatrick, Charles James, Sabine Fuchs, Maria Iris Hermanns, Kirsten Peters, and Ronald E. Unger. 2007. "Cell Culture Models of Higher Complexity in Tissue Engineering and Regenerative Medicine." *Biomaterials* 28: 5193–98.

Kirshner, Julia, Kyle J. Thulien, Lorri D. Martin, Carina Debes Marun, Tony Reiman, Andrew R. Belch, and Linda M. Pilarski. 2008. "A Unique Three-Dimensional Model for Evaluating the Impact of Therapy on Multiple Myeloma." *Blood* 112 (7): 2935–45. https://doi.org/10.1182/blood-2008-02-142430.

Knight, Eleanor, and Stefan Przyborski. 2015. "Advances in 3D Cell Culture Technologies Enabling Tissue-like Structures to Be Created in Vitro." *Journal of Anatomy* 227 (6):

746–56. https://doi.org/10.1111/joa.12257.

Knowlton, Stephanie, Shivesh Anand, Twisha Shah, and Savas Tasoglu. 2017. "Bioprinting for Neural Tissue Engineering" xx: 1–16.

Kruse, Magnus, Peter Walter, Benedict Bauer, Stephan Rütten, Karola Schaefer, Niklas Plange, Thomas Gries, Stefan Jockenhoevel, and Matthias Fuest. 2018. "Electro-Spun Membranes as Scaffolds for Human Corneal Endothelial Cells." *Current Eye Research* 43 (1): 1–11. https://doi.org/10.1080/02713683.2017.1377258.

Langer, Robert, and Joseph P Vacanti. 1993. "Tissue Engineering." *Science* 260.

Langhans, Sigrid A. 2018. "Three-Dimensional in Vitro Cell Culture Models in Drug Discovery and Drug Repositioning." *Frontiers in Pharmacology* 9 (JAN): 1–14. https://doi.org/10.3389/fphar.2018.00006.

Lee, Jungwoo, G Daniel Lilly, R Christopher Doty, Paul Podsiadlo, and Nicholas A Kotov. 2009. "In Vitro Toxicity Testing of Nanoparticles in 3D Cell Culture." *Small* 5 (10): 1213–21. https://doi.org/10.1002/smll.200801788.

Li, Jipeng, Mingjiao Chen, Xianqun Fan, and Huifang Zhou. 2016. "Recent Advances in Bioprinting Techniques : Approaches , Applications and Future Prospects," 1–15. https://doi.org/10.1186/s12967-016-1028-0.

Lian, Jiaxin, Bradley W. Mansel, Bridget Ingham, Sujay Prabakar, and Martin A.K. Williams. 2017. "Controlling Chain Flexibility in Collagen Networks to Produce Hydrogels with Distinct Properties." *Soft Materials*. https://doi.org/10.1080/1539445X.2016.1268626.

Liang, Renjie, Yuqing Gu, Yicong Wu, Varitsara Bunpetch, and Shufang Zhang. 2021. "Lithography-Based 3D Bioprinting and Bioinks for Bone Repair and Regeneration." *ACS Biomaterials Science and Engineering* 7: 806–16.

Lin, Ruei-Zhen, and Hwan-You Chang. 2008. "Recent Advances in Three-dimensional Multicellular Spheroid Culture for Biomedical Research." *Biotechnology Journal*, no. 3: 1172–84.

Liu, Xiaoyan, Wenfu Zheng, and Xingyu Jiang. 2019. "Cell-Based Assays on Microfluidics for Drug Screening." *ACS Sensors* 4: 1465–75.

Lovitt, Carrie J., Todd B. Shelper, and Vicky M. Avery. 2014. "Advanced Cell Culture Techniques for Cancer Drug Discovery." *Biology* 3 (2): 345–67. https://doi.org/10.3390/biology3020345.

Lu, Helen H., Saadiq F. El-Amin, Kimberli D. Scott, and Cato T. Laurencin. 2003. "Three-Dimensional, Bioactive, Biodegradable, Polymer-Bioactive Glass Composite Scaffolds with Improved Mechanical Properties Support Collagen Synthesis and Mineralization of Human Osteoblast-like Cells in Vitro." *Journal of Biomedical Materials Research - Part A* 64 (3): 465–74. https://doi.org/10.1002/jbm.a.10399.

Luo, Yong, Xiuli Zhang, Yujiao Li, Jiu Deng, Xiaorui Li, Yueyang Qu, Yao Lu, Tingjiao Liu, Zhigang Gao, and Bingcheng Lin. 2018. "High-Glucose 3D INS-1 Cell Model Combined with a Microfluidic Circular Concentration Gradient Generator for High Throughput Screening of Drugs against Type 2 Diabetes." *RCS Advances* 8: 25409–16.

Marrazzo, Pasquale, Cristina Angeloni, and Silvana Hrelia. 2019. "Combined Treatment with Three Natural Antioxidants Enhances Neuroprotection in a SH-SY5Y3D Culture Model." *Antioxidants* 8 (420).

Matai, Ishita, Gurvinder Kaur, Amir Seyedsalehi, Aneesah Mcclinton, and Cato T Laurencin. 2019. "Progress in 3D Bioprinting Technology for Tissue/Organ Regenerative Engineering." *Biomaterials*, 119536. https://doi.org/10.1016/j.biomaterials.2019.119536.

Matak, Damian, Klaudia K. Brodaczewska, Monika Lipiec, Łukasz Szymanski, Cezary Szczylik, and Anna M. Czarnecka. 2017. "Colony, Hanging Drop, and Methylcellulose Three Dimensional Hypoxic Growth Optimization of Renal Cell Carcinoma Cell Lines." *Cytotechnology* 69: 565–78.

Min, Jia, Swee Leong, Wai Yee, Jia Min Lee, Swee Leong Sing, Miaomiao Zhou, and Wai Yee Yeong. 2018. "3D Bioprinting Processes : A Perspective on Classification and Terminology 3D Bioprinting Processes : A Perspective on Classification and

Terminology," 0–10. https://doi.org/10.18063/ijb.v4i2.151.

Mishriki, S., A. R. Abdel Fattah, T. Kammann, R. P. Sahu, F. Geng, and I. K. Puri. 2019. "Rapid Magnetic 3D Printing of Cellular Structures with MCF-7 Cell Inks." *Research* 2019: 1–13. https://doi.org/10.34133/2019/9854593.

Monteiro, Maria V., Victor M. Gaspar, Luis P. Ferreira, and Joao F. Mano. 2020. "Hydrogel 3D in Vitro Tumor Models for Screening Cell Aggregation Mediated Drug Response." *Biomaterials Science* 8 (1855).

Mørch, YÄrr A., Ivan Donati, Berit L. Strand, and Gudmund Skja˚ K-Bræk. 2006. "Effect of Ca2+,Ba2+, and Sr2+on Alginate Microbeads." *Biomacromolecules* 7: 1471–80. https://doi.org/10.1021/bm060010d.

Mueller-Klieser, Wolfgang. 2000. "Tumor Biology and Experimental Therapeutics." *Oncology/Hematology*, 123–39.

Müller, Werner E.G., Heinz C. Schröder, Qingling Feng, Ute Schlossmacher, Thorben Link, and Xiaohong Wang. 2015. "Development of a Morphogenetically Active Scaffold for Three-Dimensional Growth of Bone Cells: Biosilica-Alginate Hydrogel for SaOS-2 Cell Cultivation." *Journal of Tissue Engineering and Regenerative Medicine*. https://doi.org/10.1002/term.1745.

Namkaew, Jirapat, Thiranut Jaroonwitchawan, Narawadee Rujanapun, Jantip Saelee, and Parinya Noisa. 2018. "Combined Effects of Curcumin and Doxorubicin on Cell Death and Cell Migration of SH-SY5Y Human Neuroblastoma Cells." *In Vitro Cellular & Developmantal B.Ology-Animal* 54: 629–39.

Narenderan, S. T., S. N. Meyyanathan, and Veera Venkata Satyanarayana Reddy Karri. 2019. "Experimental Design in Pesticide Extraction Methods: A Review." *Food Chemistry* 289 (March): 384–95. https://doi.org/10.1016/j.foodchem.2019.03.045.

Nath, Sritama, and Gayathri R Devi. 2016. "Three-Dimensional Culture Systems in Cancer Research: Focus on Tumor Spheroid Model." *Pharmacology and Therapeutics*, no. 163: 94–108. https://doi.org/10.1016/j.pharmthera.2016.03.013.

Nirmalanandhan, Victor Sanjit, Alicia Duren, Peter Hendricks, George Vielhauer, and

Gurusingham Sitta Sittampalam. 2010. “Activity of Anticancer Agents in a Three-Dimensional Cell Culture Model,” no. 5: 581–90. https://doi.org/10.1089/adt.2010.0276.

Nunamaker, Elizabeth A., Kevin J. Otto, and Daryl R. Kipke. 2011. “Investigation of the Material Properties of Alginate for the Development of Hydrogel Repair of Dura Mater.” *Journal of the Mechanical Behavior of Biomedical Materials* 4 (1): 16–33. https://doi.org/10.1016/j.jmbbm.2010.08.006.

Onbas, Rabia, Rumeysa Bilginer, and Ahu Arslan Yildiz. 2021. “On-Chip Drug Screening Technologies for Nanopharmaceutical and Nanomedicine Applications.” In *Nanopharmaceuticals: Principles and Applications Vol. 1*, edited by Vinod Kumar Yata, Shivendu Ranjan, Nandita Dasgupta, and Eric Lichtfouse, 311–46. Cham: Springer International Publishing. https://doi.org/10.1007/978-3-030-44925-4_8.

Onbas, Rabia, and Ahu Arslan Yildiz. 2021. “Fabrication of Tunable 3D Cellular Structures in High Volume Using Magnetic Levitation Guided Assembly.” https://doi.org/10.1021/acsabm.0c01523.

Othman, Sheril Amira, Chin Fhong Soon, Nyuk Ling Ma, Kian Sek Tee, Gim Pao Lim, Marlia Morsin, Mohd Khairul Ahmad, Alyaa Idrees Abdulmaged, and Sok Ching Cheong. 2020. “Alginate-Gelatin Bioink for Bioprinting of Hela Spheroids in Alginate-Gelatin Hexagon Shaped Scaffolds.” *Polymer Bulletin*. https://doi.org/10.1007/s00289-020-03421-y.

Ozawa, Fumisato, Kosuke Ino, Toshiharu Arai, Javier Ramo, Yasufumi Takahashi, Hitoshi Shiku, and Tomokazu Matsue. 2013. “Alginate Gel Microwell Arrays Using Electrodeposition for Three-Dimensional Cell Culture.” *Lab Chip* 13: 3128–35. https://doi.org/10.1039/c3lc50455g.

Page, Henry, Peter Flood, and Emmanuel G. Reynaud. 2013. “Three-Dimensional Tissue Cultures: Current Trends and Beyond.” *Cell and Tissue Research* 352 (1): 123–31. https://doi.org/10.1007/s00441-012-1441-5.

Pampaloni, Francesco, Emmanuel G Reynaud, and Ernst H K Stelzer. 2007. “The Third Dimension Bridges the Gap between Cell Culture and Live Tissue” 8 (october): 839–

45.

Park, Joseph, Isaac Wetzel, Didier Dréau, and Hansang Cho. 2017. "3D Miniaturization of Human Organs for Drug Discovery" 1700551: 1–26. https://doi.org/10.1002/adhm.201700551.

Patil, Ujwal S, Shiva Adireddy, Ashvin Jaiswal, Sree Mandava, and Benjamin R Lee. 2015. *In Vitro / In Vivo Toxicity Evaluation and Quantification of Iron Oxide Nanoparticles*. https://doi.org/10.3390/ijms161024417.

Perdew, John P, Kieron Burke, and Matthias Ernzerhof. 1996. "Generalized Gradient Approximation Made Simple." *The American Physical Society*, no. 3: 3865–68.

Physik, Theoretische, Technische Universitat Wien, and Wiedner Hauptstrasse. 1993. "Ab Initio Molecular Dynamics for Liquid Metals." *Rapid Communications* 47 (1).

Polonchuk, Liudmila, Mamta Chabria, Laura Badi, Jean Christophe Hoflack, Gemma Figtree, Michael J. Davies, and Carmine Gentile. 2017. "Cardiac Spheroids as Promising in Vitro Models to Study the Human Heart Microenvironment." *Scientific Reports*. https://doi.org/10.1038/s41598-017-06385-8.

Pradhan, Shantanu, Iman Hassani, Wen J. Seeto, and Elizabeth A. Lipke. 2017. "PEG-fibrinogen Hydrogels for Three-dimensional Breast Cancer Cell Culture." *Journal of Biomedical Materials Research: Part A* 105 (1): 236–52.

Radhakrishnan, Janani, Sudha Varadaraj, Sanat Kumar, and Akriti Sharma. 2020. "Organotypic Cancer Tissue Models for Drug Screening : 3D Constructs , Bioprinting and Microfluidic Chips." *Drug Discovery Today* 00 (00). https://doi.org/10.1016/j.drudis.2020.03.002.

Ravi, Maddaly, V. Paramesh, S. R. Kaviya, E. Anuradha, and F. D. Paul Solomon. 2015. "3D Cell Culture Systems: Advantages and Applications." *Journal of Cellular Physiology* 230 (1): 16–26. https://doi.org/10.1002/jcp.24683.

Rimann, Markus, and Ursula Graf-Hausner. 2012. "Synthetic 3D Multicellular Systems for Drug Development." *Current Opinion in Biotechnology* 23 (5): 803–9. https://doi.org/10.1016/j.copbio.2012.01.011.

Rimann, Markus, Sandra Laternser, Ana Gvozdenovic, Roman Muff, Bruno Fuchs, Jens M. Kelm, and Ursula Graf-Hausner. 2014. "An in Vitro Osteosarcoma 3D Microtissue Model for Drug Development." *Journal of Biotechnology* 189: 129–35. https://doi.org/10.1016/j.jbiotec.2014.09.005.

Robles-Martinez, Pamela, Xiaoyan Xu, Sarah J. Trenfield, Atheer Awad, Alvaro Goyanes, Richard Telford, Abdul W. Basit, and Simon Gaisford. 2019. "3D Printing of a Multi-Layered Polypill Containing Six Drugs Using a Novel Stereolithographic Method." *Pharmaceuticals* 11: 274.

Saji Joseph, Jitcy, Sibusiso Tebogo Malindisa, and Monde Ntwasa. 2019. "Two-Dimensional (2D) and Three-Dimensional (3D) Cell Culturing in Drug Discovery." *Cell Culture*. https://doi.org/10.5772/intechopen.81552.

Santander, J, L Fonseca, S Udina, and S Marco. 2007. "Wood-Based Nanocellulose and Bioactive Glass Modified Gelatin-Alginate Bioinks for 3D Bioprinting of Bone Cells." *Biofabrication*. https://doi.org/10.1016/j.snb.2007.07.003.

Shimizu, Kazunori, Akira Ito, and Hiroyuki Honda. 2006. "Enhanced Cell-Seeding into 3D Porous Scaffolds by Use of Magnetite Nanoparticles." *Journal of Biomedical Materials Research - Part B Applied Biomaterials* 77 (2): 265–72. https://doi.org/10.1002/jbm.b.30443.

Shri, Meena, Himanshu Agrawal, Payal Rani, Dheer Singh, and Suneel Kumar Onteru. 2017. "Hanging Drop, a Best Three-Dimensional (3D) Culture Method for Primary Buffalo and Sheep Hepatocytes." *Scientific Reports* 7 (1): 1–13. https://doi.org/10.1038/s41598-017-01355-6.

Souza, Glauco R, Jennifer R Molina, Robert M Raphael, Michael G Ozawa, J Daniel, Carly S Levin, Lawrence F Bronk, et al. 2015. "HHS Public Access" 5 (4): 291–96. https://doi.org/10.1038/nnano.2010.23.Three-dimensional.

Souza, Glauco R, Jennifer R Molina, Robert M Raphael, Michael G Ozawa, Daniel J Stark, Carly S Levin, Lawrence F Bronk, et al. 2010. "Three-Dimensional Tissue Culture Based on Magnetic Cell Levitation." *Nature Nanotechnology* 5 (4): 291–96. https://doi.org/10.1038/nnano.2010.23.

Stock, Kristin, Marta F. Estrada, Suzana Vidic, Kjersti Gjerde, Albin Rudisch, Vítor E. Santo, Michaël Barbier, et al. 2016. "Capturing Tumor Complexity in Vitro: Comparative Analysis of 2D and 3D Tumor Models for Drug Discovery." *Scientific Reports*. https://doi.org/10.1038/srep28951.

Sutherland, Robert M. 1988. "Cell and Enrivonment Ineractions in Tumor Microregions : The Spheroid Model." *Science* 240 (4849): 177–84.

Thoma, Claudio R., Miriam Zimmermann, Irina Agarkova, Jens M. Kelm, and Wilhelm Krek. 2014. "3D Cell Culture Systems Modeling Tumor Growth Determinants in Cancer Target Discovery." *Advanced Drug Delivery Reviews* 69–70: 29–41. https://doi.org/10.1016/j.addr.2014.03.001.

Tibbitt, Mark W, and Kristi S Anseth. 2009. "Hydrogels as Extracellular Matrix Mimics for 3D Cell Culture." *Biotechnology and Bioengineering*, no. 103: 655–63. https://doi.org/10.1002/bit.22361.

Topuz, Fuat, Artur Henke, Walter Richtering, and Jürgen Groll. 2012. "Magnesium Ions and Alginate Do Form Hydrogels: A Rheological Study." *Soft Matter* 8 (18): 4877–81. https://doi.org/10.1039/c2sm07465f.

Tseng, Hubert, Liezl R. Balaoing, Bagrat Grigoryan, Robert M. Raphael, T. C. Killian, Glauco R. Souza, and K. Jane Grande-Allen. 2014. "A Three-Dimensional Co-Culture Model of the Aortic Valve Using Magnetic Levitation." *Acta Biomaterialia* 10 (1): 173–82. https://doi.org/10.1016/j.actbio.2013.09.003.

Tseng, Hubert, Jacob A. Gage, William L. Haisler, Shane K. Neeley, Tsaiwei Shen, Chris Hebel, Herbert G. Barthlow, Matthew Wagoner, and Glauco R. Souza. 2016. "A High-Throughput in Vitro Ring Assay for Vasoactivity Using Magnetic 3D Bioprinting." *Scientific Reports* 6 (1): 1–8. https://doi.org/10.1038/srep30640.

Tseng, Hubert, Jacob A. Gage, Robert M. Raphael, Robert H. Moore, Thomas C. Killian, K. Jane Grande-Allen, and Glauco R. Souza. 2013. "Assembly of a Three-Dimensional Multitype Bronchiole Coculture Model Using Magnetic Levitation." *Tissue Engineering - Part C: Methods* 19 (9): 665–75. https://doi.org/10.1089/ten.tec.2012.0157.

Tseng, Hubert, Jacob A. Gage, Tsaiwei Shen, William L. Haisler, Shane K. Neeley, Sue Shiao, Jianbo Chen, et al. 2015a. "A Spheroid Toxicity Assay Using Magnetic 3D Bioprinting and Real-Time Mobile Device-Based Imaging." *Scientific Reports* 5: 1–11. https://doi.org/10.1038/srep13987.

Tseng, Hubert, Jacob A Gage, Tsaiwei Shen, William L Haisler, Shane K Neeley, Sue Shiao, Jianbo Chen, et al. 2015b. "A Spheroid Toxicity Assay Using Magnetic 3D Bioprinting and Real- Time Mobile Device-Based Imaging." *Nature Publishing Group* 5: 1–11. https://doi.org/10.1038/srep13987.

Tung, Yi Chung, Amy Y. Hsiao, Steven G. Allen, Yu Suke Torisawa, Mitchell Ho, and Shuichi Takayama. 2011. "High-Throughput 3D Spheroid Culture and Drug Testing Using a 384 Hanging Drop Array." *Analyst* 136 (3): 473–78. https://doi.org/10.1039/c0an00609b.

Türker, Esra, Nida Demirçak, and Ahu Arslan Yildiz. 2018. "Scaffold-Free Cell Culturing in Three-Dimension Using Magnetic Levitation." *Biomaterials Science* 6: 1745–53. https://doi.org/10.1039/C8BM00122G.

Verjans, Eddy Tim, Jordi Doijen, Walter Luyten, Bart Landuyt, and Liliane Schoofs. 2018. "Three-Dimensional Cell Culture Models for Anticancer Drug Screening: Worth the Effort?" *Journal of Cellular Physiology* 233 (4): 2993–3003. https://doi.org/10.1002/jcp.26052.

Vicini, Silvia, Marco Mauri, Joanna Wichert, and Maila Castellano. 2017. "Alginate Gelling Process : Use of Bivalent Ions Rich Microspheres," 1–6. https://doi.org/10.1002/pen.

Wang, Xinlong, Wei Song, Naoki Kawazoe, and Guoping Chen. 2013. "The Osteogenic Differentiation of Mesenchymal Stem Cells by Controlled Cell–Cell Interaction on Micropatterned Surfaces." *Journal of Biomedical Materials Research A* 101A (12): 3388–95.

Wen, Z, Q Liao, Y Hu, L You, L Zhou, and Y Zhao. 2013. "A Spheroid-Based 3-D Culture Model for Pancreatic Cancer Drug Testing , Using the Acid Phosphatase Assay." *Brazilian Journal of Medical and Biological Research* 46: 634–42.

Willerth, Stephanie M., Kelly J. Arendas, David I. Gottlieb, and Shelly Elese Sakiyama-Elbert. 2006. "Optimization of Fibrin Scaffolds for Differentiation of Murine Embryonic Stem Cells into Neural Lineage Cells." *Biomaterials* 27 (36): 5990–6003. https://doi.org/10.1016/j.biomaterials.2006.07.036.

Worthington, Peter, Darrin J. Pochan, and Sigrid A. Langhans. 2015. "Peptide Hydrogels – Versatile Matrices for 3D Cell Culture in Cancer Medicine." *Frontiers in Oncology*.

Ye, Nannan, Jianhua Qin, Weiwei Shi, Xin Liu, and Bingcheng Lin. 2007. "Cell-Based High Content Screening Using an Integrated Microfluidic Device." *Lab Chip* 7 (12): 1696–1704. https://doi.org/10.1039/b711513j.

Zhang, Yu Shrike, and Ali Khademhosseini. 2017. "Advances in Engineering Hydrogels." *Science*, 356. https://doi.org/10.1126/science.aaf3627.

Zhao, Yu, Rui Yao, Liliang Ouyang, Hongxu Ding, Ting Zhang, Kaitai Zhang, Shujun Cheng, and Wei Sun. 2014. "Three-Dimensional Printing of Hela Cells for Cervical Tumor Model in Vitro." *Biofabrication* 6 (3). https://doi.org/10.1088/1758-5082/6/3/035001.

Zhu, Junmin. 2011. "Design Properties of Hydrogel Tissue-Engineering Scaffolds" 8 (5): 607–26.